Design and Analysis of Solar Powered Multilevel Inverter Fed Induction Motor Drive for Water Pumping Application

(Case Study on Koka in Adama, South-East Ethiopia)

Bereket Fola Gugunto

A Thesis Submitted to

The Department of Electrical Power and Control Engineering

School of Electrical Engineering and Computing

Presented in Partial Fulfillment of the Requirement for the Master of Science Degree in Electrical Power and Control Engineering (Power Electronics)

Office of Graduate Studies

Adama Science and Technology University

Adama, Ethiopia

October-2020

Design and Analysis of Solar Powered Multilevel Inverter Fed Induction Motor Drive for Water Pumping Application

(Case Study on Koka in Adama, South-East Ethiopia)

Bereket Fola Gugunto

Advisor: Dr. Tefera T. Yetayew

A Thesis Submitted to

The Department of Electrical Power and Control Engineering

School of Electrical Engineering and Computing

Presented in Partial Fulfillment of the Requirement for the Master of Science Degree in Electrical Power and Control Engineering (Power Electronics)

Office of Graduate Studies

Adama Science and Technology University

Adama, Ethiopia

October-2020

APPROVAL OF BOARD OF EXAMINERS

We, the undersigned, members of the Board of Examiners of the final open defense by Bereket Fola Gugunto have read and evaluated his thesis entitled “Design and Analysis of Solar Powered Multilevel Inverter Fed Induction Motor Drive for Water Pumping Application” and examined the candidate. This is, therefore, to certify that the thesis has been accepted in partial fulfillment of the requirement of the Degree of Master’s in Power Electronics.

Name	Signature	Date
_____ Name of Student	_____	_____
_____ Advisor	_____	_____
_____ Internal Examiner	_____	_____
_____ External Examiner	_____	_____
_____ Chair Person	_____	_____
_____ Head of Department	_____	_____
_____ School Dean	_____	_____
_____ Postgraduate Dean	_____	_____

DECLARATION

I hereby declare that this MSc thesis is my original work and has not been presented for a degree in any other university, and all sources of material used for this thesis have been duly acknowledged.

Name:_____

Signature:_____

This MSc thesis has been submitted for examination with my approval as thesis advisor.

Name:_____

Signature:_____

Date of submission:_____

Advisor Approval Sheet

To: Electrical Power and Control Engineering (EPCE) Department

This is to certify that the thesis entitled “Design and Analysis of Solar Powered Multilevel Inverter Fed Induction Motor Drive for Water Pumping Application” submitted in partial fulfilment of the requirements of the Master of Science Degree in Electrical Power and Control Engineering, post graduate in Power Electronics, and has been carried out by Bereket Fola Gugunto Id No. PGR/18207/11 under my supervision. Therefore, I recommend that the student has fulfilled the requirements and hence hereby he can submit the thesis to the department.

_____	_____	_____
Name of Advisor	Signature	Date

ACKNOWLEDGEMENT

First and foremost, I would like to express my most heartfelt and profound gratitude to my supervisor, **Dr. Tefera T. Yetayew** for his unlimited professional guidance and support throughout my research. I thank him not only for his valuable advice on my research work but also, for his help in personal matters. He was much more than an academic supervisor to me.

I would moreover like to thank **Mr. Minyamer Gelawe Wase (MSc.)** for his advising and being with me in all my research work.

Furthermore, I am also very grateful to all Electrical Power and Control Engineering department staff members for their unwillingness support, patience, and encouragement throughout my work.

I am also very grateful to my whole family. Especially, my father, my mother, my brothers, my sisters and my friends who showed great patience during the long period of my full dedication to this research work.

Most of all, I would like to thank the almighty God who I strongly believe gave me the power and the strength to accomplish this task.

TABLE OF CONTENTS

LIST OF TABLES

LIST OF FIGURES

LIST OF ACRONYMS

AC	Alternating Current
APOD	Alternative Phase Opposition Disposition
CCM	Continues Conduction Mode
DC	Direct Current
DCM	Discontinuous Conduction Mode
GDP	Gross Domestic Product
GTO	Gate Turn Off Thyristor
HOMER	Hybrid Optimization modeling for Electric Renewable
IEC	International Electrotechnical Commission
IGBT	Insulated Gate Bipolar Transistor
IPD	In Phase Disposition
MLI	Multilevel Inverter
MOSFET	Metallic Oxide Silicon Field Effect Transistor
MOV	Metal Oxide Varistor
MPPT	Maximum Power Point Tracker
NASA	National Aeronautics and Space Administration
OCPD	Over Current Protective Device
P&O	Perturb and Observe
PID	Proportional Integral Derivative
POD	Phase Opposition Disposition
PWM	Pulse Width Modulation
PVC	Polyvinyl Chloride
SCR	Silicon Controlled Rectifier
SHE-PWM	Selective Harmonic Elimination Pulse Width Modulation
SMPS	Switch Mode Power Supply
SPWM	Sinusoidal Pulse Width Modulation
STATCOM	Static Compensator
SVM	Space Vector Modulation
TDH	Total Dynamic Head
THD	Total Harmonic Distortion

LIST OF SYMBOLS

I	Output Current
N	Diode Ideality Factor
Q	Electron Charge
K	Boltzmann Constant
R_s	Series Resistance
R_{sh}	Shunt Resistance
I_{ph}	Photon Generated Current
I_s	Saturation Current
V	Output Voltage
I_d	Diode Saturation Current
I_{sh}	Shunt Current
T_c	Cell Temperature
V_T	Thermal Voltage
G	Solar Insolation
K_i	Short Circuit Current Temperature Coefficient
I_{sc}	Short Circuit Current
V_{oc}	Open Circuit Voltage
E_g	Band Gap Energy
N_s	Number of Cells Connected in Series
N_p	Number of Cells Connected in Parallel
I_{RS}	Reverse Saturation Current
T_{ref}	Reference Temperature
G_{ref}	Reference Solar Insolation
Q	Water Discharge Rate
G	Gravity
P	Water Density
Δ	Declination Angle
Φ	Latitude
B	Slope
Γ	Surface Azimuth Angle
Ω	Hour Angle

Θ	Angle of Incidence
θ_z	Zenith Angle
α_s	Solar Altitude Angle
γ_s	Solar Azimuth Angle
ω_s	Sun Rise/Sun Set Angle
G_{on}	Extra-terrestrial Radiation, Measured on the Plane Normal to the Radiation
G_o	Extra-terrestrial Radiation on Horizontal Surface
H_o	Daily Extra-terrestrial Radiation on Horizontal Surface
H	Monthly Average Daily Radiation
n_d	n^{th} Day of the Year
n	Sunshine Hours
N	Maximum Possible Daily Hours of Bright Sunshine

ABSTRACT

The ability to use renewable energy resources has grown continuously over the past few decades due to fear over warnings of global warming and the depletion of fossil fuels. These fundamental things have initiated researchers to do scientific research into it. Pumping of water requires excessive energy for its operation by consuming a massive amount of diesel, gasoline, and electric power etc. However, the high operational cost and the emission of greenhouse gases of diesel pump set forces farmers to practice deficit irrigation of crops, considerably reducing their yield and income. Induction motor drives are most widely used in both industrial and irrigation sectors. Solar water pumping systems constitute a cost-effective alternative to irrigation pump sets that run diesel. In this research, the design and analysis of solar powered multilevel inverter fed induction motor drive for water pumping system was carried out using MATLAB and HOMER softwares. In this regard, the components of standalone photovoltaic water pumping system such as, Photovoltaic panel, buck converter, three phase inverter, and direct current link capacitor are carefully sized to design system. To achieve this, the mathematical modeling of the (photovoltaic, induction motor, and converter) system has been done. Also, for the implementation purpose the energy demand of deferable load 112.533kWh/day with peak load of 8.44kW has been involved in HOMER optimization. The result shows that 30kW solar, 9kW converter with the best optimum solar energy system with cost of energy 0.236$/kW and net present cost of $60,217 is required for the selected area. Furthermore, a detailed electrical characteristic of 15,600W photovoltaic array with 13 series and 5 parallel configurations was determined on current versus voltage and power versus voltage plane by taking manufacturer's data sheet of the photovoltaic module as input. With the use of a multi-level inverter, the total harmonic distortion is improved from 7.6% to 2.22%. When increasing the modulation index, the voltage profile of the system is increased from 314V to 395.5V and the performance of the machine is improved. Finally, a model for solar powered multilevel inverter fed induction motor is developed and simulated using MATLAB/2016a and HOMER softwares.

***Keywords**: Induction motor, Multilevel inverter, Photovoltaic, Total harmonic distortion.*

CHAPTER 1

INTRODUCTION

1.1. Background

Energy has the great importance for our life and economy. The energy demand has greatly increased due to the industrial revolution. Fossil fuels have been started to be gradually depleted. The sustainability of our civilization is seriously threatened. On the other hand, the greenhouse gas emissions are still increasing due to the conventional generation of energy. It is a really global challenge to reduce carbon dioxide emissions and ensuring secure, clean and affordable energy, and to achieve more sustainable energy systems. Renewable energy sources are considered as a perfect option for generating clean and sustainable energy, among the renewable energy sources, solar energy is sustainable with less carbon emissions. Solar power system finds extensive application in remote areas where access to the grid supply is impractical [1].

Agricultural production and rural water supplies in developing countries are mostly dependent on rain and are adversely affected if sufficient water is not available. The poor irrigation facilities result in significant crop yield losses which can improve if timely adequate water for irrigation is available. Thus, for improving irrigation and urban/rural water supplies, water has to be pumped to reduce the dependence on rain. Most of the population in Ethiopia lives in highland area, with 85 percent being rural and dependent on agriculture with a low level of productivity. But our country, Ethiopia has many rivers and ground water potential. If these water resources are used extensively for irrigation, our country's farmers will be productive [2].

From livestock watering to remote home or village water supply needs are met from the solar based water pumps. Most of the PV water pumping systems are connected directly to the solar arrays and use DC motor driven pumps. This system is easy to operate but is inefficient and requires frequent maintenance. Solar pump operated with AC drive uses an inverter with AC motor. Induction motor offer better choice in terms of size, ruggedness, efficiency and maintainability. Development of high power and low-cost power electronic devices in the recent past has provided a larger area of application for the AC drives. Hence,

AC drives like induction motor drives along with power electronic converters have replaced the dc motor drives in irrigation system [3].

Today, most of the research is focused on the effective utilization of non-conventional energy sources. Of all the existing non-conventional sources of energy, solar Photovoltaic (PV) technology is popularly used as it has many advantages. The benefits of solar Photovoltaic panel are: it absorbs the everlasting solar energy at free of cost and it is eco-friendly without generating any kind of pollution into the atmosphere and offers low noise and low maintenance, when compared with conventional energy sources. It directly converts the solar energy from Sun into DC electric power [4], [5]

When doing the research, selecting the appropriate site plays a crucial role. Site selection is vital for a sustainable water supply scheme, yet many designers in sizing PV water pumping systems frequently underestimate its importance. Installing the best system without a reliable water source is a waste of financial resources. When selecting the site for this research, the availability, type, and quality of water resource and the amount of water required for the intended uses. Based on these criteria's, Koka in Adama located in South Eastern part of Ethiopia is selected for this research.

In two level inverter technology output waveforms is of two level include increase harmonic distortion, ripple factor, and higher voltage stress in induction motor. Multilevel inverter is considered as a state of art in power conversion from DC to AC for high power and power quality demanding applications [6], [7]. It is useful in some application as transport, mining, manufacturing, irrigation, and others. Recently, they have been proposed to enable new possibility for other important applications like electronic and hybrid vehicle, wind energy conversion, UPS, photovoltaic solar energy conversion, and others. For this research, MATLAB/Simulink 2016a and HOMER softwares are used to design and analyze solar powered multilevel inverter fed induction motor drive for water pumping system for farm irrigation application. This research work enhances the method to produce a wave which is similar to that of a sine wave from a DC source.

1.2. Renewable Energy Scenario in Ethiopia

Ethiopia has large amount of renewable energy resources and has the ability to generate over 60,000 megawatts (MW) of electric power from hydroelectric, wind, solar and geothermal sources. The need for electricity has been steadily increasing due to Ethiopia's

rapid GDP growth over the previous decade. The country is experiencing energy shortages as it struggles to meet growing electricity demand which is forecast to grow by approximately 30% per year despite Ethiopia's huge energy potential. Table 2.1 shows the energy resource potential of the Ethiopia [8].

Table 1.1 Energy resource potential of Ethiopia [8]

Resource	Unit	Exploitable Reserve	Exploited Percent
Hydropower	MW	45,000	<5%
Solar/day	kWh/m^2	4 – 6	<1%
Wind: Power Speed	GW m/s	100 >7	<1%
Geothermal	MW	<10,000	<1%
Wood	Million tons	1120	50%
Agricultural waste	Million tons	15-20	30%
Natural Gas	Billion m^3	113	0%
Coal	Million tons	300	0%
Oil shale	Million tons	253	0%

1.3. Motivation of the Study

In Ethiopia, many farmers have to face a lot of problems regarding irrigation. In winter, due to lack of rainfall drought happens and there is interruption of electricity due to load shedding. As a result, crops do not get the required water, and it dies. Now a days, many countries have an agreement to replace gasoline-based irrigation system to photovoltaic system due to the cost of fossil fuels and environmental pollution. Solar energy can be of great use in irrigation. Farmers had to face a huge loss for it. So, to avoid this problem; solar powered multilevel inverter fed induction motor drive for water pumping system is the best solution.

1.4. Statement of the Problem

Energy demand in Ethiopia has grown very rapidly. However, the proportion of clean energy supply for water pumping in off-grid area has not grown at the same rate. Fossil fuels are the main sources of energy which are currently believed to be running out. Moreover, these conventional energies are the main sources of greenhouse gases and also responsible for the global warming. This environmental challenge can be minimized by looking for alternative renewable energy resources.

In Ethiopia, many farmers had to face a lot of problems regarding to the irrigation. In winter, due to lack of rainfall drought happens. As a result, crops do not get the required water, and it dies. Conventional methods like diesel driven generators and direct coupled DC motors are used to avoid these problems. Diesel pumps and DC motors have many drawbacks such as high running and maintenance cost, unreliable supply of fuel, and poor availability of spare parts. Unlike DC motors, induction motors have no brushes to replace, reliable and low maintenance operation. Solar is one of the renewable energy sources which is free of air pollution. However, the output of the solar energy is more than the required due to the load design. For this DC to DC converter is used to get the required voltage for three phase induction motor drive. Usually AC motors used two level inverters to convert DC to AC. This introduces harmonics to the system. Multilevel inverters are one of the alternative solutions to reduce harmonics and it is implemented to the induction motor drive for this work. Therefore, by using solar powered induction motor water pumping using multilevel inverter for farm irrigation overcome the above problems.

1.5. Research Questions

This work intends to answer the following fundamental research questions.

- Are PV water pumping systems technically, economically, and environmentally feasible for farm irrigation?
- How to improve the total harmonic distortion involved in inverters?

1.6. Objectives of the Study

1.6.1. General Objective

The general objective of this research work is to design and analyze water pumping system using multilevel inverter feed three phase induction motor for farm irrigation application.

1.6.2. Specific Objectives

The specific objectives of this research thesis are:

- To design the maximum load of the system.
- To model the selected PV module and design an appropriate DC-DC converter.
- To design IPD-SPWM five level CMLI for comparing and analyzing the THD value by using different modulation index and switching frequency techniques.
- To simulate the overall system by using MATLAB and HOMER software tools.

1.7. Scope of the Study

The deficit in electricity and high diesel costs affects the pumping requirements of community water supplies and irrigation. Therefore, using solar energy for water pumping is a promising alternative to conventional electricity and diesel-based pumping systems. The scope of this thesis is designing and analyzing solar powered water pumping system using multilevel inverter for farm irrigation using MATLAB/Simulink 2016a and HOMER software.

1.8. Limitations of the Study

This research work is limited to the simulation of the system using MATLAB/Simulink and HOMER software by showing how the different components of the system interact with each other. The reason behind this is the implementation of a real system, which is difficult to procure the components. Along with it takes the additional time and cost incurred in making the actual prototype implementation.

1.9. Significance of the Study

The purpose of this research is to present the benefits of replacing diesel water pumping system by photovoltaic water pumping system in farm irrigation. The benefit will be demonstrated in terms of environmental perspectives to show how much reduction in CO_2 emissions is when using photovoltaic system. The wastage of energy and air pollution are the major issues in the world as well as our country Ethiopia. Therefore, the world is replacing non-renewable energy source into renewable energy source. Due to the above-mentioned reasons, the renewable energy is accepted in many countries.

1.10. Thesis Organization

This research thesis comprises five chapters.

Chapter 1: Presents introduction of the research work, statement of the problem, research questions, objectives, scope, limitation, motivation and significance of the research thesis.
Chapter 2: Describes theoretical background and literature reviews.
Chapter 3: Provides the methodologies followed in this research thesis.
Chapter 4: Presents the proposed results and discussions.
Chapter 5: Discusses conclusion and recommendations.

CHAPTER 2

THEORETICAL BACKGROUND AND LITERATURE REVIEW

2.1. Introduction

This chapter discusses on the overall thesis theory and concept. The purpose of this is to explain the perspective and method that is used in previous research and to classify how much this thesis relate with those research and theory. Moreover, this chapter will show the theory and concept used to solve the problem. Theoretical understanding is very important as a guide in doing any kind of research. Electrical and diesel-powered water pumping systems are widely utilized for irrigation applications in Ethiopia.

2.2. Renewable Energy

In spite of the fact that, the fossil fuels are still widely used at the modern day, they are being spent by the humankind much faster than they are replaced by the natural resources. As a consequence, fossil fuels are regarded as being non-renewable at the current rate of the consumption. For that reason, recent research indicated that the demand for renewable sources of energy is an issue of primary concern at the present moment. Today, the renewable sources of energy are tied with the solar energy and its primary and secondary impacts on the planet [9].

These impacts include (solar radiation, the power of wind, the power of water, and certain types of florae, biomass, to be precise). In addition, the renewable energy sources are connected to gravitational forces (for example, tides), and geothermal forces (the heat of the core of the planet). Renewable sources of energy are known to refill themselves on the course of the human life span and might be utilized in addition to the appropriate technological machineries in order to generate foreseeable amounts of energy when needed. In addition, the renewable energy systems appear to be more consistently disseminated on the planet in comparison to other resources, for example, fossil fuels and nuclear power [9].

At this time, the renewable resources of energy are responsible for around 13.6 percent of the worldwide energy usage. Furthermore, by the year 2040, the contribution of the

renewable energy sources to the global energy consumption is projected to be around 47.7%. One of the most significant advantages of renewable energy is their input in the reduction of environmental pollution and its possible elimination on a massive scale [10].

2.2.1. Solar Energy in Ethiopia

Solar power has got powerful potential of energy which can be harnessed using a variety of devices. With the added advantage of minimum maintenance, solar energy systems are easily available for industrial and domestic use with recent developments. Ethiopia has huge solar energy resources. The estimated national annual average irradiance is to be 5.2 kWh/m^2/day with seasonal variations that range between the minimum of 4.5 kWh/m^2/day in July to a maximum of 5.6 kWh/m^2/day in February and March. The solar resource is relatively lower in the most populous Northern, Central and Western highlands of the country while the rift valley regions, Western and Eastern lowlands of the country get higher annual average irradiance well above 6 kWh/m^2/day. Figure 2.1 below shows the global horizontal solar radiation annually for Ethiopia [11].

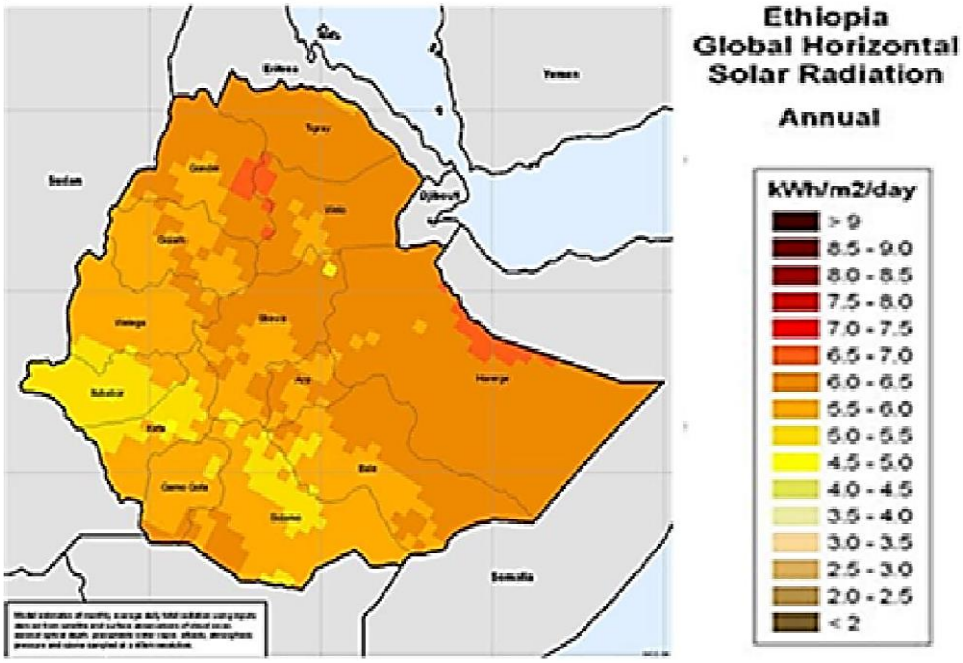

Figure 2.1 Global horizontal solar radiation annually for Ethiopia [12]

2.3. Distribution of Solar Radiation

As shown in the Figure 2.2, the earth receives 174 petawatts (PW) of incoming solar radiation at the upper atmosphere.

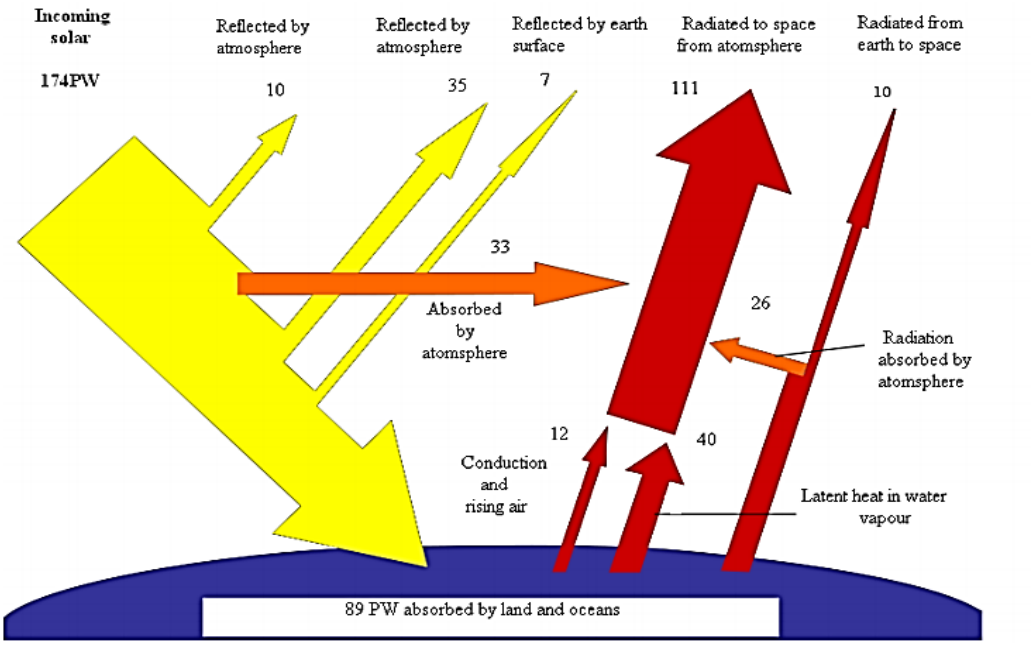

Figure 2.2 Solar radiation distribution [13]

Approximately 30% is reflected back to space and only 89 pw is absorbed by oceans and land masses. The spectrum of solar light at the Earth's surface is generally spread across the visible and near-infrared reason with a small part in the near ultraviolet [13].

2.4. Solar Radiation Reaching Earth Surface

The intensity of solar radiation reaching earth surface which is 1369 watts per square meter is known as Solar Constant. It is important to realize that it is not the intensity per square meter of the Earth’s surface but per square meter on a sphere with the radius of 149,596,000 km and with the Sun at its center. The total amount solar radiation intercepted by the Earth is the Solar Constant multiplied by the cross-section area of the Earth. If we now divide the calculated number by the surface area of the Earth, we shall find how much solar radiation is received in an average per square meter of the Earth's surface [13].

2.5. Spectrum of Sun

The performance of Photovoltaic device is reliant on the spectral distribution of solar radiation. The standard spectral distribution is mainly used as reference for evaluation of PV devices.

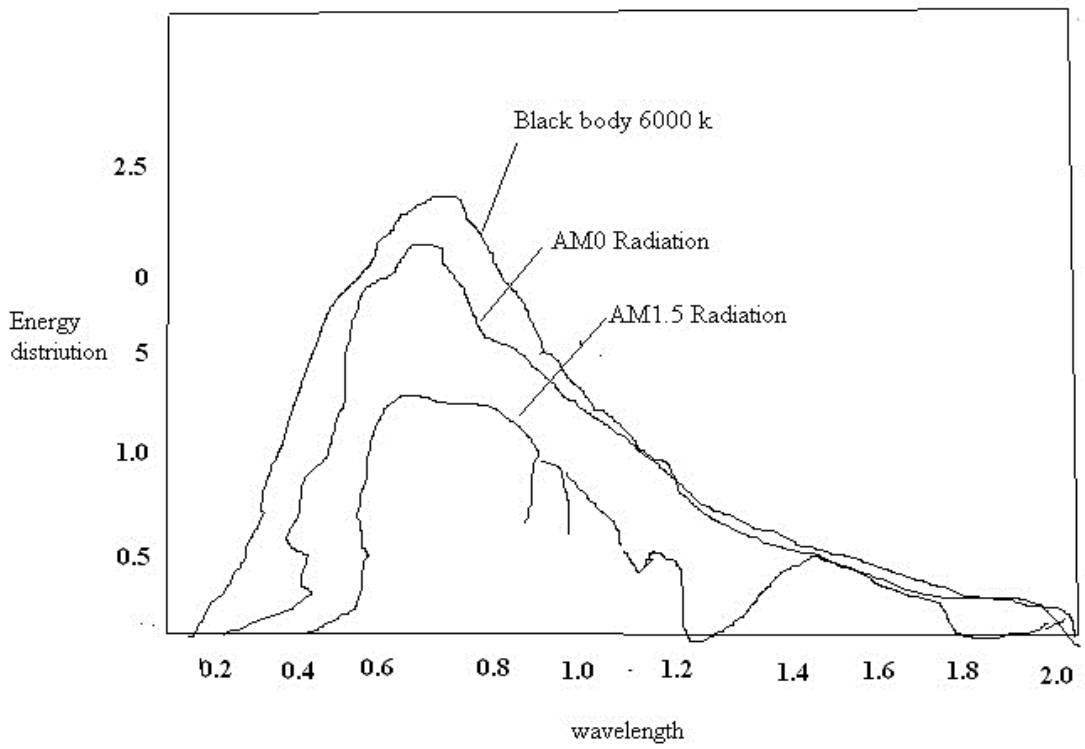

Figure 2.3 Spectrum distribution of black radiation and sun radiation [14]

There are two standard terrestrial distribution defined by the American Society for Testing and Materials (ASTM), global AM1.5 and direct normal. The solar radiation that is perpendicular to a plane directly facing the sun is known as direct normal. The global corresponds to the spectrum of the diffuse radiations. Diffuse radiations are the radiations which are reflected on earth's surface or influenced by atmospheric conditions.

Figure 2.3 shows the distribution of black body radiation and sun radiation. The air mass in this circumstance means the mass of air between a surface and the sun [14]. The length of the path of solar radiation from the sun through the atmosphere is indicated by the number AMx. The longer the path the more is the deviation of light. The AM0 in the above figure means the spectral distribution and intensity of sunlight in near-earth space without atmospheric attenuation [14].

2.6. Standard Test Conditions

The comparison between different photovoltaic cells can be done on the basis of their performance and characteristic curve. The parameters are always given in datasheet. The datasheet makes available the notable parameter regarding the characteristics and performance of PV cells with respect to standard test condition.

Standard test conditions are as follows:

- Irradiance= 1000[w/m]
- Temperature= 25[^{0}C]
- Spectrum of x= 1.5 i.e, AM1.5 [15].

2.7. Photovoltaic System Arrangement

The PV manufacturers use crystalline silicon wafers or thin film technologies to make modules. Single crystal silicon (single-Si), polycrystalline silicon (poly- Si) or ribbon silicon (ribbon-Si) wafers are made into solar cells in the former. The cells are assembled in to modules by solar cell manufacturers.

A typical crystalline silicon module consists of a series circuit of 36 cells, encapsulated in a glass and plastic package for prevention from the environment. This plastic package is framed and provided with an electrical connection enclosure, or junction box. Typical conversion of solar energy to electrical energy efficiencies for common crystalline silicon modules are in the 11 to 15% range [16]. Figure 2.4 shows the arrangement of photovoltaic system.

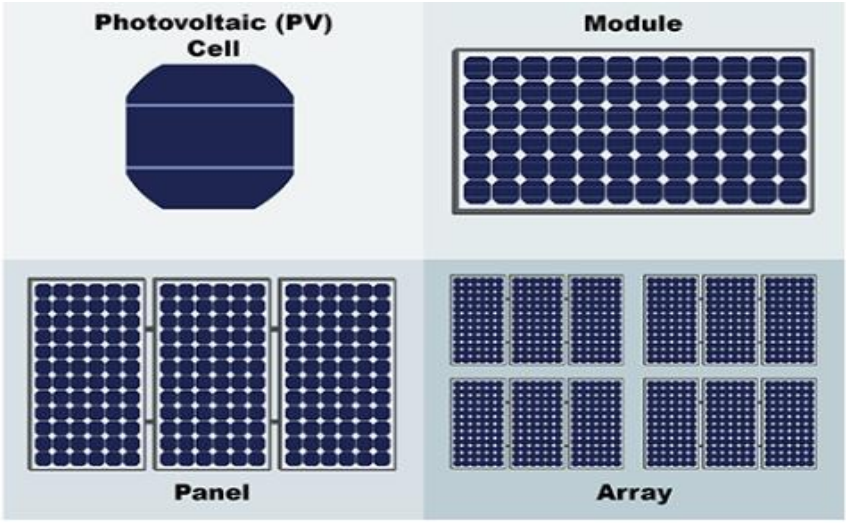

Figure 2.4 Photovoltaic cells, modules, panels and arrays [16]

2.7.1. Working Principle of Photovoltaic Cell

Semiconductor diode whose p–n junction is exposed to light is called photovoltaic cell. Silicon PV cells are made of a thin layer of bulk Si or a thin Si film connected to electric terminals. To form the p–n junction, one of the sides of the Si layer is doped and, on the Sun-facing surface of the semiconductor, a thin metallic grid is placed. When sunlight

strikes its surface, some portion of the solar energy is absorbed in the semiconductor material PV cell. The electron from valence band jumps to the conduction band if absorbed energy is greater than the band gap energy of the semiconductor. Figure 2.5 illustrates the physical structure of a PV cell.

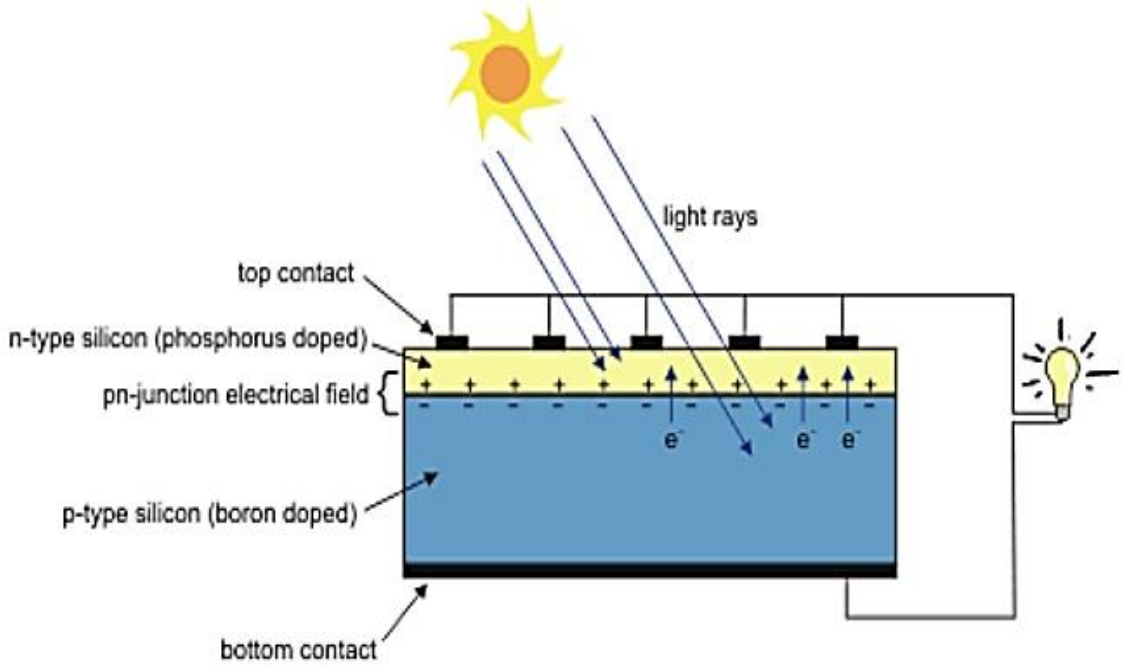

Figure 2.5 Working principle of PV cell [17]

By this process, pairs of hole-electrons are created in the illuminated region of the semiconductor. Thus, electrons which are created in the conduction band are now free to move. By the action of electric field present in the PV cells, these free electrons are forced to move in a particular direction. These flowing electrons contains current and can be drawn for external use by connecting a metal plate on top and bottom of PV cell. The required power is produced due to this current and voltage (created because of its built-in electric fields).

2.8. Types of Photovoltaic Technology

There are mainly three types of PV cells are available today. These are monocrystalline, polycrystalline, and thin film. Each type has its own unique advantages and disadvantages. The solar panel type best suited for the installation depends on factors specific to property and desired system characteristics. This section discusses on the different types of the PV cells that are currently in the manufacturing, research and development stage. Table 2.1 summarizes the performance of the different PV cells.

Table 2.1 Summary of PV cell performance [18]

CELL TYPE	CRYSTALLINE SILICON		THIN FILM	
	Monocrystalline	Polycrystalline	Cadmium Telluride	Amorphous Silicon
Efficiency	14-17.5%	13-15%	9-11%	5-7%
High Temp. Performance	Drop 10-15%	Drop 20%	Drop 0%	Drop 0%
Optimal Temperature	Perform well in cool weather, but poorly in extreme heat.	Performs well in the cool weather. But, poorly in the extreme heat	Perform well in a hot weather, but even extreme heat	Performs well in the hot weather. But even extreme heat.
Cost	Expensive crystalline Silicon	Cheaper crystalline Silicon	Cheaper than crystalline Silicon.	Cheaper than crystalline Silicon
Additional Details	Oldest solar cell technology & the most widely used	Economical choice due to its cost to the performance ratio	Cadmium is toxic, through very small amounts used	Requires a lot of roof space and can take longer to install.

2.9. Effects of Ambient Conditions on PV System

The output of a PV power system can be affected by various ambient conditions. So that the customer has realistic expectations of overall system output, these factors should be taken into consideration. The parameter that has great influence in the characteristic of a PV system is module temperature, as it modifies system efficiency and output energy. In addition to this, the atmospheric parameters such as irradiance level, ambient temperature, dirt/dust and the particular installing conditions also have great influence in the PV system. The result of a connatural characteristic of crystalline silicon cell-based modules are the temperature effects. As the temperature drops, they tend to produce higher voltage and, conversely, to lose voltage in high temperatures. Any PV module or system derating calculation must include adjustment for the temperature effect [19].

2.9.1. Irradiance

The measure of the amount of sunlight falling on a given surface is called irradiance. The more energy a cell will produce when the higher irradiance on a solar cell. It is obvious that, the PV output voltage and current increases as the irradiation level increases. In general, when there is no change in the cell temperature, the increment in the irradiation level leads to a theoretical increment in the maximum power voltage. Figure 2.6 shows the effects of irradiance on PV cell characteristics.

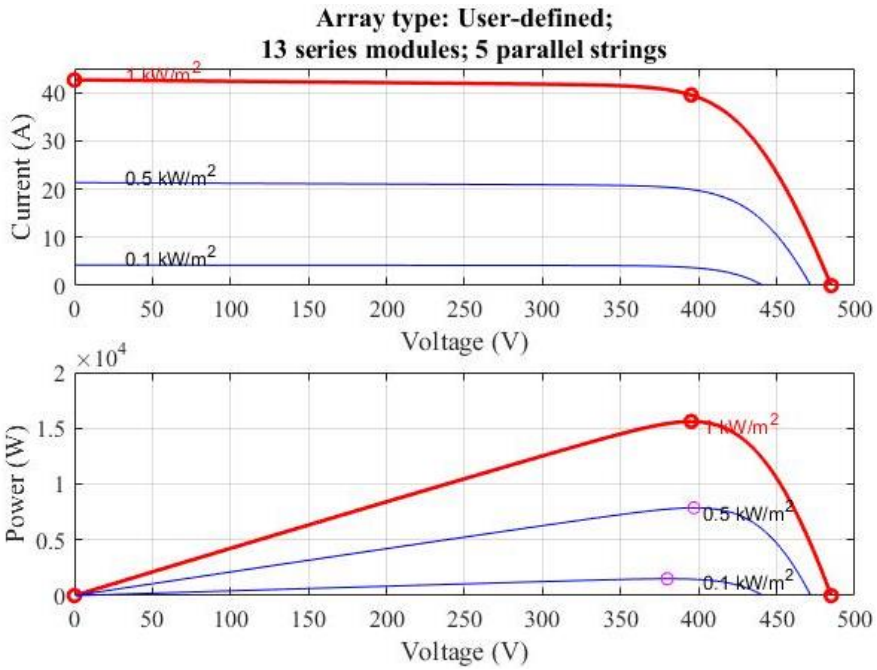

Figure 2.6 Effects of irradiance on PV cell characteristics

On the other hand, the short circuit current I_{sc} depends totally and linearly on the irradiance level therefore the maximum power current is changed as shown below. However, the overall energy received by the system from the sun remains relatively constant from year to year. The angle of the sun, hazy weathers, passing clouds, and air pollution can affect irradiance levels.

2.9.2. Temperature

The band gap of the semiconductor shrinks and the open circuit voltage V_{oc} decreases as the temperature increases following the p–n junction voltage temperature dependency of seen in the diode factor q/kT. Therefore, PV cells have a negative temperature coefficient of V_{oc}. Moreover, a lower output power results given the same photocurrent I_{ph} because the charge carriers are liberated at a lower potential [18]. Again, the band gap of the intrinsic

semiconductor shrinks as temperature increases and more incident energy is absorbed. To raise charge carriers from the valence band to the conduction band, a greater percentage of the incident light has enough energy. A larger photocurrent results; therefore, I_{sc} increases for a given insulation, and PV cells have a positive temperature coefficient of I_{sc}. Figure 2.7 shows the effects of cell temperature on PV cell characteristics.

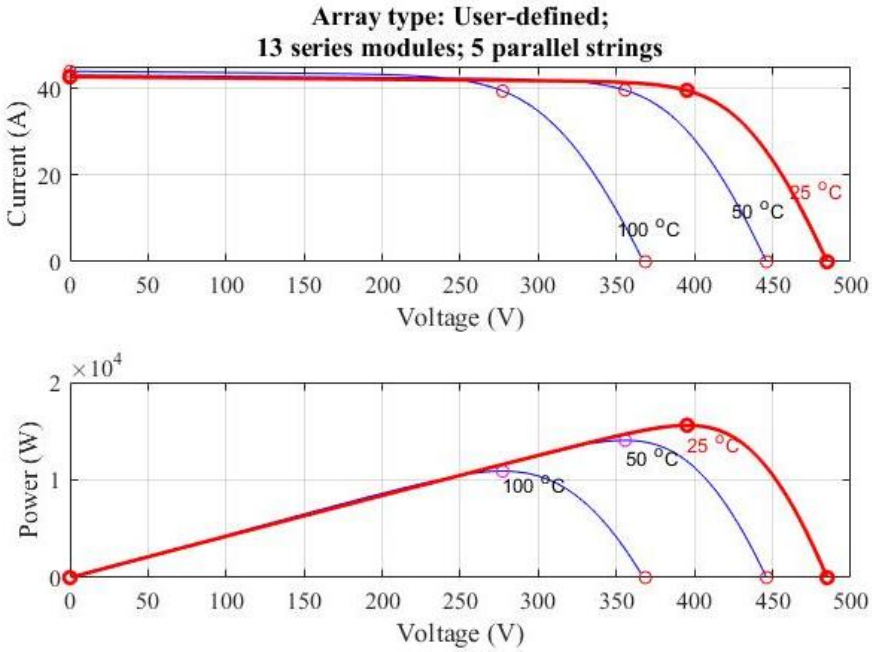

Figure 2.7 Effects of cell temperature on PV cell characteristics

The influences of irradiance and cell temperature on the cell characteristics are shown in Figure 2.6 and Figure 2.7 respectively. As seen from Figure 2.6, by increasing the solar radiation, open circuit voltage increases logarithmically whereas the short circuit current increases linearly. The influence of the cell temperature on the cell characteristics is shown in Figure 2.7. On the open circuit voltage, there is the main effect of increase in cell temperature which decreases linearly with the cell temperature. Thus, the cell efficiency drops. As can be seen, with the increase of the cell temperature, the short circuit current increases slightly.

2.9.3. Energy Conversion Efficiency

The percentage of power converted (from absorbed light to electrical energy) and collected, when a PV cell is connected to an electrical circuit is PV cell ‘s energy conversion efficiency. By reducing the operating temperature of its surface, the efficiency improved and the rate of thermal degradation of a PV module is reduced. By reducing the heat stored

inside the PV cells and cooling the module during operation, this can be achieved efficiently.

2.10. Advantages and Disadvantages of Using PV System

In this section the advantages and disadvantages of photovoltaic system will be discussed briefly [21]. The advantages and disadvantages of photovoltaic system is listed in Table 2.2.

Table 2.2 Advantages and disadvantages of photovoltaic system [21]

Advantages	Disadvantages
Reliability	Cost
Low maintenance cost	Variability of available solar radiation
Universally applications	Energy storage
Environmentally safe	Education

2.11. Inverters

Inverters which are also known as Power conditioning units are necessary in any stand-alone PV system with ac loads. The choice of inverter will be a factor in setting the DC operating voltage of your system. When specifying an inverter, it is necessary to consider requirements of both the dc input and the ac output [51]. All requirements that the ac load will place on the inverter should be considered, not only how much power but what variation in voltage, frequency, and waveform can be tolerated. On the input side, the dc voltage, surge capacity, and acceptable voltage variation must be specified. Selecting the best inverter for an application requires a study of many parameters. The choice of inverter will affect the performance and reliability of a PV system.

2.11.1. Types of Inverter

There are two basic types of inverters commonly employed in adjustable AC drives system. These are:

- Voltage Source Inverter (VSI)
- Current Source Inverter (CSI)

The variable voltage inverter (VVI), or square-wave six-step voltage source inverter (VSI), receives DC power from an adjustable voltage source and adjusts the frequency and voltage [51]. The current source inverter (CSI) receives DC power from an adjustable current source and adjusts the frequency and current. Table 2.3 shows the comparison between voltage

source inverter and current source inverter.

Table 2.3 Comparison between VSI and CSI [51]

Voltage source inverter (VSI)	Current source inverter (CSI)
Inverter fed by a stiff voltage source	Inverter fed by a stiff current source
DC source has low internal impedance	DC source has high internal impedance
Half bridge, full bridge, square wave and pulse width modulated inverters fall under VSI	Capacitor commutated CSI and auto sequential commutated inverters (ASCI) fall under CSI
Need feedback diodes	No feedback diodes required

Since pulse width modulated inverters are fall under voltage source inverter (VSI), and it is used for this research work.

2.12. Photovoltaic System

There are different types of PV systems that are available. These systems are categorized by the main categories of standalone system, grid connected and hybrid system. The system comprises different sources of energy such as PV arrays, diesel generators and wind generators [20]. However, this research thesis describes the study carried out using a direct coupled system. A direct coupled PV pumping system is a group of interactive pieces of equipment designed to collect and convert the solar radiation into electrical energy and to convert the electrical energy into mechanical energy to provide enough mechanical torque to spin a pump to circulate a fluid. In direct-coupled solar water pumping systems used in this research work, the electricity from the PV modules is transferred directly to the pump, which pumps water through a pipe to a specific land.

This system is designed to pump water only during the day. The amount of water pumped is totally dependent on the amount of sunlight hitting the PV panels and the type of pump. Since the pump runs entirely on sunlight the amount of water pumped by this system varies throughout the day in direct correlation to the intensity and amount of sun is striking the PV panel at any given moment [20]. The PV water pumping system considered in this thesis is a stand-alone system to fulfil the interest of people in the rural locations for farm irrigation. The power from the photovoltaic array in the stand-alone system is directly fed to the load without connection to the utility system. The different types of photovoltaic system are discussed below.

2.12.1. Stand Alone Systems

Where the energy is generated and consumed in the same place and which does not interact with the main grid [21].

Table 2.4 Comparisons of different stand-alone type water pumping systems [22]

System Type	Advantages	Disadvantages
PV Powered System	Low maintenance Reliable long life No fuel & no fumes Easy to install	Relatively high initial cost. Low outputs in the cloudy weather.
Diesel Powered System	Moderate capital costs Easy to install Can be portable	It needs maintenance and replacement Site visits necessary Consists noise, fume, dirty problems Fuel is often expensive and supply intermittent
Windmill	No fuel and fumes Potentially long lasting and works well in windy sites	High maintenance & difficult find parts that are costly repair Installation is based on labor intensive & needs special tools

Normally, the electricity consuming/utilizing device is part of the system, i.e. solar home systems, solar street lighting system, solar lanterns and solar power plants. Table 2.4 shows the comparisons of stand-alone type water pumping systems.

2.12.2. Grid Connected Systems

where the solar PV system is connected to the grid. The grid-connected system can either be a grid-tied system, which can only feed power into the grid and such system cannot deliver power locally during blackouts and emergencies because these systems have to be completely disconnected from the grid and have to be shut down as per national and international electrical safety standards [21]. Some grid-connected PV systems with energy storage can also provide power locally in an islanding mode.

2.12.3. Solar PV Hybrid Systems

In a hybrid system, another source(s) of energy, such as wind, biomass or diesel, can be hybridized with the solar PV system to provide the required demand [21]. In such type of system, main objective is to bring more reliability into the overall system at an affordable way by adding one or more energy source(s).

2.13. Water Pumps

Pumps provide additional energy in order to boost or transport liquids, in this case, water, between two different locations. These are usually applied in applications, for example, industrial, domestic and agriculture application. The selection of a certain pumping system for a particular use is a rather central decision and it will be dependent on the necessary energy demand and discharge, head, performance, possible subsequent upkeep and financial expenses [23]. There are several types of pumps with different subcategories (centrifugal pumps and positive displacement pumps are the most popular types), each of them used in a specific field.

For water pumping applications, several types of pumps may be used. They can be categorized according to their design type (rotating or positive displacement pumps), to their location (surface or submersible), or to the type of motor they use (AC or DC). Rotating pumps (e.g. centrifugal pumps) are usually preferred for deep wells or boreholes and large water requirements. The use of displacement pumps is usually limited to low volumes. Positive displacement pumps (e.g. diaphragm pumps, piston pumps and progressive cavity pumps) usually have good lift capabilities but are less accessible than surface pumps and are more sensitive to dirt in the water. Figure 2.8. shows the diagram of centrifugal pump.

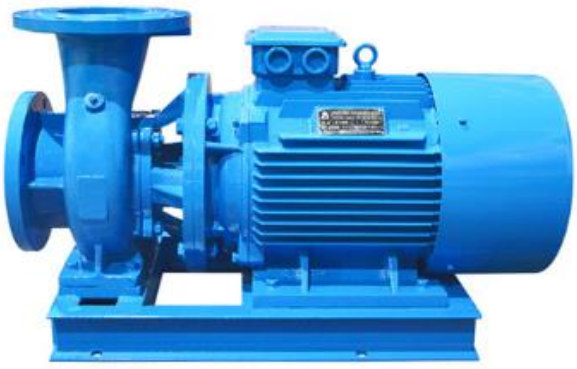

Figure 2.8 Centrifugal pump diagram [17]

2.14. Motor Based PV Pumping System

Currently, several types of electric motors are used for water pumping application. Due to their shortcomings all motors are not equally used. In the Figure 2.9, the classification feature of electric motors can be organized as follows.

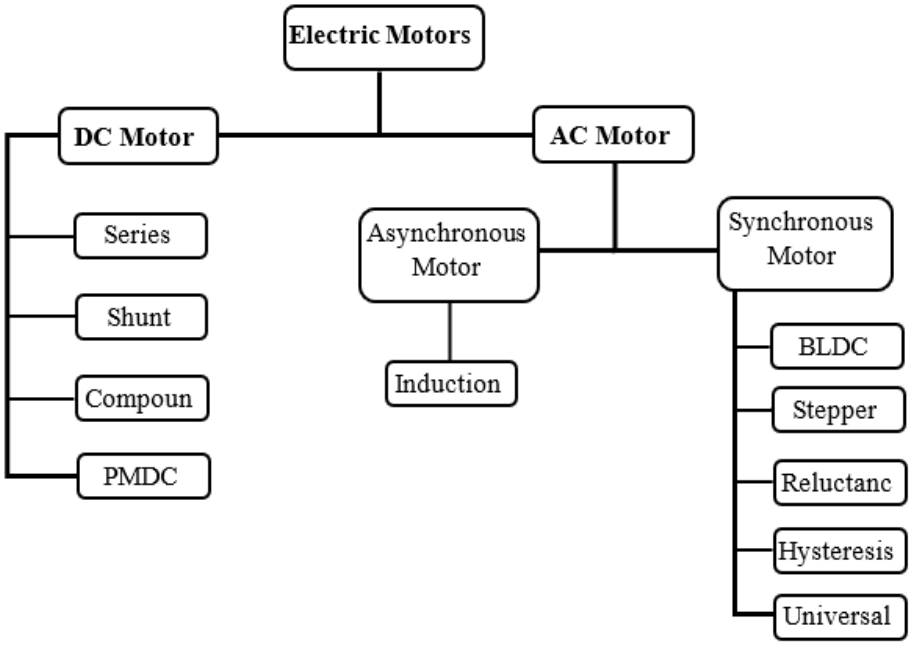

Figure 2.9 Motor Classification

Motors are generally grouped into two types DC and AC. The simplest and cheapest type of AC motor is the squirrel-cage induction motor [24]. Its low cost and rugged construction make it the most commonly used motor for wind/PV applications. Induction motors are classified as squirrel-cage (asynchronous) motors and wound-rotor motors. Wound-rotor motors are generally used for industrial applications. Types of Induction motor (AC motor) pumping system: Induction motor (AC motor) pumping systems can be further classified into single and three phase pumping systems.

The three phase water pumping systems consist of PV array, DC– DC converter, inverter, an induction motor, and the water pump. As the AC pumping motor cannot be directly attached to the PV cells, the DC– DC converter with the P&O MPPT tracking algorithm is used which is connected to the inverter to convert the DC voltage to variable voltage for the induction motor [24]. To increase the speed of the pump, the motor speed needs to be increased, which can be achieved by increasing the frequency of the inverter [24]. Table 2.5 below summarizes the comparison between DC motor and induction motor.

Table 2.5 Comparing AC motor and DC motor

Basics	AC Motors	DC Motors
Nature of the input current	AC current is the main input power in the AC motor.	DC current is the main input power in the DC motor.
Supply phase	Both single phase and three phase supply are used.	Only single-phase supply is used.
Position of armature	In AC motors armatures don't rotate but magnetic field rotates.	In DC motor, armature rotates while magnetic field doesn't rotate.
Maintenance cost	Repairing of AC motor is not costly.	Repairing DC motor is costly.
Carbon brushes	AC motor does not use carbon brushes.	DC motor uses carbon brushes.
Life spam	AC motors have longer life spam.	The DC motors have no longer life spam.
Speed control	The speed of AC motor is controlled by varying the frequency of current.	Speed of DC motors is controlled by varying the armature winding's current.
Commutation process	Commutation process is absent in AC motors.	Commutation process is present in DC motors.

2.14.1. Induction Motor

An induction motor is an AC electric motor in which the magnetic field of the stator winding induces the magnetic flux in the rotor, intern produces the rotating torque on it. It has two important parts that is rotor and stator. Stationary part of induction motor is stator and it has winding on it and rotating part is a rotor. The rotor is connected to the mechanical load devices by using the shaft [25].

According to input supply, induction motors are divided into two types, single and three phase induction motor. Out of both types of induction motors, three phase induction motor is a self-starting motor. Single phase and three-phase IM motor working principle is same but slightly differs in controlling mechanism. The block diagram of induction motor is shown in Figure 2.10.

Figure 2.10 Induction motor block diagram [17]

2.14.2. Speed Control of Induction Motor

There are various method for speed control of induction motor, slip energy loss and to improve overall poor efficiency of system [26]. There are several speed control methods of induction motor. These are mentioned below:

- V/F Control or Frequency Control,
- Controlling Supply Voltage,
- Adding Rheostat in The Stator Circuit,
- Adding External Resistance on Rotor Side,
- Multilevel Inverter Based SPWM Speed Control Method.

Among the above-mentioned speed control methods, the multilevel inverter based SPWM speed control method is used in this research work. The advancement in Power Electronics and semiconductor technology has triggered the development of high power and high-speed semiconductor devices in order to achieve a smooth, continuous and step less variation in motor speed. Applications of solid-state converters/ inverters for adjustable speed of induction motor drive are wide spread in electromechanical systems for a large spectrum of industrial systems [26].

2.15. Selection of Piping Material

When selecting the piping materials, the followings have to be considered.

- The chosen pipe must meet the mechanical requirements of the system.
- It should have sufficient corrosion resistance to prevent corrosion build-up.
- It should be cost-effective.

According to the different piping hand book (Mc Graw-Hill), the most commonly used piping material for water pumping applications is polyvinyl chloride (PVC) piping due to its several advantages.

- It has excellent chemical resistance.
- It is favorable working pressure rating.

There are two common types of PVC pipe. These are schedule 40 PVC and Schedule 80 PVC. Schedule 40 PVC is usually white in colour and schedule 80 PVC is usually a dark gray (they can also be found in other colours). Schedule 80 pipe is designed with thicker wall. This means the pipe is thicker and stronger, and as a result it can handle higher pressure. Schedule 40 pipe is best suited for drainage, irrigation and other cold-water systems. It is strong, rigid and can handle pressure applications. In this thesis, schedule 40 PVC pipe is used due to cost. Based on it's application, schedule 40 pipe is used in this research work. The diameter selection of schedule 40 PVC pipe is shown in Appendix A.

2.16. Photovoltaic Water Pumping Energy Storage

Direct-coupled PV pumps deliver water only when the sun is shining. This may require some type of water storage in order to satisfy the need when the sun is not out. Batteries are usually not recommended for solar-powered water pumping systems because they reduce the overall efficiency of the system and add to the maintenance and cost. Instead of storing electricity in batteries, it is generally simpler and more economical to install 3 to 10 days' worth of water storage. The storage canal is a place which is used for storing water which is an elevated to create pressure at the ground-level outlet. The water in this system is used to feed the plants under cloudy conditions and night time if the water is required for the crop. The water can be continuously supply from the main canal to storage canal [27].

2.17. Irrigation System

Irrigation is the artificial application of water to plants on garden or farm land that is as old as a man, since agriculture is basic thing for human life sustainability. There are many types of irrigation systems depending on the application of water to the land. These are manual irrigation, flood irrigation, surface irrigation, sprinkler irrigation and drip irrigation [27]. Due to its several advantages over other types of irrigation, drip irrigation method is used for this research work.

2.18. Related Works

In this section, other related previous works are reviewed and the gap between previews work and this work is discussed briefly.

Design, simulation and analysis of photovoltaic water pumping system for irrigation of a potato farm at Gerenbo southern Ethiopia in literature [28]. This paper aims to present the benefits of replacing diesel water pumping system by photovoltaic water pumping system in irrigation of a potato farm using river (surface) water available in the area. The finding of this research shows us using solar power for the water pumping system is a good opportunity in terms of solar availability, carbon emission control and economically effective.

Study of PV based water pumping system for agricultural sector aiming to evaluate ways of efficient PV powered water pumping system is discussed in literature [29]. The Photovoltaic-battery hybrid system feds the vector control of an asynchronous motor, PV generator, converter of DC-DC, battery, converter of DC-AC, an induction motor controlled by a vector and the centrifugal pump are investigated in this paper.

The effect of pumping head on solar water pumping system is presented in literature [30]. The aim of this work is to determine the effect of pumping head on PVWPS using the optimum PV array configuration, adequate to supply a DC Helical pump with an optimum energy amount, under the outdoor conditions of Madinah site. Four different pumping head have been tested (50 m, 60 m, 70 m and 80 m). The tests have been carried for different heads, under sunny daylight hours, in a real well at a farm in Madinah site. The flow rate Q depends basically on two factors: the pumping head H and the global solar irradiation Hg.

Study a review of solar-powered water pumping systems comparing to diesel powered pumping system in different countries is presented in literature [31]. The result of this research paper shows, almost all the installed solar-powered water pumping systems heads do not exceed 200m, since as increase in system head there is increase in power supply, and this system are more economical at low pumping capacities compared to diesel and wind-powered water pumping systems. A solar-powered water pumping system contributes to a clean environment by reducing the carbon emission compared to other power supply system.

The viability of the solar/ wind and hybrid water pumping system for off-grid rural areas in Ethiopia is presented in literature [32]. This can be achieved by studying Solar and Wind Potential at the selected site and design a water pumping system for both solar and wind

and by combining the two-energy source solar and wind, the Hybrid water pump has been designed. In this paper maximum power point tracking and energy storage battery was not used. The paper concludes that the Hybrid water pumping system is more feasible than a standalone PV and Windmill.

The above literatures show the effect of TDH in water pumping systems, control of carbon emission by using renewable energy. In this research work, many limitations have been addressed, such as previously directly coupled PV panel to DC motor Pump with battery has been used but this has its own disadvantages; DC motor has high starting torque which is mismatch with variable load torque, this is due to variable solar irradiances and temperature. This may cause damage of equipment or not operate properly. DC motor is expensive and also it needs high maintenance. Nowadays, AC motor is more appropriate for water pumping systems, because it has constant torque, less expensive than DC motor, simple, easily maintained. In PV based water pumping system, using water storage instead of using solar battery is recommended.

CHAPTER 3

METHODOLOGY

3.1. Introduction

This chapter deals with the data collection, designing process of solar powered water pumping system, mathematical modelling for photovoltaic cell, designing and modelling of buck converter, and designing of cascaded multilevel inverter.

3.2. Materials

In this research work, software such as Microsoft office 2019, MathType 6.0 equation, HOMER and MATLAB/2016a are used. Microsoft office is used for editing the thesis documentation. MATLAB is the computing software which consists of technical toolboxes and Simulink. The solar system Optimization Model for Electric Renewable (HOMER) is a computer model developed by the U.S. National Renewable Energy Laboratory (NREL). MathType 6.0 is used for writing mathematical formulas and equations in Microsoft office word and Power point presentation tools.

3.3. Methodologies

The method used in this research to accomplish the required task is shown in Figure 3.1. First the related works are reviewed and then, the necessary data to the research is collected and analyzed. After that, the load demand of the system is determined and PV module is designed based on the load demand. The DC-DC buck converter is designed to get the required output voltage. This voltage is given as input to multilevel inverter which converts the DC to AC voltage and drives induction motor. Finally, the proposed system is developed by using MATLAB/Simulink and the result is discussed and conclusion is drawn.

3.4. Block Diagram of the Proposed System

The methodology of this research involves a number of different tasks that are performed to lead towards completion. The proposed system mainly consists PV array, MPPT, DC-DC converter, multilevel inverter, induction motor, and pump load. In this research work, PV array is used to generate the DC power from the solar energy and MPPT is incorporated with

it to track the maximum power. Then the output voltage of the PV array is stepped down by using the DC transformer so called buck converter.

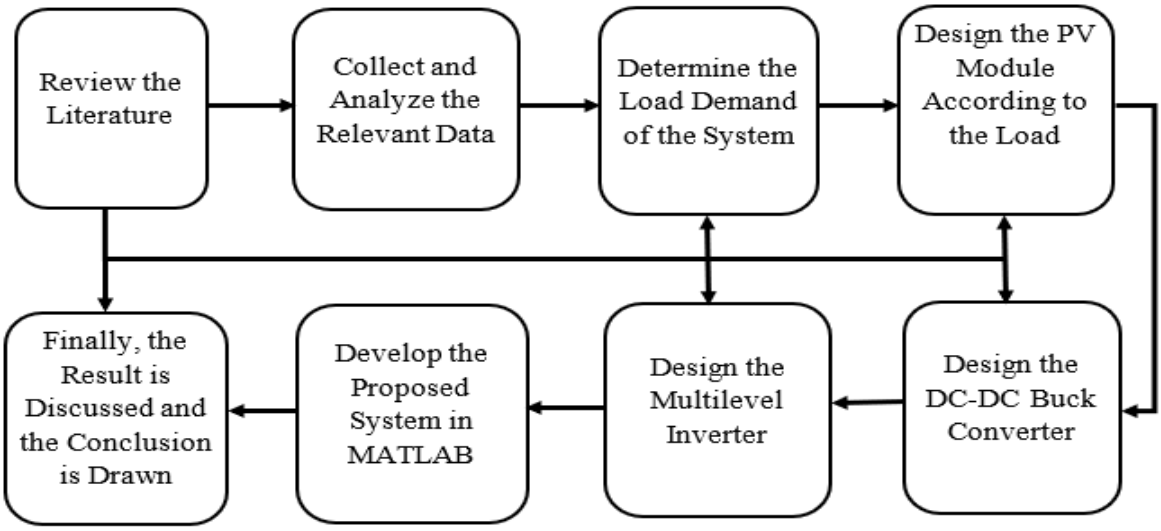

Figure 3.1 Block diagram of the research methodology

To get a stable and smooth response, the output of the buck converter is controlled by using PID controller. Then, the output of buck converter is converted to AC power with the help of multilevel inverter, which is followed by signal generator PWM techniques. To generate gating pulse, the sinusoidal reference of amplitude with carrier wave sets of amplitude are compared. The overall completed multilevel inverter fed the induction drive water pumping system for remote areas farm irrigation. The layout of the proposed system is shown in Figure 3.2.

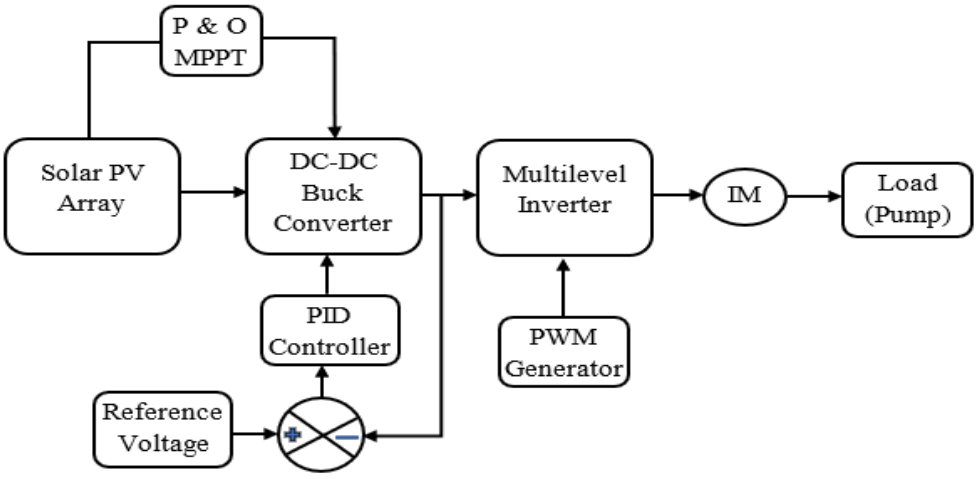

Figure 3.2 The layout of proposed system

3.5. Estimation of the Solar Radiation

In order to design and analyze solar systems, the amount and intensity of sunlight available in the area should be determined. The sun light which is received on the surface of the earth is depending on different factors. The position of the sun in the sky, the slop and orientation of collector surface, the surrounding area (whether it is reflector or absorber), the shading and obstructing object are the most common factor. As shown in Figure 3.3, the angle formed between the plane of the equator and a line drawn from the center of the sun to the center of the earth is called the solar declination, δ. It varies between the extremes of ± 23.45^0. Where n is the number of the day of the year starting 1 at January 1.

$$\delta = 23.45 \sin\left(360.\frac{284+n}{365}\right) \tag{3.1}$$

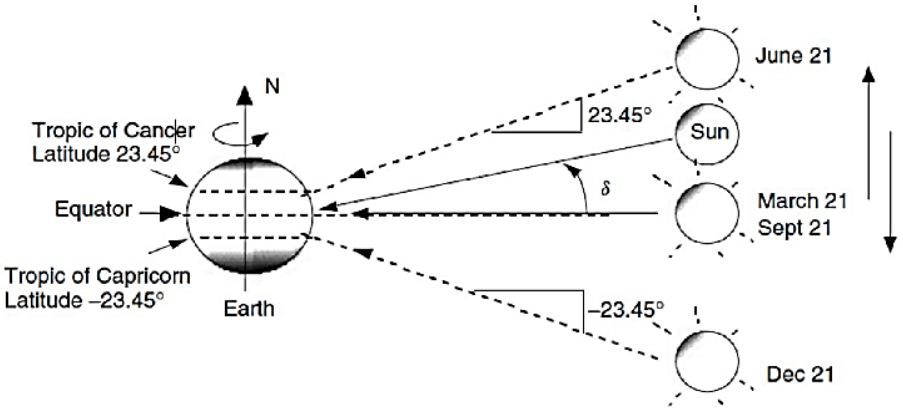

Figure 3.3 The angle between the sun and the declination [33]

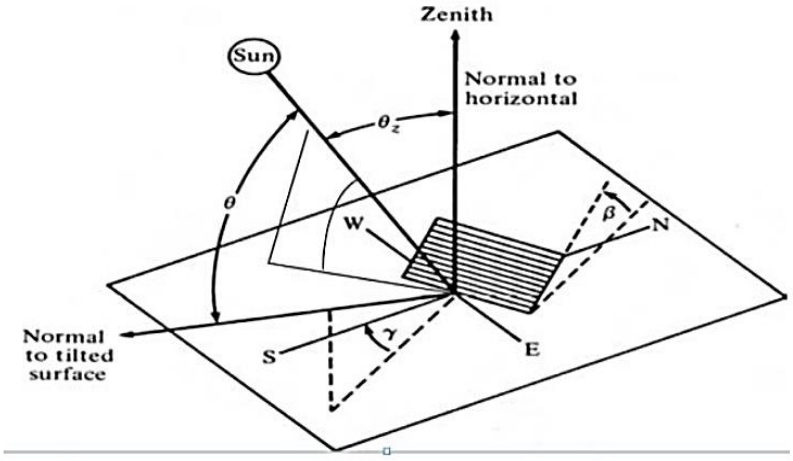

Figure 3.4 The position of sun relative to plane [34]

The geometric relationships between a plane of any particular orientation relative to the earth at any time (weather plane is fixed or moving relative to the earth) and the incoming beam solar radiation, that is, the position of the sun relative to that plane can be described in terms of several angles. Some of the angles are indicated in the Figure 3.4 [34].

Where:

- Φ: Latitude, the angular location north or south of the equator, north positive; $-90^0 \leq \Phi \leq 90^0$. The latitude of the selected site is 8.5263^0 North.
- β: Slope, the angle between the plane of the surface in question and the horizontal; $0^0 \leq \beta \leq 180^0$. ($\beta > 90^0$ means that the surface has a down word facing component).
- γ: Surface azimuth angle, the deviation of the projection on a horizontal plane of the normal to the surface from the local meridian, with zero due south, east negative, west positive; $-180^0 \leq \gamma \leq 180^0$.
- Ω: Hour angle, the angular displacement of the sun east or west of the local meridian due to rotation of the earth on its axis at 150 per hour, morning negative afternoon positive.
- θ: Angle of incidence, the angle between the beam radiation on a surface and the normal to that surface.

Additional angles to define the position of the sun in the sky are:

- θ_z: Zenith angle, the angle between the vertical and the line to the sun, i.e., the angle of incidence of beam radiation on a horizontal surface.
- α_s: Solar altitude angle, the angle between the horizontal and the line to the sun, to mean that the complement of zenith angle.
- γ_s: Solar azimuth angle, the angular displacement from south of the projection of the beam radiation on the horizontal plane. Displacement east of south is negative and west of south is positive.

From the above listed angles, the numerical expression to get the radiation to interest can be calculated. The angle of incidence θ, can be expressed interims of the other angels [34].

$$\sin\alpha_s = \sin\Phi\sin\delta + \cos\Phi\cos\omega\cos\delta \tag{3.2}$$

$$\cos\theta_z = \sin(90^0 - \theta_z) = \sin\alpha_s \tag{3.3}$$

$$\sin\gamma_s = \sin\omega\cos\delta \Big/ \sin\alpha_s \tag{3.4}$$

$$\omega = 15^0(12 - t_{loc}) \tag{3.5}$$

$$\omega_s = \cos^{-1}(\tan\Phi \tan\delta) \tag{3.6}$$

Where ω_s is sunrise or sunset angle and t_{loc} is local solar time in hours.

Considering the two sources of variation in extra-terrestrial radiation, the following equation can be written, i.e., variation in the radiation emitted by the sun and the sun earth distance variation.

$$G_{on} = G_{sc}\left[1 + 0.033\cos\frac{360n}{365}\right] \tag{3.7}$$

Where G_{on} is the extra-terrestrial radiation, measured on the plane normal to the radiation on the nth day of the year.

The extra-terrestrial radiation on a horizontal surface is given by:

$$G_o = G_{on}\cos\theta_z \tag{3.8}$$

$$\cos\theta_z = \cos\delta\cos\omega + \sin\delta\sin\Phi \tag{3.9}$$

$$G_o = G_{sc}(1 + 0.033\cos\frac{360n}{365}) * (\cos\Phi\cos\delta\cos\omega + \sin\delta\sin\delta\sin\Phi) \tag{3.10}$$

To get daily extra-terrestrial radiation on horizontal surface H_o, equation 3.10 is integrated from sun rise to sun set angles and the following equation is obtained.

$$H_o = \frac{24*3600*G_{sc}}{\pi}\left(1 + 0.033\cos\frac{360nd}{365}\right) * \left(\cos\Phi\cos\delta\sin\omega_s + \frac{\pi\omega_s}{180}\sin\delta\sin\Phi\right) \tag{3.11}$$

Where ω_s is the sunset hour angle, n_d is the n^{th} day of the year.

Radiation data are the best source of information for estimating average incident radiation. Lacking these data from nearby location of similar climate, it is possible to use empirical relationships to estimate radiation from hours of sunshine or cloudiness. The original Angstrom type regration equation related to monthly average daily radiation, H, to extra-terrestrial radiation, Ho, for the location [29].

$$H = H_o\left(a + b\frac{n}{N}\right) \tag{3.12}$$

Where a and b are the constants depending on the location, n is the sunshine hours. The maximum possible daily hours of bright sunshine given (N) is given by equation:

$$N = \frac{2}{15}\cos^{-1}(\tan\delta \tan\Phi) \tag{3.13}$$

The values of constants "a" and "b" depends on the location i.e., the surrounding area and has the average value a=0.33 and b=0.43 and the value of Φ is 8.5263^0 North [35]. Declination is the angle made between the plane of the equator and the line joining the two centers of the earth and the sun.

$$\delta = 23.45\sin\left(360.\frac{284+n}{365}\right) \tag{3.14}$$

Table 3.1 The average days of months and the declination angle

Month	n for i^{th} Day of Month	For the Average Day of the Month		
		n		δ
		Day	Day of Year	Declination (^{0})
January	I	17	17	-20.9
February	31+i	16	47	-13.0
March	59+i	16	75	-2.4
April	90+i	15	105	9.4
May	120+i	15	135	18.8
June	151+i	11	162	23.1
July	181+i	17	198	21.2
August	212+i	16	228	13.5
September	243+i	15	258	2.2
October	273+i	15	288	-9.6
November	304+i	14	318	-18.9
December	334+i	10	344	-23.0

Where n is the number day of the year starting from 1st January. Table 3.1 shows the average days of the month and the declination angle. Using monthly average daily global solar radiation, the monthly average extra-terrestrial daily radiation can be calculated. Here, n is the number typical of day of the month. The total solar radiation on a tilted surface is made up of the direct or beam solar radiation, diffuse radiation and ground reflected radiation,

assuming isotropic reflection. As a consequence, the monthly average daily solar radiation on a tilted surface with these declinations is worked in this system. As observed from the Table 3.1, the declination varies between $-23.45° \leq \delta \leq 23.45°$ and is positive during summer and negative during winter.

3.5.1. Sunshine Per Hour Data of Metrology

Table 3.2 shows sunshine per hour data of the selected area.

Table 3.2 Sunshine per hour data of the selected area

Year	Jan	Feb	Ma	Apr	May	Jun	Jul	Aug	Sep	Oct	Nov	Dec
2013	8.9	10.1	8.5	8.1	8.4	7.9	5.3	6.9	8.4	8.3	8.8.	10.1
2014	9.5	8.7	8.6	9	8.7	8.7	6.4	6.9	6.6	8.8	9.4	9.7
2015	9.8	10.1	9.6	8.8	7.7	7.6	9.4	8	8.4	9	9.1	8.9
2016	7.7	8.9	9.4	6.7	6.2	7.9	6.5	6.8	7.2	9.9	9.1	9.8
2017	9.9	9	9.3	9.6	7.9	8	6.2	6	6.8	8.7	10	9.4
Ave	9.16	9.36	9.08	8.44	7.78	8.02	6.76	6.92	7.48	8.94	9.4	9.58

Table 3.3 Solar radiation from different sources

Month	N	N	n/N	ω_s (^{0})	H_O MJ/m^2	H(Calculated) MJ/m^2	NASA
Jan	9.16	12.44	0.74	93.28	32.43	5.84	6.08
Feb	9.36	12.26	0.76	91.98	34.97	6.38	6.57
Mar	9.08	12.05	0.75	90.36	37.10	6.73	6.52
Apr	8.44	11.81	0.71	88.58	37.76	6.66	6.31
May	7.78	11.61	0.67	87.08	37.01	6.36	6.36
Jun	8.02	11.51	0.70	86.34	36.25	6.35	5.77
Jul	6.76	11.56	0.58	86.67	36.4	5.86	5.23
Aug	6.92	11.73	0.59	87.94	37.22	6.04	5.36
Sept	7.48	11.96	0.63	89.67	37.15	6.20	5.84
Oct	8.94	12.19	0.73	91.45	35.20	6.30	6.31
Nov	9.4	12.39	0.76	92.94	32.94	6.01	6.27
Dec	9.58	12.49	0.77	93.64	31.59	5.80	6.08

By using Equation 3.12 and the value of a=0.33 and b=0.43 the following result is found for comparison. Table 3.3 shows the solar radiation from different sources. As it is observed from the Table 3.3, the solar radiation value from NASA and calculated is almost similar. For this purpose, the value of solar radiation which is found from the NASA is used as the input for the HOMER software. Figure 3.6 shows the graphical representation of solar radiation of different sources. Due to the above calculation, the panel angle is adjusted in the July because less amount so sunshine is radiated. Therefore, the panel is mounted at the angle of 21.2^0 and the radiation is 5.23.

3.6. Designing Process of Solar Powered Pumping System

3.6.1. Site Selection

Site selection is vital for a sustainable water supply scheme, yet many designers in sizing PV water pumping systems frequently underestimate its importance. The main criteria for site selection include availability, quality and type of water resource, and the amount of water required for the intended use. Installing the best system without a reliable water source is a waste of financial resources. Similarly, designing a system without estimating the realistic water demand might result in insufficient water supplies or unnecessary financial expenditures for a system that is too large [36]. Based on the above-mentioned criteria's, the selected site is Koka in Adama South-Eastern part of Ethiopia.

3.6.2. Water Requirement

The water requirement has to be considered while designing a solar water pump system is to determine the water requirement. For this irrigation system, the average requirement of water for the crop grown on the field has to be calculated. This requirement differs from place to place so to perform this system one has to be more specific. It is difficult to get the exact water requirement for the tomato. Estimated water demand for various types of crop irrigation is presented in Table 3.4.

Table 3.4 Estimated water demand for various types of crop irrigation [36]

Type of crops	Daily water requirement (Litter/ha)
Tomato	46,200
Maize	50,000
Bean	48,000
Vegetables	25,000

By using estimated water demand for various types of crop irrigation, the water requirement for the system is obtained [36]. This system will be implemented on Koka in Adama South-Eastern part of Ethiopia. For this location, 92,400 Litter water is needed which is the maximum requirement for this specific location. In this research, tomato is selected to cultivate on two hectares of land.

3.6.3. Water Source

The other thing is determining the water source from where water supplied to the field. The available water source may be ground water, surface water or rain water. The common sources are the well, borehole, river, pond and spring. Before choosing the source of water, the researchers have to consider static water level and dynamic water level of the source. In this research, the borehole source is used. Static level is the distance from the surface of the water to the top of the well. This static water level can change over time depending on season. Dynamic level is the distance from the top of the well to the surface of the water when pump is running. Dynamic water level can be measured while pump run because normally it decreases when pump runs. The water level may vary due to the various season so some observation or test have to be done so that the dynamic water level remains same for the whole year. It is important not to exceed the capacity of the source because this can lead to the pump running dry and risking severe damage [36].

3.6.4. System Layout

The schematic layout of standalone PV system is shown in Figure 3.5.

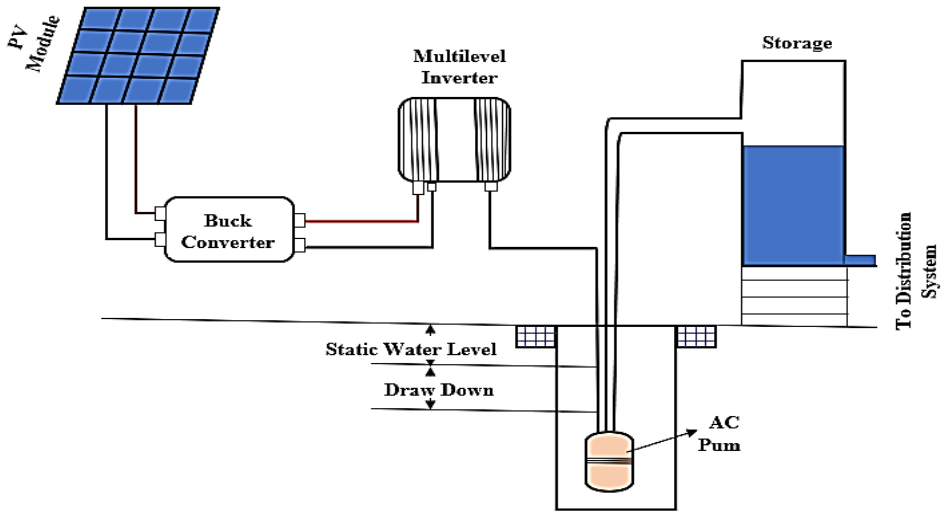

Figure 3.5 Schematic layout of standalone PV system

To get a picture of the system at first, a simple draft schematic of the whole system was preferred to a picture of what the real implementation looks like. The sketch includes where the different component should be located will also include distance and elevation between the components. Determining Flow Rate for the Pump

The pump is designed based on flow rate which is based on the sun peak hours for the chosen designed month and the daily water requirement. For this design, the month which has the least amount of insolation has been chosen. This is because to ensure that the system is not undersized for any month of the year. The pump's design flow rate is based on the operations estimated daily water needs divided by the number of peak-sun hours per day. Average sun hour per day=6.05 (Table 3.3). The design flow rate for the pump can be calculated using:

$$\text{Design flow rate} = \frac{\text{daily water requirement}}{\text{peak} - \text{sun hours}} \tag{3.15}$$

$$= \frac{92,400\text{Lit}}{6.05\,\text{peak} - \text{sun hour} * 60\,\text{min/ hr}}$$

$$= 256\ {}^{l}\!/_{\text{min}}$$

The selected well depth is 150m, static water level is 60m and draw down is 20m and safe yield in that area is (6.7 L/s). Then, the recommended pump position depends on the above data.

3.7. Total System Dynamic Head

In solar powered water pumping system, the total lifting height is the main parameter to determine the necessary power to move the water from the well depth level to the targeted place.

$$T_h = P_h + V_{Rh} + f_h + V_h + D_h + H_{pipe} \tag{3.16}$$

Where: P_h is pump level head, V_{Rh} is vertical rise head, f_h is head due to friction loss, V_h is the velocity head, D_h is the dynamic head loss, H_{pipe} is the horizontal length of pipe.

3.7.1. Determination of Head Loss Due to Friction

By using Darcy-Weisbach formula, the head loss due to friction is calculated.

$$f_h = \frac{fLC^2}{2dg} \tag{3.17}$$

Where: f is friction factor, d is pipe diameter, L is length of pipe, C is mean velocity of fluid. However, the process of determining the friction factor is too complex or problematic. For smooth flow and smooth pipes, Blasius equation is applicable.

$$f = \frac{0.079}{R_e^{1.4}} \tag{3.18}$$

The most simplified form of Blasius equation is:

$$f = \frac{64}{R_e} \tag{3.19}$$

Where R_e is Reynolds number, μ is the dynamic viscosity, ρ is the density of water

$$V = \frac{Q}{A} = \frac{4*Q}{\pi * d^2} \tag{3.20}$$

Then, i can be calculated as,

$$V = \frac{4*0.0043 m^3/\sec}{\pi * 0.05^2} = 2.2 \, m/\sec$$

The Reynolds value can be obtained as,

$$R_e = \frac{\rho V d}{\mu} = \frac{1000 Kg/m^3 * 2.2 m/\sec * 0.05 m}{1.14 * 10^{-3} Ns/m^2} = 96,491$$

Table 3.5 shows common pipe materials.

Table 3.5 Common pipe materials

Material	Roughness(ft)
Drawn bass or copper	0.000005
Commercial steel	0.000150
Wrought iron	0.000150
PVC pipe	0.000005
Asphalted cast iron	0.00400
Galvanized iron	0.000500

The kind of flow is based on the value of R_e.

- If R_e<2000, the flow is called laminar.
- If R_e>4000, the flow is called turbulent.
- If 2000<R_e<4000, the flow is transition.

Since in this system R_e>4000, the flow is turbulent.

For PVC, $\varepsilon \approx 1.5*10^{-6}\text{m}$, the relative roughness is:

$$\gamma = \frac{\varepsilon}{d} = \frac{1.5*10^{-6}\text{m}}{0.05\text{m}} = 3*10^{-5} \tag{3.21}$$

Since R_e>4000, the following equation can be used to determine friction factor.

$$f = \frac{1.325}{\left[\ln\left(\frac{e}{3.7d} + \frac{5.74}{R_e^{0.9}}\right)\right]^2} = 0.021 \tag{3.22}$$

Therefore,

$$f_h = \frac{fLV^2}{2dg} = \frac{0.021*100*2.2^2}{2*9.81*0.05} = 10.4\text{m}$$

3.7.2. Determination of Dynamic Head Loss

Using Darcy Weisbach equation, the dynamic head loss is given by:

$$D_h = K\frac{V^2}{2g} \tag{3.23}$$

$$K = K_{pipe} + K_{fitting} \tag{3.24}$$

K_{pipe} is associated the straight length of the pipe used in the system defined as:

$$K_{pipe} = \frac{fL}{d} \tag{3.25}$$

$K_{fitting}$ is associated with fittings used in the pipe works of the system to pump the water from the ground to the receiving tank. Values can be obtained from the standard tables and total $K_{fitting}$ values can be calculated by adding all the $K_{fitting}$ values for each individual fitting within the system. The following table shows the calculation of $K_{fitting}$ for the system under consideration. The $K_{fitting}$ consideration is shown in the Table 3.6.

$$K_{pipe} = \frac{fL}{d} = \frac{0.021*100}{0.05} = 42$$

Therefore,

$$K = K_{pipe} + K_{fitting} = 3.95 + 42 = 45.95 \approx 46$$

So, D_h can be calculated as,

$$D_h = K\frac{V^2}{2g} = \frac{46*2.2^2}{2*9.81} = 11.34m$$

The velocity head loss can be calculated by using the following formula.

$$V_h = \frac{V^2}{2g} = \frac{2.2^2}{2*9.81} = 0.25$$

Therefore,

$$T_h = P_h + V_{Rh} + H_{pipe} + f_h + V_h + D_h$$

$$T_h = 80 + 8 + 12 + 10.4 + 0.25 + 11.35 = 122m$$

Table 3.6 $K_{fitting}$ consideration

Fitting Items	Number of Items	$K_{fitting}$ Value	Total
No return valves	1	1	1
90^0 bend	3	0.75	2.25
45^0 flanged	2	0.2	0.4
Valves (fully open)	1	0.3	0.3
Total $K_{fitting}$			3.95

3.8. Determination of Power Requirement

This is an important step to estimate what amount of power is required to take the water to the surface.

3.8.1. Pump Size

The required hydraulic power of the pump is:

$$P_h = \frac{q\rho gh}{3600*1000} \quad (3.26)$$

However, the water flow rate can be calculated as:

$$q = \frac{Q/day}{P_{oh}} \tag{3.27}$$

Where Q is water flow rate, P_{oh} is pump operating hours.

$$q = \frac{92.4}{8} = 11.55 m^3/hr$$

Therefore,

$$P_h = \frac{11.55*1000*9.81*122}{3600*1000} = 3.84kW$$

$$P_h = \frac{q\rho gh}{\eta} \tag{3.28}$$

If the efficiency of the pump is not known, the recommended value is between 65 to 70 percent (assume η=0.65).

$$P_h = \frac{3.84}{0.65} = 5.91kW$$

3.8.2. Induction Motor Size

The induction motor power is given by the formula below.

$$P_m = \frac{P_h}{\eta} \tag{3.29}$$

The induction motor pump efficiency is assumed as 0.7. Therefore,

$$P_m = \frac{5.91}{0.7} = 8.44kW$$

3.8.3. PV Panel Sizing

The system is designed to run for only eight hours during day time (2-10am.).

$$P_{uses} = 8440*8 = 67,520Wh/day$$

Where, P_{uses} is the pump uses. To estimate the needed PV energy, the total watt-hour per day is divided by the mismatch factor. The recommended standard mismatch factor is 60 to 70 percent. For this system, 60% is selected. Assume this mismatch factor includes the losses that occur during power conversions between the load and the PV panel. Therefore,

$$\text{PV energy needed} = \frac{67,520}{0.6} = 112,533.33\text{Wh / day}$$

To get the desired power of the system, divide the PV energy needed by the working hour per day.

$$\text{PV power needed} = \frac{\text{PV energy needed}}{\text{Working hour per day}} \tag{3.30}$$

$$= \frac{112,533.33}{8} = 14.1\text{kW / day}$$

For this research work, PV panel with $240W_P$ is selected based on load design, availability, and cost. Therefore,

$$\text{Number of mod ules} = \frac{\text{PV array size}}{\text{Rating power per mod ule}} \tag{3.31}$$

$$= \frac{14,100\text{W}}{240\text{W}} = 59\,\text{mod ules}$$

$$\text{Number of mod ules in series} = \frac{\text{the required voltage}}{\text{max imum voltage of the mod ule}} \tag{3.32}$$

$$= \frac{400\text{V}}{30.4\text{V}} = 13\,\text{mod ules}$$

In series connection the total current is the same as the individual current.

$$I_{total} = I_{individual} \tag{3.33}$$

But, the total voltage of the system is the summation of the individual voltage.

$$\text{Total voltage} = \sum V_{individual} \tag{3.34}$$

Therefore, the total voltage of the system is 484.9V.

$$\text{Number of parallel mod ules} = \frac{\text{Total number of mod ules}}{\text{Number of series mod ules}} = \frac{59}{13} = 5 \tag{3.35}$$

In parallel connection, the summation of total voltage is the same as the individual voltage.

$$V_{total} = V_{individual} \tag{3.36}$$

But the total current is the summation of the individual current.

$$\text{Total current} = \sum I_{\text{individual}} \tag{3.37}$$

Therefore, the total number of modules required is:

$$N_t = N_p * N_s = 5*13 = 65 \tag{3.38}$$

Therefore, to get the satisfied design, the total number of modules required are 65 modules.

3.9. Mathematical Modelling for Photovoltaic Cell

A photovoltaic system converts sunlight into electricity, where, the basic device of a photovoltaic system is the photovoltaic cell. Cells may be grouped to form panels or modules. The modelling of photovoltaic (PV) has made a great transition and form an important part of power generation in this present age. The modelling of PV module generally involves the approximation of the non-linear (I-V) curves. The circuit-based approach to characterize the PV module of which the simplest model is the current source in parallel to a diode is used. The circuit models for photovoltaic cell are listed below.

3.9.1. Ideal Photovoltaic Model

The ideal Photovoltaic cell consists of a single diode connected in parallel with a light generated current source, Iph as shown in the Figure 3.6, where, its output current, I, can be written as:

$$I = I_{ph} - I_s \left[\exp\left(\frac{V}{nV_T} \right) - 1 \right] \tag{3.39}$$

Where Is is cell saturation current, VT is thermal voltage, K is Boltzmann's constant, T_C is cell's working temperature, Q is electron charge (1.6* 10−19 C), and n is ideality factor.

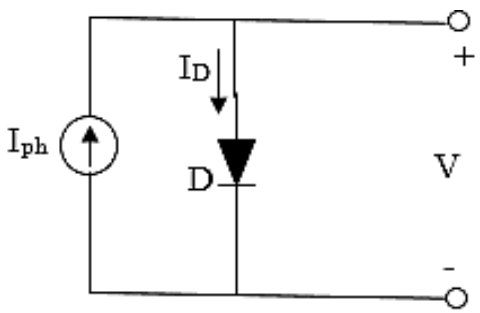

Figure 3.6 Ideal photovoltaic model

3.9.2. Non-Ideal Photovoltaic Models

The photovoltaic model with series resistance (Rs-model) depicted is achieved with the inclusion of series resistance Rs, hence, the output current can be derived as:

$$I = I_{ph} - I_s\left[\exp\left(\frac{V + IR_s}{nV_T}\right) - 1\right] \tag{3.40}$$

The photovoltaic model with series resistance is shown in Figure 3.7.

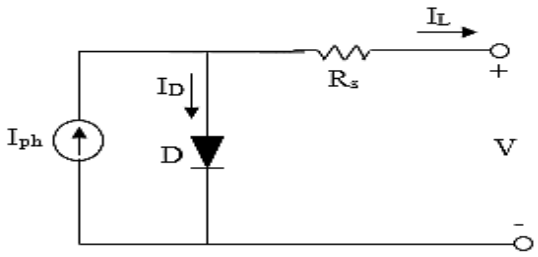

Figure 3.7 Photovoltaic model with series resistance

Equation (3.40) does not adequately represent the behavior of the cell when subjected to environmental variations, especially at low voltages. A more practical model can be seen in Figure 3.10, where series Rs, and parallel resistances Rsh**,** are introduced [37]. Series resistance is very small, which arises from the ohmic contact between metal and semiconductor internal resistance. However, shunt resistance is very large and represents the surface quality along the periphery, noting that in ideal case Rs is 0 and Rsh is ∞ [38]. Applying Kirchhoff's law to the node where Iph, diode, Rsh and Rs meet.

$$I = I_{ph} - I_d - I_{sh} \tag{3.41}$$

$$I = I_{ph} - I_s\left[\exp\left(\frac{V + IR_s}{nV_T}\right) - 1\right] - \left[\frac{V + IR_s}{R_{sh}}\right] \tag{3.42}$$

Where I_d is diode current, G is solar insolation, I_{sh} is shunt current.

This model yields more accurate results than the Rs model, but at the expense of longer computational time. A modification of this model was proposed by several authors by adding an extra diode. This additional diode represents the recombination effects of the charge carriers. In general, the two-diode model is more accurate but the computational time is much longer [37]. For simplicity, the single diode model of Figure 3.6 was used throughout the present work. The photovoltaic model with series and parallel resistance is shown in Figure 3.8.

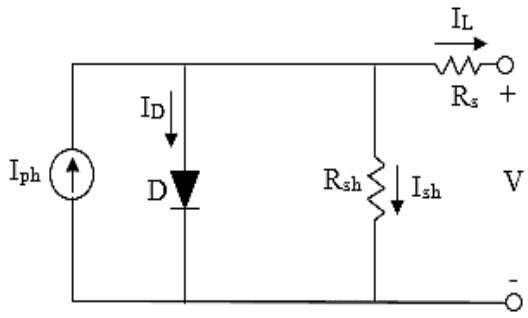

Figure 3.8 Photovoltaic model with series and parallel resistance [37]

The photocurrent mainly depends on the solar insolation and cell's working temperature, which is described as:

$$I_{ph} = \left[I_{scr} + K_i \left(T_c - T_{ref} \right) \right] \frac{G}{G_{ref}} \tag{3.43}$$

Where I_{scr}: solar cell short-circuits current, G_{ref}: reference solar insolation in W/m^2, T_{ref}: cell's reference temperature, K_i: cell's short-circuit current temperature coefficient, G: solar insolation in W/m^2.

On the other hand, the cell's saturation current varies with the cell temperature, which is described as:

$$I_S = I_{RS} \left(\frac{T_c}{T_{ref}} \right)^3 \exp\left[\frac{qE_g}{nK} \left(\frac{1}{T_{ref}} - \frac{1}{T_c} \right) \right] \tag{3.44}$$

Where I_{RS} is cell's reverse saturation current, Eg is band-gap energy of the Si solar cell (1.10 eV), and n is dependent on PV technology.

The reverse saturation current at reference temperature can be approximately obtained as:

$$I_{RS} = \frac{I_{sc}}{\exp\left(\frac{qV_{oc}}{nKT_c} \right) - 1} \tag{3.45}$$

Based on mathematical equations of the photovoltaic cells, a model was written for MATLAB software package applications. The MATLAB/2016a model has been developed which calculates the current module from data of voltage, solar radiation, and temperature. From which, the current versus voltage and power versus voltage, as well as, maximum power point could be obtained. The overall MATLAB block implementation of the PV Module is shown in Figure 3.9.

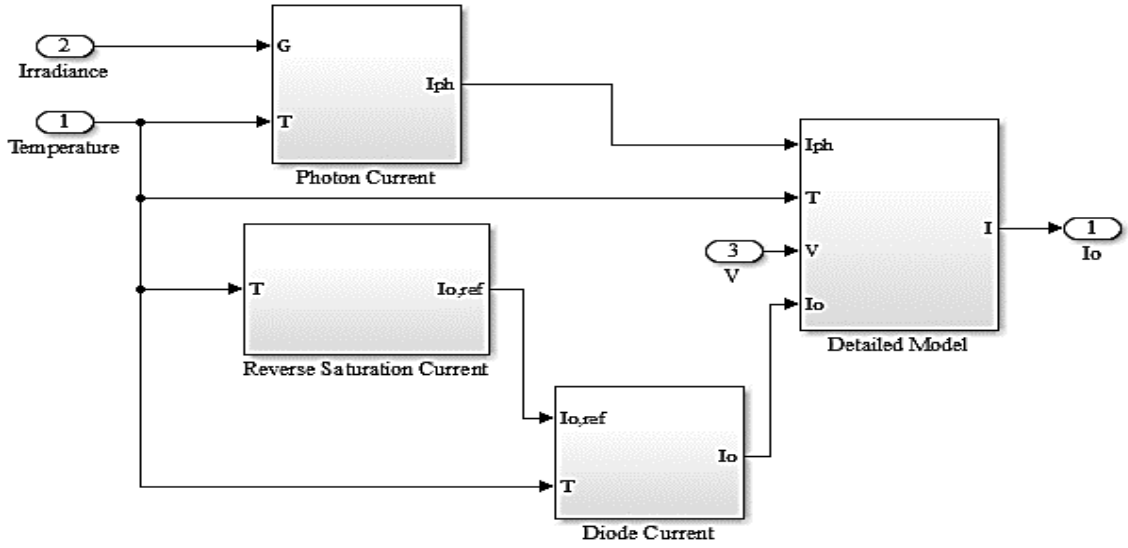

Figure 3.9 Block representation of PV module

3.10. Characteristics of the Photovoltaic Cell

Photovoltaic cells generally demonstrate a nonlinear I-V and P-V characteristics which vary with the solar irradiation and cell temperature. The most important fundamental parameters used for characterizing the photovoltaic cell are: short circuit current I_{sc}, open circuit voltage V_{oc}, Maximum Power Point (MPP), efficiency (η) and Fill Factor (FF) [39].

3.10.1. Short Circuit Current

Short circuit current is the current that reduces the effect of impedance in the circuit. When the cell is short-circuited, negligible current flows in the diode. It is calculated when V=0. However, it is largest amount current produced from the PV cell due to the photon excitation.

$$I_{ph(V=0)} = I_{sc} \tag{3.46}$$

3.10.2. Open Circuit Voltage

Open circuit voltage is the voltage when the PV cell is not connected to any load in a circuit and no current passing through the cell. It is calculated when the voltage is equal to zero. Moreover, it is the maximum voltage difference across the PV cell when I=0. Mathematically,

$$V_{OC} = \frac{AKT}{q} \ln\left(\frac{I_{ph}}{I_s} + 1\right) = V_{th} * \ln\left(\frac{I_{ph}}{I_s} + 1\right) \tag{3.47}$$

Where: V_{th} is the thermal voltage, T is the operating temperature of the PV cell.

3.10.3. Maximum Power Point

It is the operating point where the power is maximum across the load. Mathematically,

$$P_k = V_k * I_k = \delta V_{OC} * I_{SC} \tag{3.48}$$

Where P_k is the maximum power, V_k is the maximum voltage, I_k is the maximum current and δ is the fill factor.

3.10.4. Efficiency

It is defined as the ratio of maximum power to the incident light power. Mathematically,

$$\eta = \left(\frac{P_k}{P_{in}} \right) * 100 = \left(\frac{V_k * I_k}{P_{in}} \right) * 100 \tag{3.49}$$

3.10.5. Fill Factor

Fill Factor which is abbreviated by FF, is a parameter defined as the ratio of the maximum power from the solar cell to the product of I_{sc} and V_{oc}, expressed as:

$$FF = \frac{P_{max}}{V_{OC} I_{SC}} \tag{3.50}$$

Typically fill factors ranges from 0.5 to 0.82. Its value is more than 0.7 for good PV cells. The fill factor decreases with the increase of cell temperature. In this research, Perform Poly240W photovoltaic module is used to analyze the electrical performance parameters. The Perform Poly240W module contains 60 poly-crystalline solar cells configured as 13 series and 5 parallel connection. The key specification and electrical characteristics of Perform Poly240W, 240W PV cell is shown in Table 3.7.

Table 3.7 Electrical characteristics of Perform Poly240W, PV module

Parameters	Values
Nominal power [Wp] P_{mpp}	>240W
Voltage at nominal power [V] V_{mpp}	30.4V
Open-circuit voltage [V] V_{oc}	37.3V
Current at nominal power [A] I_{mpp}	7.9A
Short-circuit current [A] I_{sc}	8.52
Cells per module N_S	60
Module Efficiency [%] η	14.3%

The model of the PV module was executed using a MATLAB/Simulink 2016a. The PV module is influenced by temperature, light intensity etc. The output power of PV cell and output current depends on cell's operating voltage, temperature and solar insolation.

3.11. Modelling Maximum Power Point Tracker

Maximum power point tracker is used to improve the efficiency of the solar panel. The output power of any circuit can be maximized by adjusting source impedance equal to the load impedance according to maximum power point theorem. So, the algorithm of MPPT is equivalent to the problem of impedance matching. In this thesis, the Buck Converter is used as impedance matching device between input and output by changing the duty cycle of the converter circuit.

The output voltage of converter depends on the duty cycle. Therefore, MPPT is used to calculate the duty cycle for obtain the maximum output voltage because if output voltage increases than power also increases. In this research, Perturb and Observe (P&O) algorithm is used to track maximum output power from PV module and to command DC-DC buck converter, because this requires less complexity and low-cost implementations. Figure 3.10 shows flow chart of the perturb and observe MPPT.

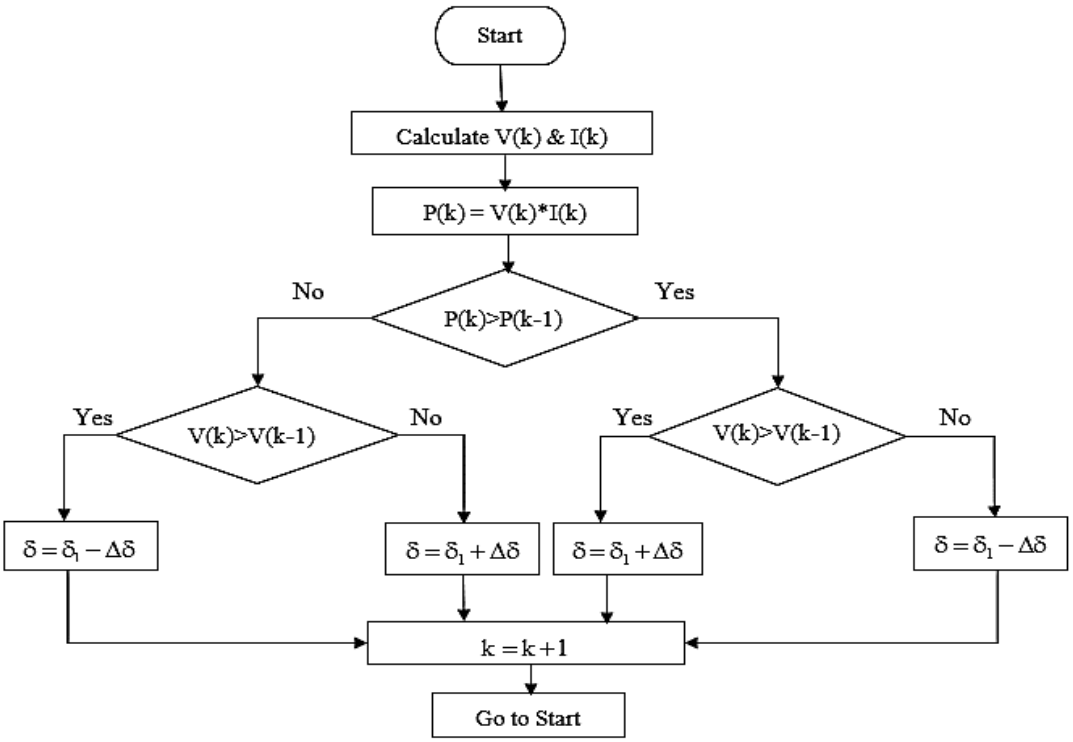

Figure 3.10 Flow chart of the perturb and observe MPPT

3.11.1. Perturb and Observe MPPT Algorithm

Among other methods of MPPT, it is the simplest method to implement. It is easy to implement because in this method only voltage is sensed. In this method, the power output of the system is checked by varying the voltage supply. If on increasing the voltage power also increases, then ‘δ’ is increased. Otherwise ‘δ' is decreased to regulate the power.

Similarly, while reducing voltage if power increases, the duty cycle is decreased. These steps continue till maximum power point is achieved. The corresponding voltage at which MPP is reached is called reference point (V_{ref}). The MATLAB implementation of perturb and observe method is shown in Figure 3.11.

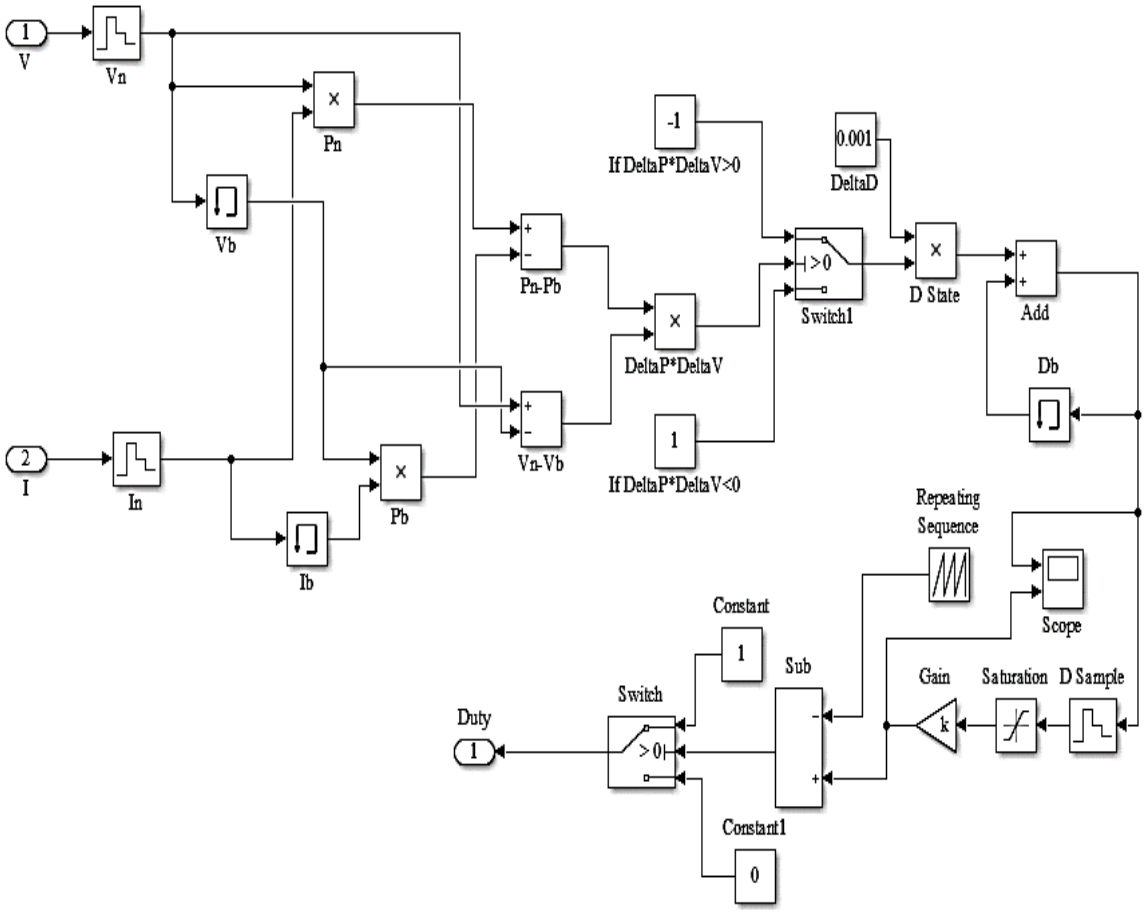

Figure 3.11 The MATLAB implementation of perturb and observe method

3.12. DC-DC Converters

DC-DC converters are the electronic devices that are used to change DC electrical power efficiently from one voltage level to another. The switched mode DC-DC converter is considered as the main part of MPPT system. These are widely used to convert unregulated DC inputs into controlled DC output at a desired voltage and current levels in DC power

supplies, DC motors and input of inverter [40]. They use an inductor and a capacitor as energy storage elements so that energy can be transferred from the input to the output.

The DC-DC converters are widely used in switched-mode power supplies (SMPS) and have a wide range of uses today and are becoming increasingly more important in everyday use. There are different types of DC-DC converters. The most commonly known are buck converter, boost converter and buck-boost converter.

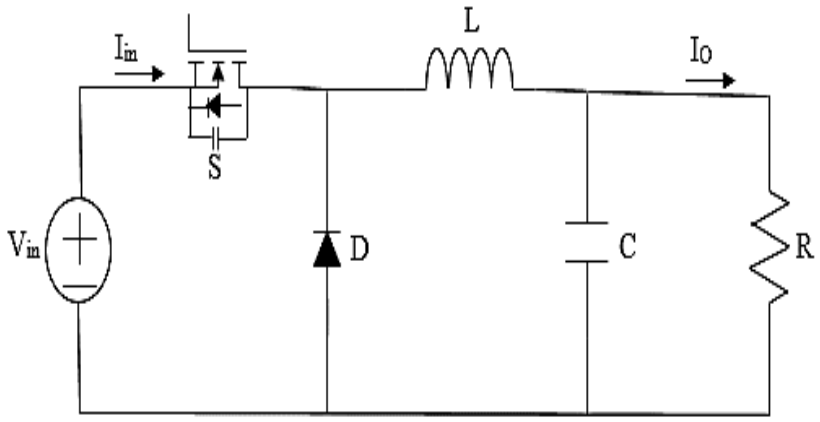

Figure 3.12 Schematic diagram of buck converter

Buck converter is a type of converter which is used to convert unregulated DC input voltage to a controlled DC output voltage with a desired voltage level. It is sometimes called step down power stage. The topology gets its name from producing an output voltage that is lower in magnitude than the input voltage. In this thesis work, the modelling and design of the buck converter is used and discussed. Figure 3.12 demonstrates the circuit diagram of buck converter.

3.12.1. Power Semiconductor Switch

In its crudest form, a switch can be a toggle switch which switches between supply voltage and ground. Here transistors chosen for use in switching power supplies must have fast switching times and should be able to withstand the voltage spikes produced by the inductor [41]. The most popular switching devices are SCR, GTO, IGBT and MOSFET. Among different types of switches MOSFET and IGBT are compared on the Table 3.8. Due to its several advantages over the MOSFET, the IGBT switch is used in this research work.

Table 3.8 Comparison between MOSFET and IGBT

MOSFET	IGBT
MOSFET is the voltage-controlled device.	IGBT is voltage-controlled device
Three terminals of the MOSFET are gate (G), drain(D) and source (S).	IGBT has also three terminals: gate (G), drain (D) and source(S).
The input impedance of MOSFET is very high.	Input impedance of IGBT is very high.
MOSFET has positive temperature coefficient. When compared to the IGBT, with increase in temperature on-state resistance increases.	IGBT has positive temperature coefficient. With the increase in the temperature the on-state resistance increases but rate of increment is less than increase in MOSFET.
MOSFET has large voltage drop.	IGBT has very low voltage drop.
The on-state voltage drop of the MOSFET increases by three times for the temperature rise from room temperature to 200^0C.	The increment of on-state voltage drop of IGBT is very small.

3.13. Designing and Modelling of Buck Converter

Buck converters convert unregulated DC supply into a regulated DC voltage and the output voltage is lesser than the input voltage. The waveforms of buck converter for continuous conduction mode of operation are shown in the Figure 3.13 below.

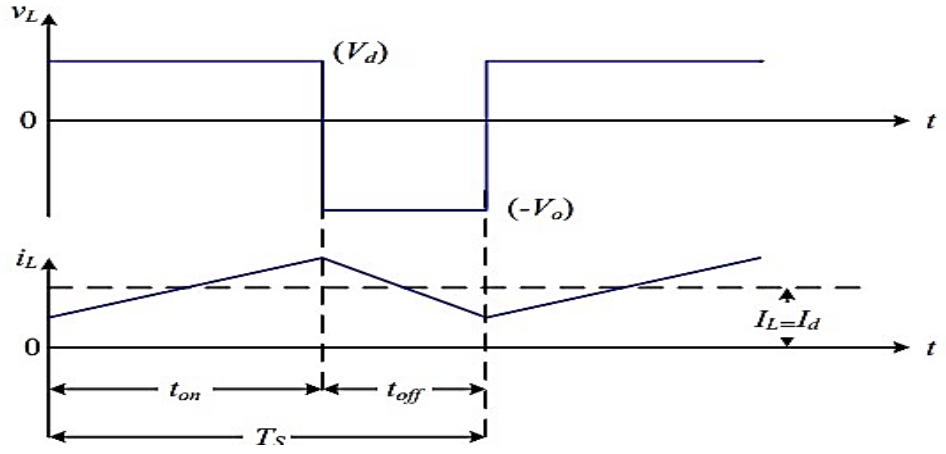

Figure 3.13 Waveforms of buck converter

3.13.1. Analyses of Buck Converter When the Switch is Closed

The equivalent circuit of buck converter when the switch closed is as shown below in Figure 3.14 below.

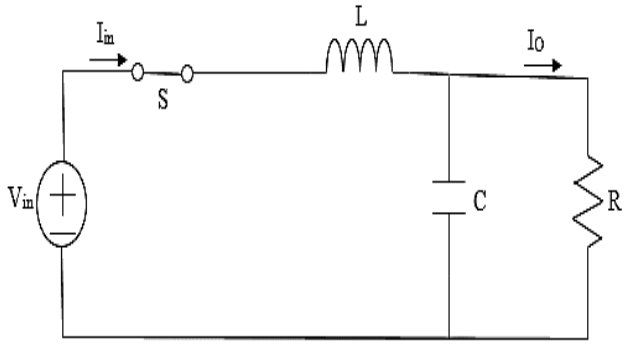

Figure 3.14 Equivalent circuit of buck converter when switch is closed

When the switch is closed (ON) for time duration ton, the switch conducts the inductor current and the diode becomes reverse biased. This results in a positive voltage across the inductor.

$$V_{in} = L\frac{di_L}{dt} + V_o \tag{3.51}$$

Rearranging Equation (3.51) gives,

$$L\frac{di_L}{dt} = V_{in} - V_o \tag{3.52}$$

Equation (5.52) can be rewritten as,

$$\frac{\Delta i_L}{\Delta t} = \frac{V_{in} - V_o}{L} \tag{3.53}$$

Since the duration of time when the switch ON is given as $\Delta t = DT$, Equation (5.53) can be modified as,

$$\Delta i_L(\text{closed}) = \left(\frac{V_{in} - V_o}{L}\right)DT \tag{3.54}$$

Where D is the duty ratio.

3.13.2. Analyses of Buck Converter When Switch is Open

When the switch is turned off, because of the inductive energy storage, inductor current continues to flow. During this time diode is forward biased and the current flow through it. The equivalent circuit of buck converter is shown in Figure 3.15 when the switch is open.

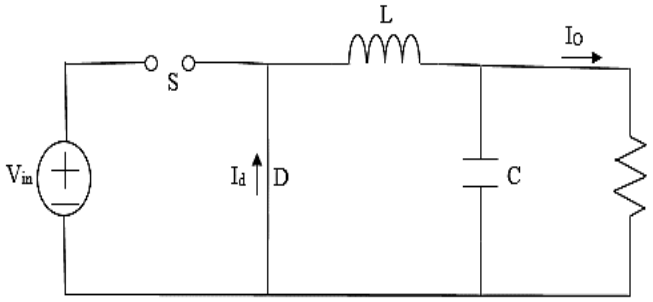

Figure 3.15 Equivalent circuit of buck converter when switch is open

$$L\frac{di_L}{dt} = -V_o \tag{3.55}$$

Then, Equation (5.55) can be rewritten as,

$$\frac{\Delta i_L}{\Delta t} = \frac{-V_o}{L} \tag{3.56}$$

Since the duration of time when the switch OFF is given $\Delta t = (1-D)T$ as, then, Equation (5.56) is given as,

$$\Delta i_{L(open)} = \frac{-V_o}{L}(1-D)T \tag{3.57}$$

For steady state operation, the net change in inductor current must be zero over one period of time.

$$\Delta i_{L(closed)} + i_{L(open)} = 0 \tag{3.58}$$

The most simplified form of the Equation (5.57) gives,

$$D = \frac{V_o}{V_{in}} \tag{3.59}$$

In other ways, since in steady-state operation waveform must repeat from one time period to the next, the integral of the inductor voltage V_L over one time period must be zero.

$$\int_0^T V_L dt = \int_0^{t_{on}} V_L dt + \int_{t_{on}}^T V_L dt \tag{3.60}$$

Where T is switching period (i.e. T = ton + toff) and integrating over switching period gives,

$$(V_{in} - V_o)t_{on} = V_o(T - t_{on}) \tag{3.61}$$

Simplifying Equation (5.61) gives,

$$D = \frac{V_o}{Vin} = \frac{t_{on}}{T} \tag{3.62}$$

The detailed representation of the masked buck converter system is shown in Figure 3.16 below. The converter contains IGBT switch and freewheeling diode. Also, input and output filters are incorporated. The inductor is in charge of diminishing the output current ripple; the bigger the inductor, the smaller the ripple.

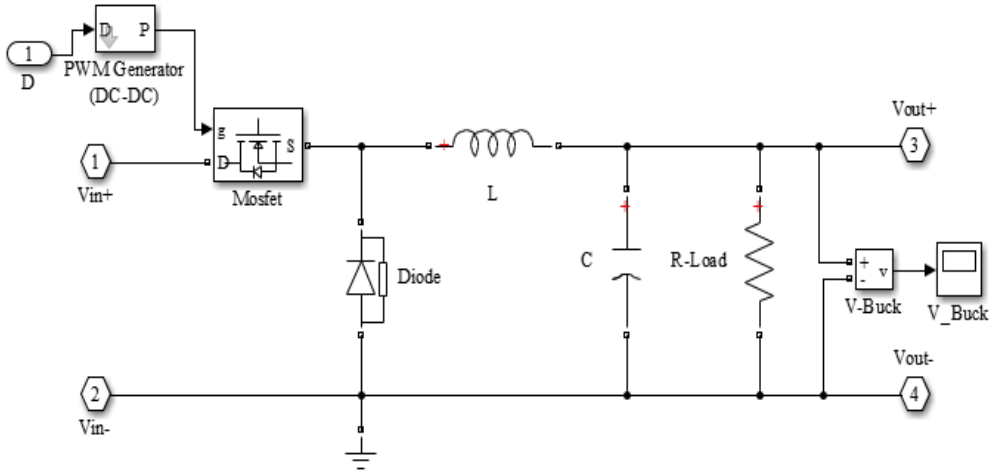

Figure 3.16 The MATLAB implementation of buck converter

To calculate the inductor value, assuming no power losses in the converter, power absorbed by the load must be equal with power supplied by the source.

$$P_o = P_s \tag{3.63}$$

Equation (5.63) can be rewritten as,

$$\frac{V^2_o}{R} = V_{in} I_s \tag{3.64}$$

Average source current is related to average inductor current as,

$$I_s = I_L D \tag{3.65}$$

Equation (5.65) can be rewritten as,

$$\frac{V^2_o}{R} = V_{in} I_L D \tag{3.66}$$

Since $V_o = V_{in} D$, Equation (5.66) can be written as,

$$I_L = \frac{V_o}{R} \tag{3.67}$$

The above Equation (5.67) shows that the average inductor current is equal to the load current. The maximum and minimum inductor current is given as follows:

$$I_{L\max} = I_L + \frac{\Delta i_L}{2} \tag{3.68}$$

$$I_{L\min} = I_L - \frac{\Delta i_L}{2} \tag{3.69}$$

Substituting for I_L and ΔI_L from Equation (3.67) and (3.54) respectively into Equation (3.68) and (3.69) and simplifying gives,

$$I_{L\min} = \frac{V_o}{R} + \frac{V_o}{2L}(1-D)T \tag{3.70}$$

$$I_{L\min} = \frac{V_o}{R} - \frac{V_o}{2L}(1-D)T \tag{3.71}$$

For continuous current, the inductor current must remain positive. Therefore, to determine the boundary between continuous conduction mode and discontinuous conduction mode minimum inductor current is set to zero.

$$I_{L\min} = \frac{V_o}{R} - \frac{V_o}{2L}(1-D)T = 0 \tag{3.72}$$

Rearranging and solving for the inductor from Equation (5.72) gives,

$$L_{\min} = \frac{(1-D)}{2f_s}R \tag{3.73}$$

Where: f_s is the switching frequency ($f_s = \frac{1}{T}$). This is the value of the inductor that determines the boundary between the CCM and DCM of operation. Thus, for the buck converter to operate in continuous conduction mode, the value of inductor used is greater than the minimum value of inductor. The ripple inductor current is the difference between maximum and minimum value of the inductor current.

$$\Delta i_L = i_{L,\max} - i_{L,\min} \tag{3.74}$$

Substituting for $I_{L,max}$ and $I_{L,min}$ from Equation (3.70) and Equation (3.71) respectively into Equation (3.74) and simplifying gives,

$$\Delta i_L = \frac{V_o}{L}(1-D)T \tag{3.75}$$

The parameters of the buck converter are presented in the Table 3.9 shown below.

Table 3.9 Parameters of the buck converter

Parameters	Values
Power Rating (P_{max})	15.6kW
Input Voltage ($V_{in} = V_{pv}$)	485V
Output Voltage ($V_{dc} = V_{out}$)	200
Maximum Input Current ($I_{pv} = \frac{P_{max}}{V_{in}}$)	32.17A
Maximum Load Current ($I_L = \frac{P_{max}}{V_{out}}$)	78A
Switching Frequency	5kHz
V_{out} Ripple (ΔV_{out})	1-5%
I_{out} Ripple (ΔI_L)	20-40%
Inductance ($L = \frac{(V_{in} - V_{out})}{\Delta I_L} DT$)	≥ 1.5mH
Capacitance ($C_{min} = \frac{1-D}{8L(\frac{\Delta V_o}{V_o})f_s^2}$)	$\geq 39.3\mu$F
Duty ($D = \frac{V_o}{V_{in}}$)	0.41

To calculate the value of capacitor the following procedure is needed. The output capacitor is assumed to be so large as to yield constant output voltage. Assuming that the entire ripple component of the inductor current (Δi_L) flows through the capacitor and its average component flows through the load resistor, the maximum increase of the charge (ΔQ) which is stored in filter capacitor C is equal to shaded triangle area [42].

$$\Delta V_o = \frac{\Delta Q}{C} \tag{3.76}$$

$$\Delta Q = \frac{1}{2}\frac{T}{2}\frac{\Delta i_L}{2} \tag{3.77}$$

Substituting for ΔQ from Equation (3.77) into Equation (3.76) gives,

$$\Delta V_o = \frac{1}{C}\frac{1}{2}\frac{T}{2}\frac{\Delta i_L}{2} \tag{3.78}$$

Substituting for ΔI_L from Equation (3.76) into Equation (3.78) and rearranging and solving for capacitor,

$$C_{min} = \frac{(1-D)V_o}{8\Delta V_o L f^2} \tag{3.79}$$

This is the minimum capacitance required. To limit the peak-to-peak value of the ripple voltage below a certain value and to minimize the voltage overshoot, the filter capacitance must be greater than the minimum capacitance.

3.14. Multilevel Inverter

An inverter is a device that converts DC power into AC power at desired output voltage and frequency. There are various types of inverters which have the demerits such as less efficiency, high cost and high switching losses. To overcome the demerits of other types of inverters the multilevel inverter concept was introduced in the year 1975. The term multilevel begins with the three levels. The main features of multilevel inverter are to desire the AC voltage waveform from the several of DC voltage [43].

The main merits of the multilevel inverter are high efficiency, low cost, low switching losses and good power quality. The output of multilevel inverter looks like a staircase and sinusoidal waveform [43]. As comparing with conventional two-level inverter, multilevel inverters has several advantages that use high switching frequency pulse width modulation. The most attractive characteristics of multilevel inverters are as follows:

- They generate smaller common-mode voltage.
- They are operated through multiple switches instead of one switch.
- Multilevel inverters give higher power.

- They can operate with lower switching frequency.
- They can generate output voltages with low distortion and lower dv/dt and draw input current with very low distortion.
- It can be use as environmentally friendly energies like wind and solar energy and convert them to AC.

One particular disadvantage of multilevel inverter is the greater number of power semiconductor switches is used. Multilevel inverter is a source of high power generally used in industrial purpose [43]. It can be use either sine waves or modified sine waves. Rather than by using one converter to convert an AC current into a DC current, a multilevel inverter uses a series of semiconductor power converters for generating higher voltage. While by using conventional inverter, you would transfer energy with the flip of one switch but by using multilevel inverter you would have to flip several switches, each and every switch requiring a circuit. Because of these multiple switches and circuits, multilevel inverters are generally more expensive than conventional inverters. The multilevel inverter can be divided into three remarkable methods [44]. These are Diode clamped, Flying capacitor and Cascaded H-bridge. Due to its several advantage cascaded H-bridge multilevel inverters is used in this thesis.

3.14.1. Diode Clamped Multilevel Inverter

In Figure 3.17 the structure of diode clamped multilevel inverter is shown.

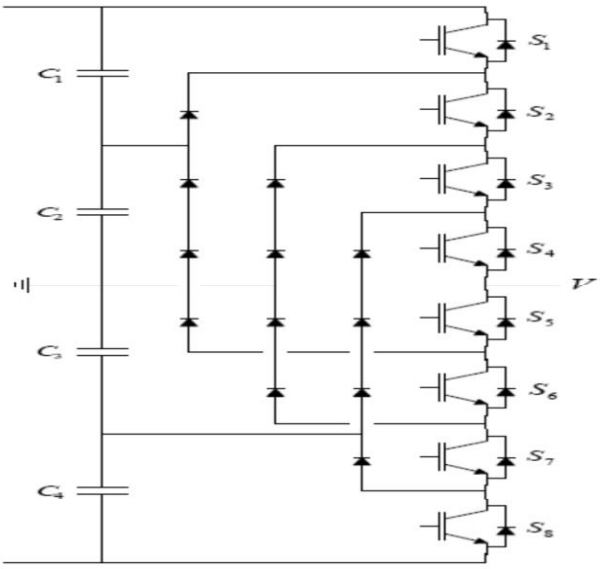

Figure 3.17 Structure of diode clamped multilevel inverter [45]

Where, N is the neutral point, Vdc is the input and C1 and C2 are the two-capacitor voltage connected to this input [46]. For three level the output voltage Van has three states: Vdc/2, 0, and –Vdc/2. For voltage level Vdc/2, switches S1 and S2 need to be turned on; for –Vdc/2, switches S1' and S need to be turned on; and for the 0 level, S2 and S1' need to be turned on.

Diode-clamped inverter have some advantage over other type of multilevel inverter such as when number of levels are high enough harmonic content are low enough. Inverter efficiency are high and control method are low. It has some major drawback also like excessive clamping diode is required when the number of levels are high also it's difficult to control real power flow of the individual converter in multi converter system.

3.14.2. Capacitor Clamped Multilevel Inverter

Figure 3.18 shows the structure of capacitor clamped multilevel inverter [47]. It is also called flywheel capacitor inverter. The basic difference between capacitor clamped multilevel inverter and diode clamped multilevel inverter is that in capacitor clamped multilevel inverter diode is replaced by capacitor. In capacitor clamped MLI also Van has three output voltage level that is Vdc/2, 0, and – Vdc/2. For voltage level Vdc/2, switches S1 and S2 need to be turned on; for – Vdc/2, switches S1' and S2' need to be turned on; and for the 0 level, either pair (S1, S1') or (S2, S2') needs to be turned on.

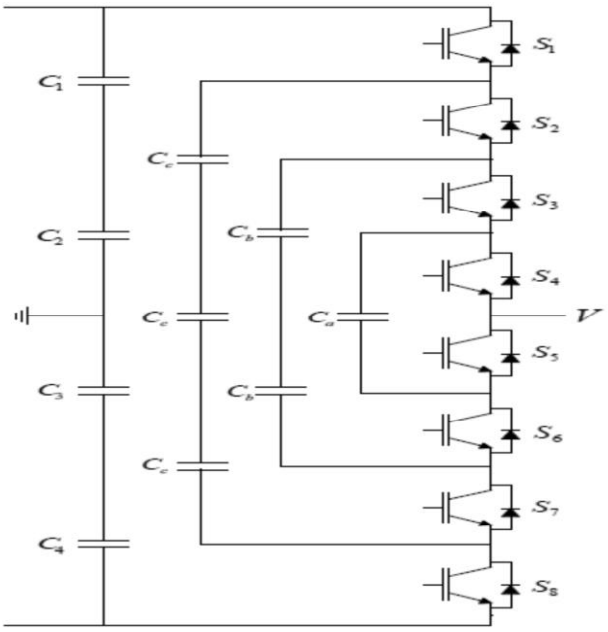

Figure 3.18 Structure of flying capacitor multilevel inverter [46]

Clamping capacitor C1 is charged when S1 and S1' are turned on, and is discharged when S2 and S2' are turned on. Its advantage is the large capacitance of capacitor can provide capability during power outage and it provide switch combination redundancy for balancing different voltage level. The major disadvantage is large number of capacitors is required when level is high also inverter control is very complicated.

3.14.3. Cascade Multilevel Inverter

Cascade H-Bridge multilevel inverters are formed by series connection of two or more single-phase H-Bridge inverter. Figure 3.19 shows the basic diagram of cascade multilevel inverter. Each single-phase full bridge inverter generates three voltage at the output +Vdc, 0, and – Vdc. The block diagram representation of the system is shown in Appendix B.

The H-Bridge inverter that are connected in series do not necessarily need to have the same dc input voltage in such manner we can generate different combination of voltage levels and eliminate redundancies. The drawback of cascaded multilevel inverter is that it needs separate DC sources for real power conversion [48].

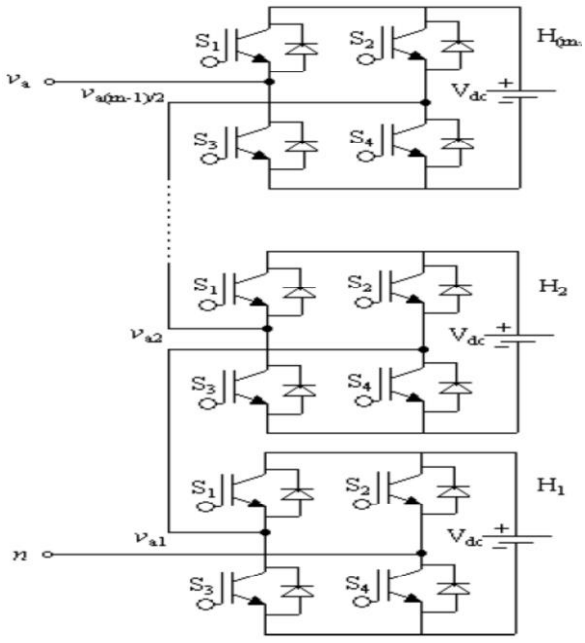

Figure 3.19 Structure of cascaded multilevel inverter [46]

Some advantages of cascade multilevel inverters are that compared to other it requires least number of components to achieve same number of voltage level also no extra clamping diode and voltage balancing capacitor is required and it has less switching loss, device stress. Table 3.10 shows the comparison between different topologies of multilevel inverter.

Table 3.10 Comparison between different topologies of multilevel inverter

Configuration of the Inverter	Diode Clamp	Flying Capacitor	Cascaded H-Bridge
Main Switching Devices	$2(n-1)$	$2(n-1)$	$2(n-1)$
Main Diodes	$2(n-1)$	$2(n-1)$	$2(n-1)$
Clamping Diodes	$(n-1)(n-2)$	0	0
Direct-Current Bus Capacitors	$(n-1)$	$(n-1)$	$\frac{(n-1)}{2}$
Balancing Capacitors	0	$\frac{(n-1)(n-2)}{2}$	0
Control Scheme	SHE-PWM, SPWM, SVM	SHE-PWM, SPWM	SPWM, SVM
Applications	Motor drive, STATCOM	Motor drive, STATCOM	PV, Motor drive, STATCOM, Batteries

3.15. PWM for Multilevel Inverter

There are two types of PWM techniques for multilevel inverter.

- Phase shifted Carrier PWM
- Level Shifted Carrier PWM

3.15.1. Phase shifted Carrier PWM

A multilevel inverter with *m* voltage levels requires (m-1) triangular carriers. In phase shifted multicarrier modulation, all the triangular carriers have the same frequency and the same peak-to-peak amplitude, but there is phase shift between any two adjacent carrier waves.

3.15.2. Level Shifted Carrier PWM

Similar to the phase shifted modulation, an *m*-level cascaded multilevel inverter level shifted multicarrier modulation schemes requires (m-1) triangular carriers, all having the same frequency and amplitude. The (m-1) triangular carrier is vertically disposed such that the bands they occupy are contiguous. In case of THD, of level shifted modulation is much lower than phase shifted modulation. Therefore, the modulation scheme of this research thesis is level shifted modulation. An m cascaded multilevel inverter using level shifted multicarrier modulation scheme requires (m-1) triangular carriers, all having the same

frequency and amplitude. The (m-1) triangular carriers are vertically disposed such that the bands they occupy are contiguous.

There are three alternative PWM strategies with different phase relationships for the level shifted multicarrier modulation: The MATLAB implementation of in phase disposition (IPD) is shown in Figure 3.20.

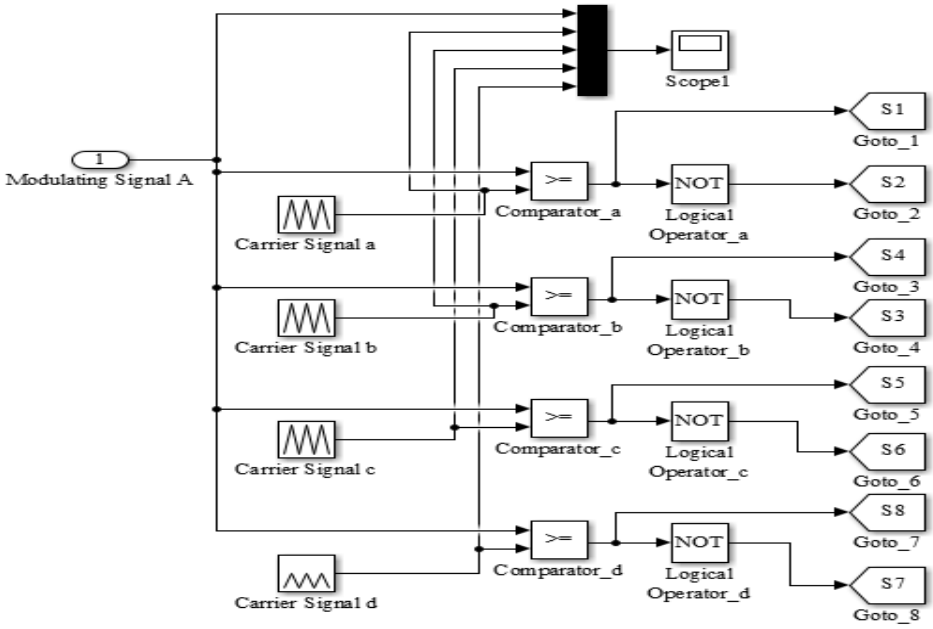

Figure 3.20 MATLAB implementation of IPD

- In phase disposition (IPD), where all carrier waveforms are in phase [49].
- Phase opposition disposition (POD), where all carrier waveforms above zero reference are in phase and are 180° out of phase with those below zero [49].
- Alternative phase opposition disposition (APOD), where every carrier waveform is in out of phase with its neighbor carrier by 180° [49].

When compared to the rest two level shifted multicarrier modulation, in phase disposition technique is used in this research work due to the lowest THD values.

3.15.3. DC Link Design

This method of calculating a minimal capacity of the DC link capacitor depends on the expected maximum input power step and the definition of a limit of allowed voltage deviation. A widely-used limit is a deviation of ten percent of the DC link voltage at any step-on and step-off load response. The expected maximum input power step is equal to the solar panel power at the maximum power point (MPP). The time constant T_r stands for the

control delay of the DC/DC converter and for instance a value of about five to ten modulation periods are a good choice [50]. This method starts with the energy ΔW which is estimated as:

$$\Delta W = \int_0^{T_r} \Delta P_{max}.dt = \Delta P_{max}.T_r \tag{3.80}$$

The stored energy of the capacitor can be written as follows:

$$W = \frac{1}{2} C_d V_d^2 \tag{3.81}$$

The variation of the stored energy in the capacitor also depends on the DC link voltage V_d, the DC link voltage deviation ΔV_d and the capacity C_d and can estimated:

$$\Delta W = \frac{1}{2} C_d (V_d + \Delta V_d)^2 - \frac{1}{2} C_d V_d^2 \tag{3.82}$$

The combination of the Equations (3.80) and (3.82) leads to the expression of the minimal capacity $C_{d,min}$:

$$C_{d,min} \geq \frac{T_r.\Delta P_{max}}{(V_d \Delta V_d + \frac{1}{2} \Delta V_d^2)} \tag{3.83}$$

Another method to appreciate the minimal DC link capacity is given in [50], where the exchanged energy ΔW by the capacitor bank is estimated as follows:

$$\Delta W = \frac{T_r.\Delta P_{max}}{2} \tag{3.84}$$

The voltage deviation is given by:

$$\Delta V_d = \frac{\Delta W}{C_d V_d} \tag{3.85}$$

Finally this leads to another equation of the minimal capacity $C_{d,min}$:

$$C_{d,min} \geq \frac{T_r.\Delta P_{max}}{2.V_d \Delta V_d} \tag{3.86}$$

Comparing the Equations (3.83) and (3.86) and assuming a DC link voltage deviation ΔV_d of commonly used ten percent, it can be seen, that the appreciation of delivers nearly twice the values of the minimum capacity than the appreciation of [50].

3.16. Sizing of the Inverter

An inverter is used in the system where AC power output is needed. For stand-alone systems, the inverter must be large enough to handle the total amount of power that will be used at one time. The inverter size should be 20–25% bigger than total power of appliances [51]. Again, the selected inverter should be capable of supplying continuous power to all AC loads and providing sufficient surge capability to start any loads that may surge when turned on and particularly if they turn on at the same time. The following steps are important for determining inverter rating**.**

- Obtain “Total power of AC appliances”, “Maximum demand “and “Surge demand”.
- Capacity or rating of the inverter should be 20–25% bigger than “Total power of AC appliances”. Capacity or rating of inverter ≥ 1. 2 X Total power of AC appliances.

So, the size of inverter suitable for the system is 25% more than AC appliances. Therefore, the size of the selected inverter is 17.625kW.

3.17. PID Controller

A proportional-integral-derivative controller (PID controller) is a generic control loop feedback mechanism widely used in industrial control systems. A PID controller attempts to correct the error between a measured process variable and a desired set point. The PID controller calculation (algorithm) involves three separate parameters; the Proportional, the Integral and Derivative values. The Proportional value determines the reaction to the current error, the Integral determines the reaction based on the sum of recent errors and the Derivative determines the reaction to the rate at which the error has been changing.

By "tuning" the three constants in the PID controller algorithm the PID can provide control action designed for specific process requirements. The response of the controller can be described in terms of the responsiveness of the controller to an error, the degree to which the controller overshoots the setpoint and the degree of system oscillation [52]. The output of PID controller u(t), is equal to the sum of three signals. The signal obtained by multiplying the error signal by a constant proportional gain Kp, plus the signal obtained by differentiating and multiplying the error signal by constant derivative gain Kd and the signal obtained by integrating and multiplying the error signal by constant internal gain Ki. The

output of PID controller is given by u(t), taking Laplace transform, and solving for transfer function, gives ideal PID transfer function given by U(s). It is given as,

$$u(t) = Kpe(t) + Kd\frac{de(t)}{dt} + Ki\int e(t)dt \tag{3.87}$$

By taking the Laplace transform of Equation (3.87):

$$G_c(s) = \left[Kp + \frac{Ki}{s} + Kds \right] \tag{3.88}$$

This is the transfer function of PID controller. Conventional PID controllers have been extensively used in industry, due to their effectiveness for linear systems, ease to understand and simple to implement. Despite their effectiveness for linear systems, conventional PID controllers are not suitable for nonlinear systems. It does not reliable and satisfactorily in case of non-linear systems. After deriving the transfer function of PID controller, the next step is finding the transfer function of the buck converter. When switch is on condition, the equation for inductor current and capacitor voltage will be:

$$\frac{diL}{dt} = \frac{-Vc}{L} + \frac{V_i d}{L} \tag{3.89}$$

$$\frac{dVc}{dt} = \frac{iL}{C} - \frac{Vc}{RC} \tag{3.90}$$

Now Equation (3.89) and Equation (3.90) can be written in state space representation as: The new variables will be introduced here. Let iL is replaced with x1, Vc is replaced with x2, d is replaced with u and y is replaced with Vc. Therefore, the state equation with the new variable can be rewritten as:

$$\frac{dx1}{dt} = \frac{-1}{L}x2 + \frac{Vi}{L}u \tag{3.91}$$

$$\frac{dx2}{dt} = \frac{1}{C}x1 - \frac{1}{RC}x2 \tag{3.92}$$

Here the input is Vi and the output is y=x2. By taking the Laplace transform of the Equation (3.89) and Equation (3.90):

$$sX1 = \frac{-1}{L}x2 + \frac{Vi}{L}u \tag{3.93}$$

$$sY = \frac{1}{C} x1 - \frac{1}{RC} y \tag{3.94}$$

By rearranging Equation (3.93) and Equation (3.94), the transfer function of the buck converter is:

$$\frac{Y(s)}{Vi(s)} = D\left[\frac{\frac{1}{LC}}{S^2 + \frac{1}{RC}S + \frac{1}{LC}}\right] \tag{3.95}$$

3.18. Mathematical Modelling of the Induction Motor

The dynamic modelling is one of the major steps in the acceptance of the design process of any drive system due to this there is elimination of mistakes during design process. From the fundamental equations of transformation, the dynamic model can be developed in dq0 (direct, quadrature and zero-sequence) axis. For the analysis of induction machines arbitrary reference frame theory is extensively used, making its use other reference frames can be developed. The modelling sets all equations for inertia, torque, and speed vs time. Differential voltages, current and also flux linkages between the moving rotor and stationary stator can be modelled.

Before deriving the mathematical model for a three-phase induction machine, few assumptions are made and they are as follows:

- Air gap is uniform;
- Squirrel cage rotor construction;
- Stator and rotor windings are balanced, and have sinusoidal winding distribution;
- Parameter change and saturation are neglected.

3.18.1. Concept of the Reference Frame

The reference frames are similar to observer platforms, wherein each platform gives a unique and distinct view of the system being studied, and simplifies it in terms of analysis. Generally, for controlling purpose, although the actual variables are sinusoidal in nature it is desirable to have them as DC quantities. This can be achieved by having a revolving reference frame whose speed is same as that of the sinusoidal quantity. Since both, the quantity as well as the reference frame is revolving at the same speed their differential speed is zero which means that they are stationary with respect to each other. Once the general

transformation is derived for an arbitrary reference frame, then any required particular frame can then be obtained by substituting the appropriate frame speed.

3.18.2. Conversion from Three-Phase to Two-Phase

For deriving the dynamic model for an induction motor, first equivalence has to be established between three-phase and two-phase. The mmf produced in the two-phase and the three-phase must be equivalent. If a three-phase winding has number of turns as Ns per phase and with equal current magnitudes, then for two-phase winding the number of turns should be 3Ns/2 for mmf equivalence. The d and q axis mmf are found by resolving the three-phase mmf's. The number of turns being common in both sides of equation gets cancelled leaving current equalities.

Under balanced conditions the three-phase stator voltages of an induction machine is given as follows,

$$V_a = \sqrt{2}Vrms\sin(\omega t) \tag{3.96}$$

$$V_b = \sqrt{2}Vrms\sin(\omega t - \frac{2\pi}{3}) \tag{3.97}$$

$$Vc = \sqrt{2}Vrms\sin(\omega t - \frac{4\pi}{3}) \tag{3.98}$$

Where V_a, V_b and V_c are the line voltages. The relation between $\alpha\beta$ and abc is as follows:

$$\begin{bmatrix} V\alpha \\ V\beta \end{bmatrix} = \frac{2}{3}\begin{bmatrix} 1 & \frac{1}{2} & -\frac{1}{2} \\ 0 & \frac{\sqrt{3}}{2} & -\frac{\sqrt{3}}{2} \end{bmatrix}\begin{bmatrix} V_a \\ V_b \\ V_c \end{bmatrix} \tag{3.99}$$

The direct axis and the quadrature axis voltages are given as,

$$\begin{bmatrix} V_d \\ V_q \end{bmatrix} = \begin{bmatrix} \cos\theta & \sin\theta \\ -\sin\theta & \cos\theta \end{bmatrix}\begin{bmatrix} V_\alpha \\ V_\beta \end{bmatrix} \tag{3.100}$$

The instantaneous values of the stator and rotor currents in a three-phase system are calculated using the transformation,

$$\begin{bmatrix} i\alpha \\ i\beta \end{bmatrix} = \begin{bmatrix} \cos\theta & -\sin\theta \\ \sin\theta & \cos\theta \end{bmatrix}\begin{bmatrix} id \\ iq \end{bmatrix} \tag{3.101}$$

Transformation to abc axis is given as,

$$\begin{bmatrix} ia \\ ib \\ ic \end{bmatrix} = \begin{bmatrix} 1 & 0 \\ -\frac{1}{2} & \frac{\sqrt{3}}{2} \\ -\frac{1}{2} & -\frac{\sqrt{3}}{2} \end{bmatrix} \begin{bmatrix} i\alpha \\ i\beta \end{bmatrix} \tag{3.102}$$

Equations of flux linkages can be given as,

$$\frac{d\varphi qs}{dt} = \omega b\left[Vqs - \left(\frac{\omega e}{\omega b}\right)\varphi ds - \left(\frac{Rs}{Xls}\right)\left(\varphi mq - \varphi qs\right)\right] \tag{3.103}$$

$$\frac{d\varphi ds}{dt} = \omega b\left[Vds - \left(\frac{\omega e}{\omega b}\right)\varphi qs - \left(\frac{Rs}{Xls}\right)\left(\varphi md - \varphi ds\right)\right] \tag{3.104}$$

$$\frac{d\varphi qr}{dt} = \omega b\left[Vqr - \left(\frac{\omega e - \omega r}{\omega b}\right)\varphi dr - \left(\frac{Rr}{Xlr}\right)\left(\varphi mq - \varphi qr\right)\right] \tag{3.105}$$

$$\frac{d\varphi dr}{dt} = \omega b\left[Vdr - \left(\frac{\omega e - \omega r}{\omega b}\right)\varphi qr - \left(\frac{Rr}{Xlr}\right)\left(\varphi md - \varphi dr\right)\right] \tag{3.106}$$

Where,

φds: q axis component of stator flux in weber, φqs: q axis component of stator flux in weber

Vqs: q axis component of stator voltage in volts, Vds: d axis component of stator voltage in volts

ωb: speed of stator supply frequency in rad/s, ωe: speed of stator reference frame in rad/s

ωr: speed of rotor in rad/s, φmd: d axis component of mutual flux in weber

φmq: q axis component of mutual flux in weber, Rs, Rr- stator and rotor resistance in **Ω**

Xls, Xlr: stator and rotor reactance respectively in **Ω**, Xml: mutual leakage reactance in **Ω**

$$Xml = 1\Big/\left[\frac{1}{Xm} + \frac{1}{Xls} + \frac{1}{Xlr}\right] \tag{3.107}$$

$$\varphi mq = Xml\left[\frac{\varphi qs}{Xls} + \frac{\varphi qr}{Xlr}\right] \tag{3.108}$$

$$\varphi md = Xml\left[\frac{\varphi ds}{Xls} + \frac{\varphi dr}{Xlr}\right] \tag{3.109}$$

Then, substituting the flux linkage equations to find the qd stator and rotor currents,

$$iqs = \frac{1}{Xls}\left(\varphi qqs - \varphi mq\right) \tag{3.110}$$

$$iqr = \frac{1}{Xlr}\left(\varphi qr - \varphi mq\right) \tag{3.111}$$

$$ids = \frac{1}{Xls}\left(\varphi ds - \varphi md\right) \tag{3.112}$$

$$idr = \frac{1}{Xlr}\left(\varphi dr - \varphi md\right) \tag{3.113}$$

The electromagnetic torque developed is given as,

$$Te = \left(\frac{3}{2}\right)\left(\frac{P}{2}\right)\left(\frac{1}{\omega b}\right)\left(\varphi ds\, iqs - \varphi qs\, ids\right) \tag{3.114}$$

$$\omega r = \int \frac{P}{2J}\left(Te - Tl\right) \tag{3.112}$$

Where: P is number of poles, J is inertia in Kg m^2, Tl is load torque in Nm.

3.19. Selection of Protective Devices

Besides the major component selection, safety measures are equally important for the solar PV system for which the protective devices to be used need to be selected properly. Failure to do so may not only lead to system efficiency but also may pose severe safety hazards. Typical protection devices which are to be selected carefully are as follows:

3.19.1. PV Source Circuit Combine Box and PV Fuse Disconnect

These fuses or circuit breakers [both known as over current protective devices (OCPD)] are installed to protect the PV modules and wiring from excessive reverse current flow that can damage PV cell interconnects and the wiring between the individual PV modules. The rating of the fuse is specified by the PV module manufacturer. As per the NEC requirement for over current protection, the fuse rating marked on the back of the PV module must be at least 156 % of short-circuit current (I_{sc}) of the PV module at STC. The fuse will generally be a dc-rated cartridge-type fuse that is installed in a finger-safe pull out-type fuse holder.

3.19.2. Grounding

Grounding is one of the most critical tasks in the entire installation of a solar PV system. It means connecting a part of the system's structure and/or wiring electrically to the earth. Grounding of a system does four things:

- It discharges accumulated charges so that lightning is not highly accumulated in the system.
- If lightning does strike, or if a high charge does build up, the ground connection provides a safe path for discharge directly to the earth rather than through the wiring.
- It reduces shock hazard from the higher voltage (AC) parts of the system and
- It reduces electrical hum and radio caused by inverters, motors, fluorescent lights and other devices.

3.19.3. Lighting Arrestor

In locations susceptible to lightning strikes, a lightning protection system must be provided, and all the exposed metallic structures of the solar PV system must be bound to the earthing system, and structures and PV module frames must be properly grounded. In certain geographical locations, solar PV systems might be exposed to the threat of lightning strikes. As lightning can cause damage to the PV modules and inverters, extra care must be required to ensure that proper lightning protection is provided for the solar PV system and the entire structure. The inverters should be protected by appropriately rated surge arrestors on the DC as well as AC side.

3.19.4. Surge Protector

Surge protection devices bypass the high voltages induced by lightning. They are recommended for additional protection in lightning-prone areas or where good grounding is not feasible (such as on a dry rocky mountain top), especially if long lines are being run to an array, pump, antenna, or between buildings. To reduce the possibility of a fire and to protect the system from a damage caused by lightings, it is recommended to have a voltage-clamping device across the DC bus bar. A metal oxide varistor (MOV) is commonly used in such applications.

3.19.5. Cables and Wires

PV array wiring should be done with minimum lengths of wire, tied into the metal framework, and then run through a metal conduit. A rule of thumb is to limit the voltage drop from the array to power inverter to 2.5 percent or less. Positive and negative wires should be run together wherever possible, rather than being kept some distance apart. This will minimize induction of lightning surges.

CHAPTER 4

RESULTS AND DISCUSSIONS

4.1. Chapter Overview

In this section, the results obtained from MATLAB/Simulink 2016a are discussed briefly. In the MATLAB Simulink model, the selected PV module is SCHOTT PERFORM poly240W. Each module has a capacity of 240Wp. The total number of modules required is 65 modules and from which 13 are conned in series and 5 are connected in parallel. The PV array used in this research work is a 15.6kW power that 13 are connected in series and 5 are connected in parallel.

4.2. Simulation Results of the PV Module

At the standard condition, irradiation and temperature 13*5 modules are connected to generate the required power of the system. For the solar PV of 15.6kW is the combination of the Poly 240W with 13 modules in series and 5 modules in parallels. The output curve of current versus voltage of the system module of SCHOTT PERFORM 240W at standard condition is shown in Figure 4.1.

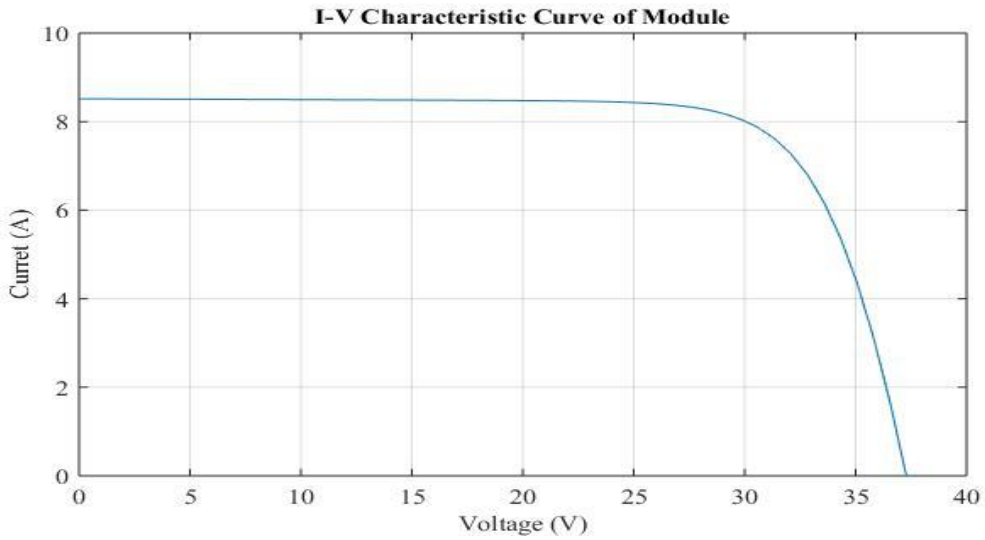

Figure 4.1 I-V characteristic curve of the module

Also, power versus voltage characteristic curve of the system module at standard condition is shown in Figure 4.2.

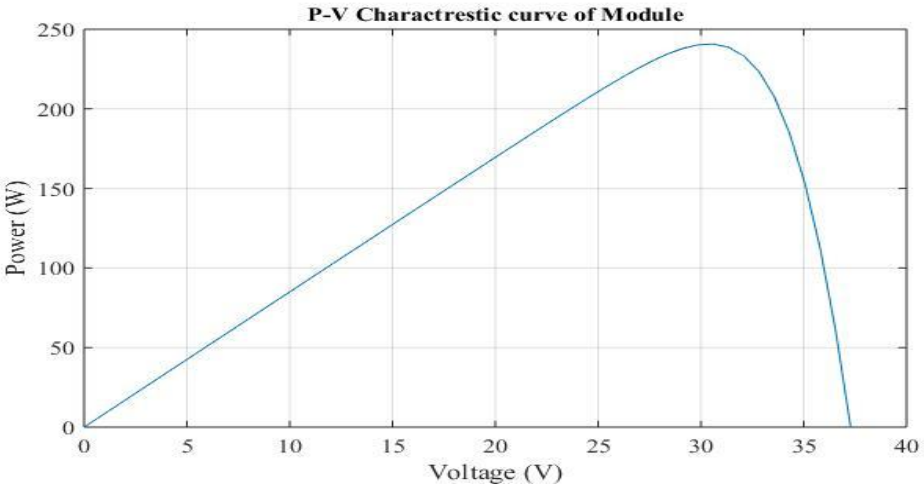

Figure 4.2 P-V characteristic curve of the module

The value of series resistance connected in series with the solar cell as 0.18Ω and the value of the shunt resistance connected in parallel to the cells selected as 520Ω. The constant 1,000 W/m^2 and 25^{0}C given as input is the irradiation and temperature respectively. The system is simulated with various range of resistors connected to it, in this condition.

The operating temperature affects the performance of the PV module. By varying the operating temperature and making irradiation constant the effect of temperature can be observed. The MATLAB implantation of the multiplot PV system is shown in Appendix C. The values of operating temperature are set at 25^{0}C, 50^{0}C, 75^{0}C, and 100^{0}C at constant irradiation of 1000W/m^2. The I-V and P-V characteristics of PV array at different temperature and constant irradiation is shown in Figure 4.3 and Figure 4.4 respectively.

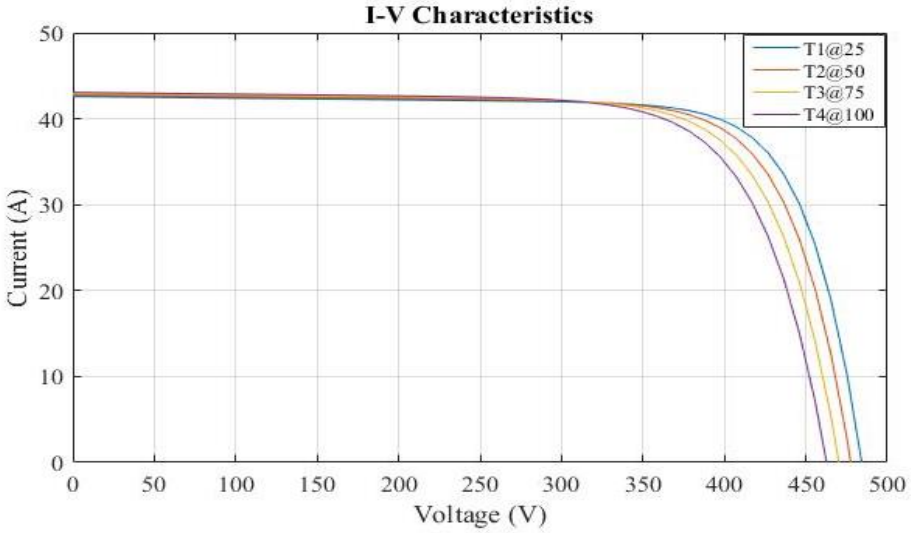

Figure 4.3 I-V characteristic of PV array at different temperature

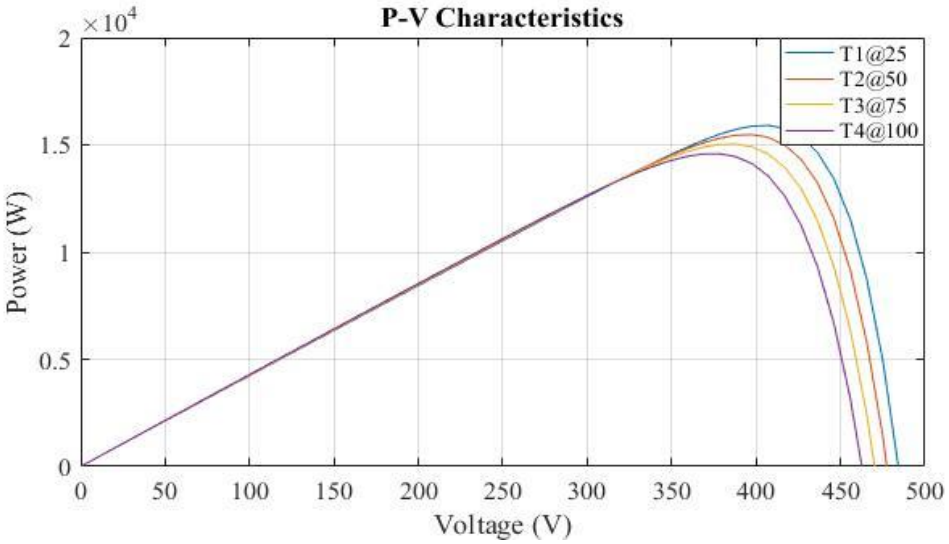

Figure 4.4 P-V characteristic of PV array at different temperature

The influences of temperature on the PV characteristics are observed in Figure 4.3 and Figure 4.4 above. As seen from the influence of the operating temperature on the open circuit voltage, there is the main effect of increase in cell temperature which decreases linearly with the cell temperature. Thus, the cell efficiency drops. As can be seen, with the increase of the cell temperature, the short circuit current increases slightly.

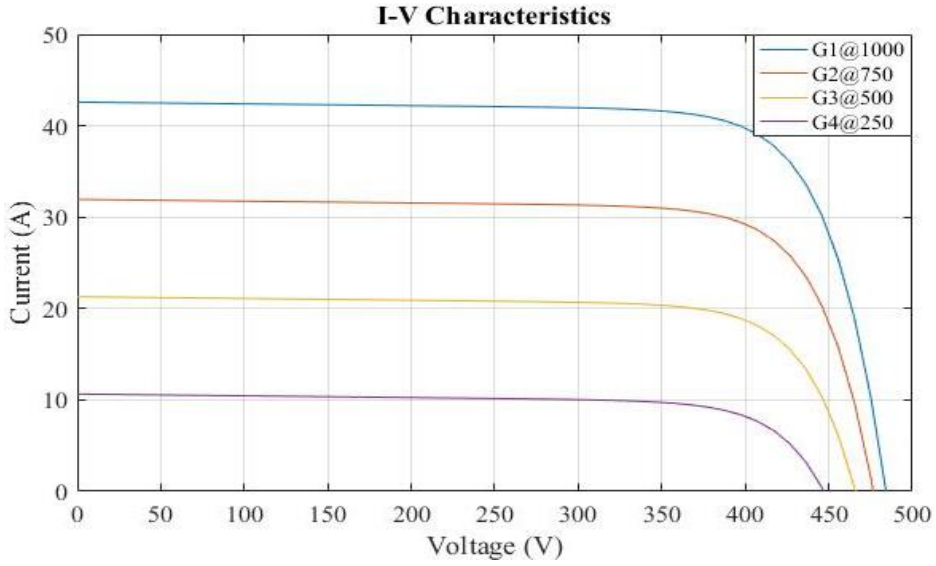

Figure 4.5 I-V characteristic of PV array at different irradiance

The solar irradiation also affects the performance of the PV module. By varying the solar irradiation and making temperature constant the effect of solar irradiation can be observed. The values of operating temperature are set at 250W/m^2, 500W/m^2, 750W/m^2 and 1000W/m^2 at constant operating temperature of 25^{0}C. The I-V and P-V characteristics of

PV array at different solar irradiation and constant operating temperature is shown in Figure 4.5 and Figure 4.6.

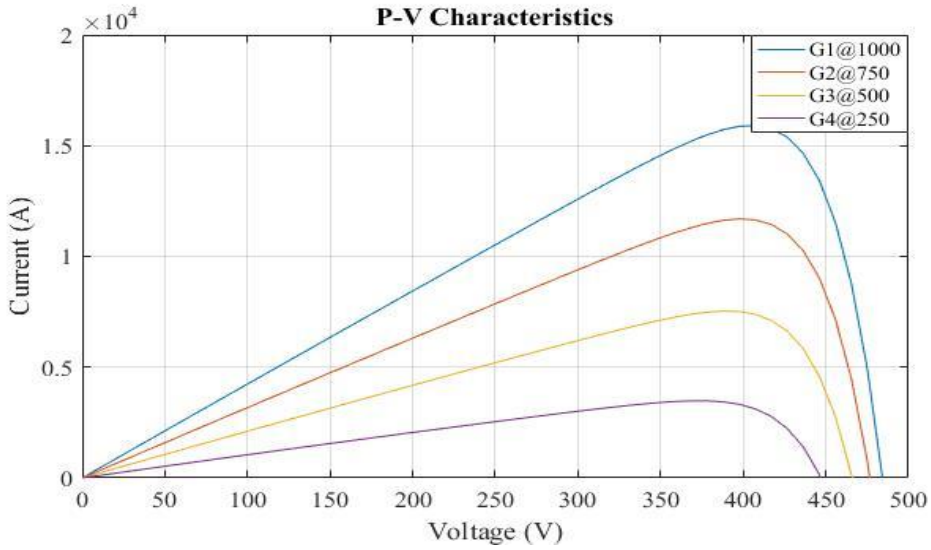

Figure 4.6 P-V characteristic of PV array at different irradiance

From the above Figure 4.5 and Figure 4.6 the influences of solar irradiation on PV module is observed. As seen from the above figure, by increasing the solar radiation, open circuit voltage increases logarithmically whereas the short circuit current increases linearly. The output current and output voltage of solar PV array at G=1000W/m^2 and T=25^{0}C are shown in the Figure 4.7.

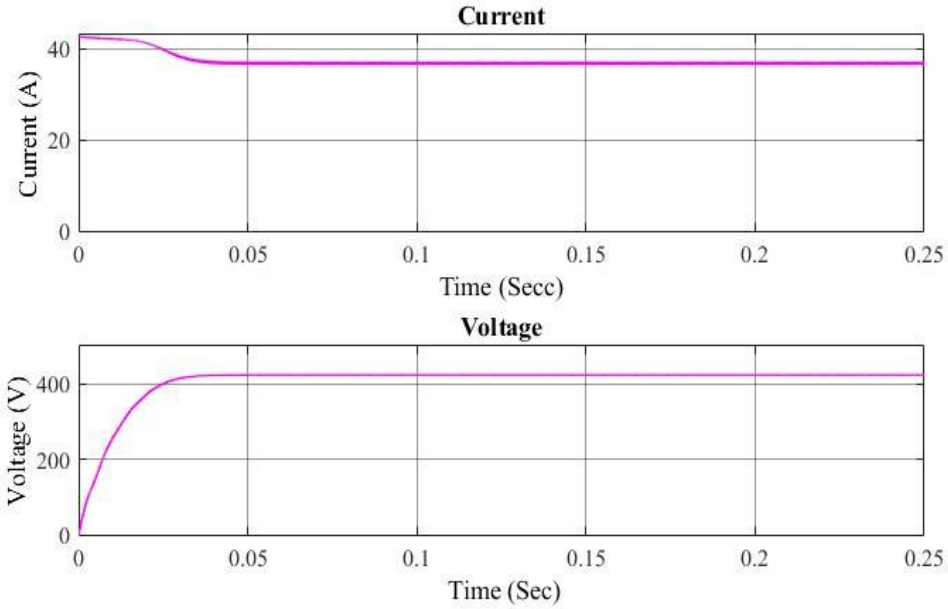

Figure 4.7 The output current and voltage of PV array

The output current and output voltage of the buck converter without the controller is shown in the Figure 4.8. As observed from Figure 4.8 the system is not stable and can not operate properly (fluctuates).

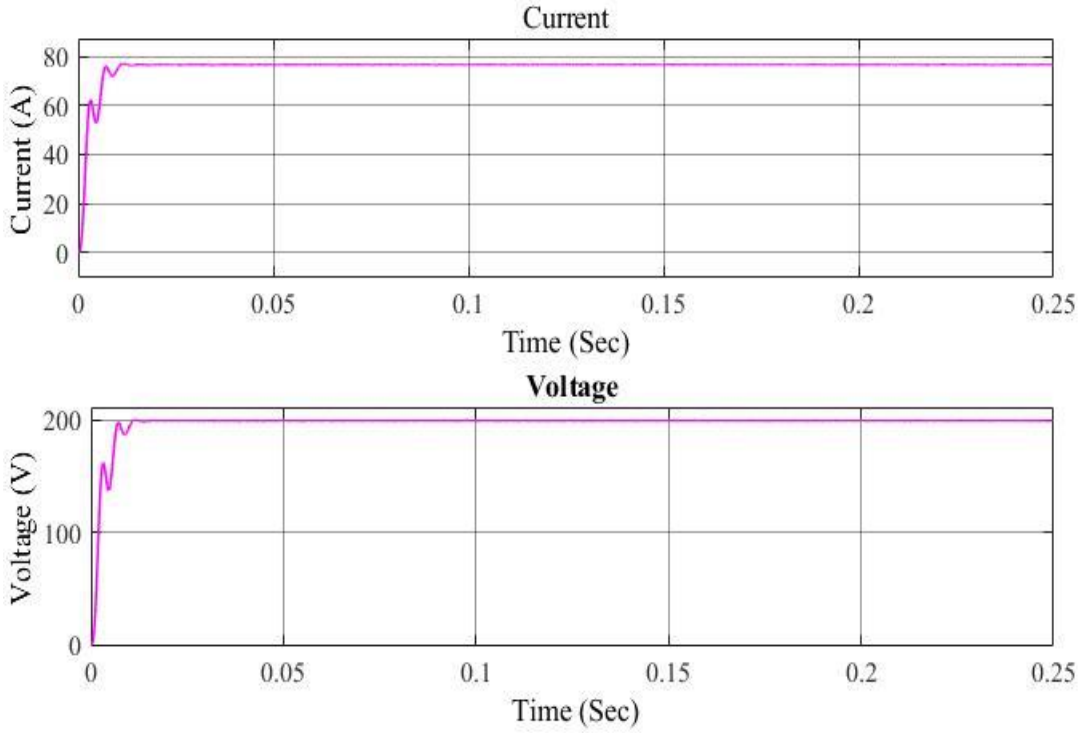

Figure 4.8 The output current and voltage of buck converter without controller

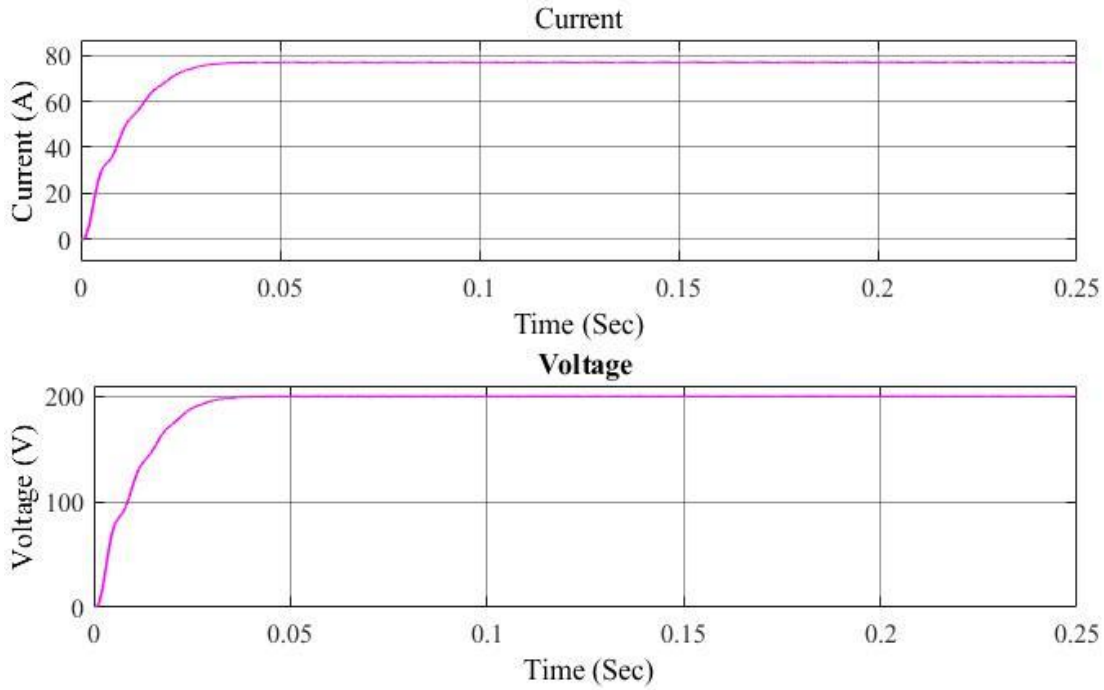

Figure 4.9 The output current and voltage of buck converter with PID controller

The output current and output voltage of buck converter with PID controller is shown in the Figure 4.9. As seen from Figure 4.9, the system is stable and the performance of the system is improved.

4.3. Simulation Results of the Multilevel Inverter

The representation of modulating signal and it's description is shown in the Figure 4.10.

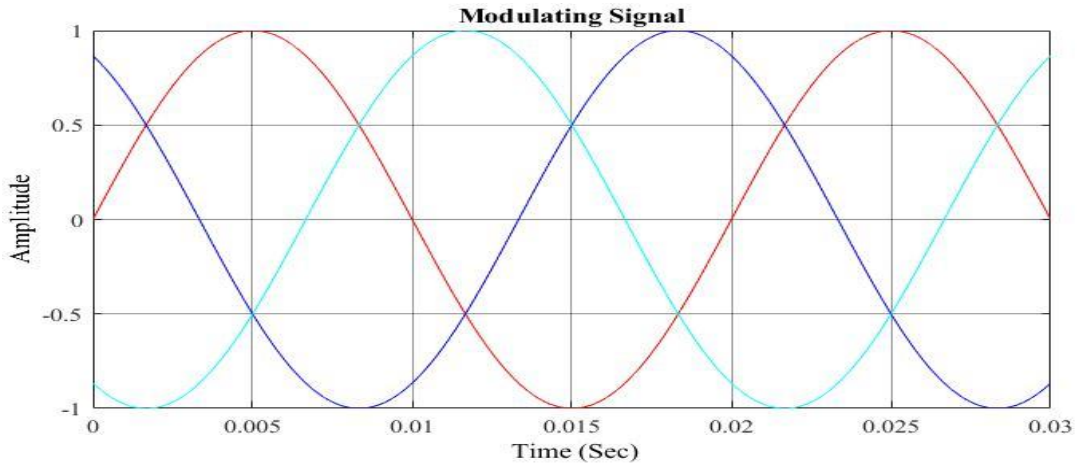

Figure 4.10 Description of modulating signal and it's output

This three phase modulating signal is compared with the carrier signal to generate the gate signal. Figure 4.11 shows the fundamental and carrier frequency wave for single phase five level cascaded multilevel inverter.

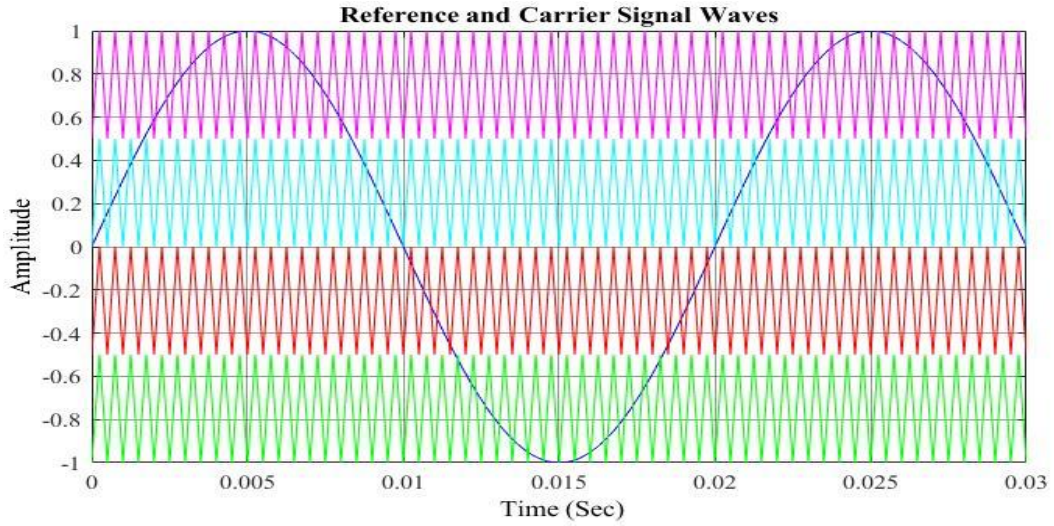

Figure 4.11 The refence and carrier signal waves

For m level inveter, m-1 triangular carriers are required. In SPWM, a referece sinusoidal voltage is compared with triangular carrier signal to genrate the PWM pulses to the IGBT

switches of the multilevel inverter. The reference signal is taken as the sinusoidal waveform whereas the carrier signal is taken as triangular waveform. In the proposed MLI the PD-PWM technique is used to generate the PWM pulses. In PD-PWM, each phase is displaced with different phases. The single phase five level cascaded multilevel inverter output voltage wave form is shown in the Figure 4.12.

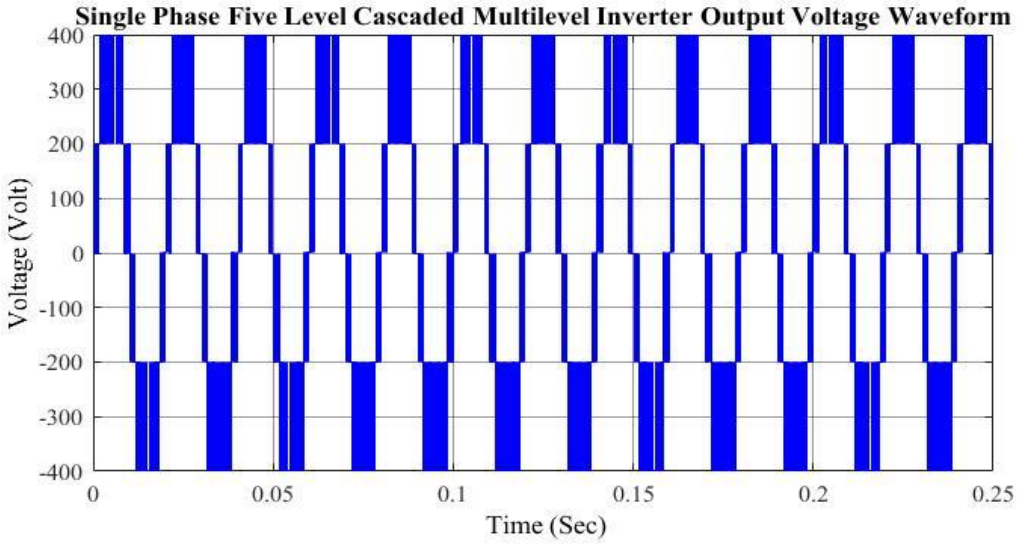

Figure 4.12 Output voltage of Single phase five level CMLI

(f_m=50Hz, f_{cr}=2000Hz, m_a=1.0)

The three phase five level cascaded multilevel inverter line voltage is shown in Figure 4.13.

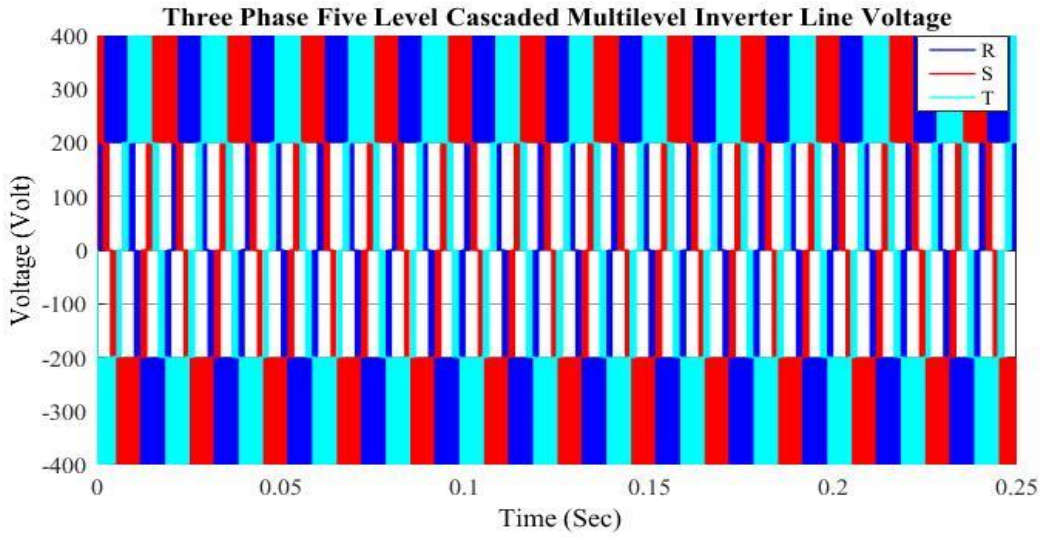

Figure 4.13 Three phase five level CMLI line voltage

The firing pulse generator for five level CMLI is shown in figure below. The generation of gating pulse is obtained by comparing modulating signal with the carrier signal. The

sinusoidal signal is generated with the amplitude of 1 volt at the frequency of 50Hz and the carrier signals are generated at the frequency of 2kHz. The pulses for positive output voltage and negative output voltage are shown in Figure 4.4 and Figure 4.5 respectively.

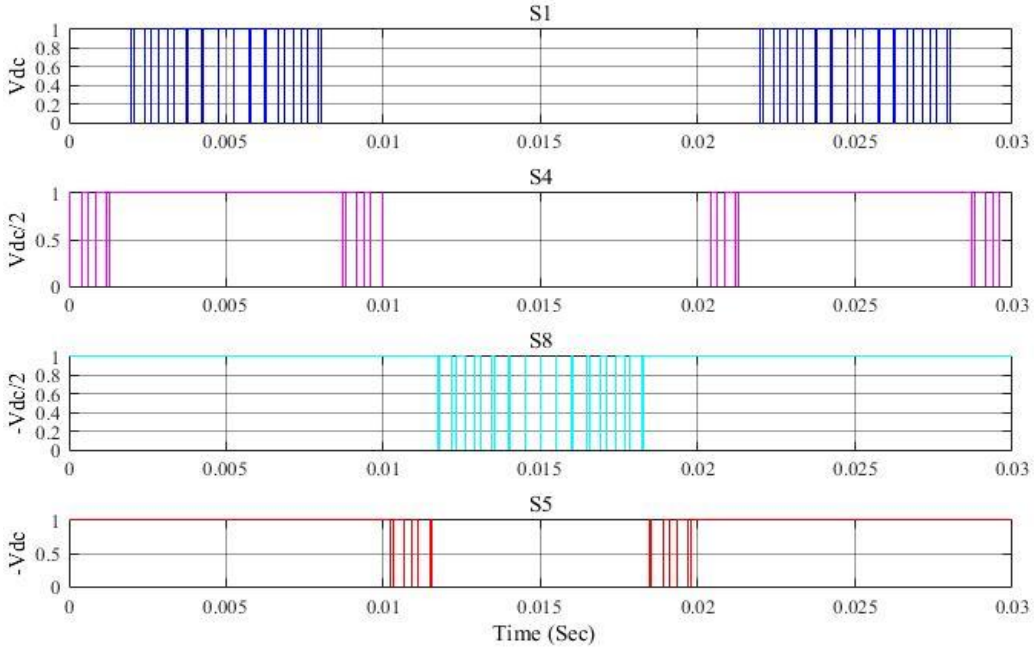

Figure 4.14 Pulses for positive output voltage

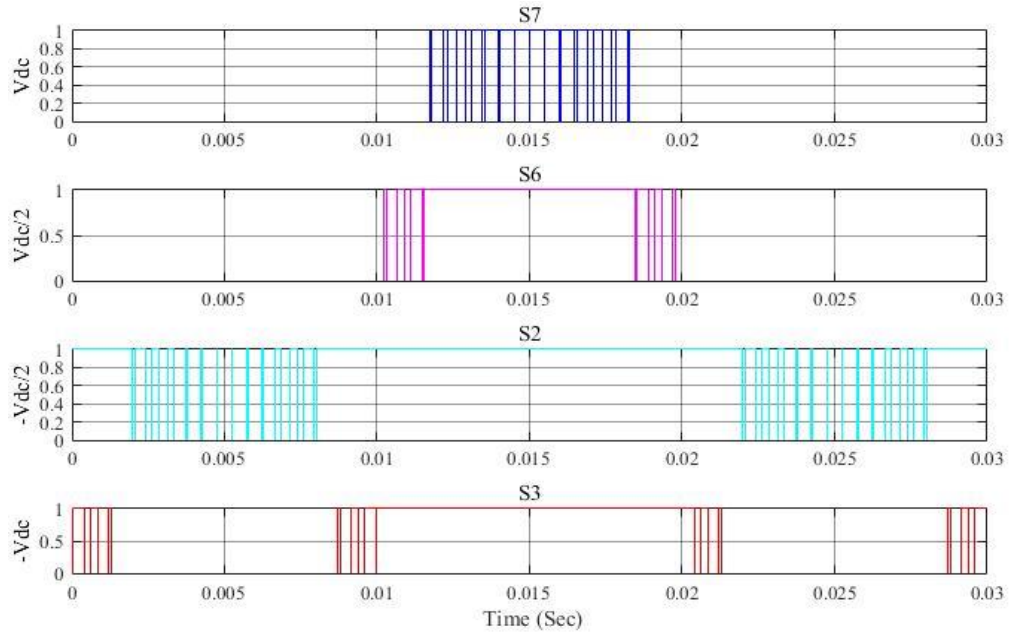

Figure 4.15 Pulses for negative output voltage

The output phase voltage waveform five level cascaded multilevel inverter and its FFT analysis is shown in Figure 4.16.

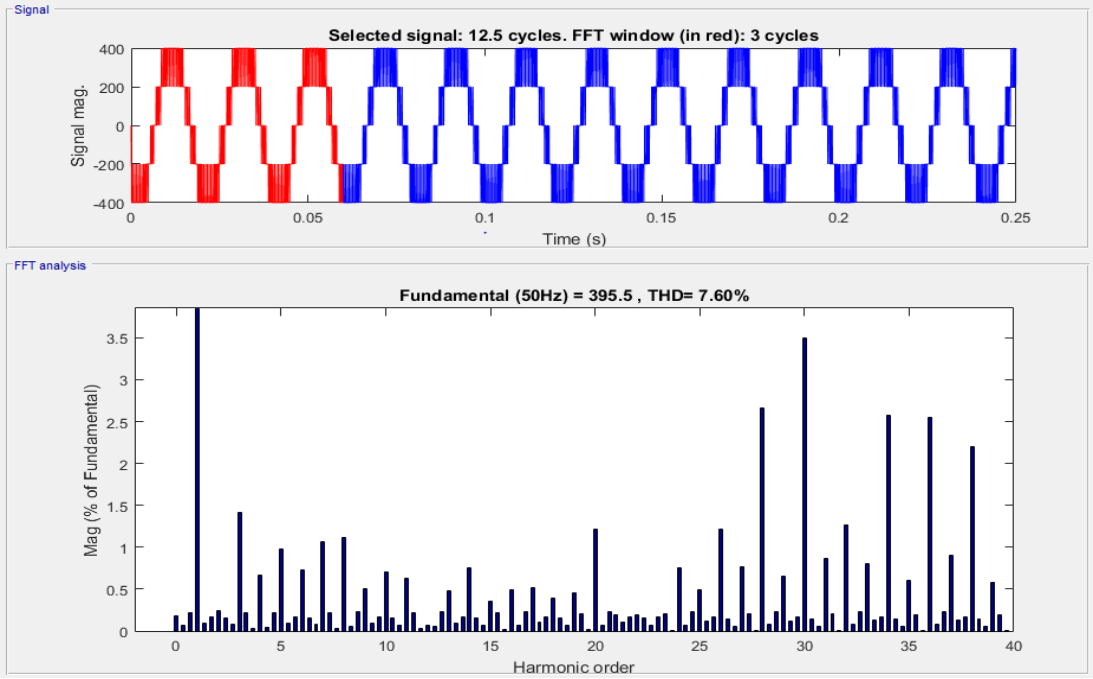

Figure 4.16 Output phase voltage and FFT analysis

(f_m=50Hz, f_{cr}=2000Hz, m_a=1.0)

The output phase voltage waveform five level cascaded multilevel inverter and its FFT analysis is shown in Figure 4.17.

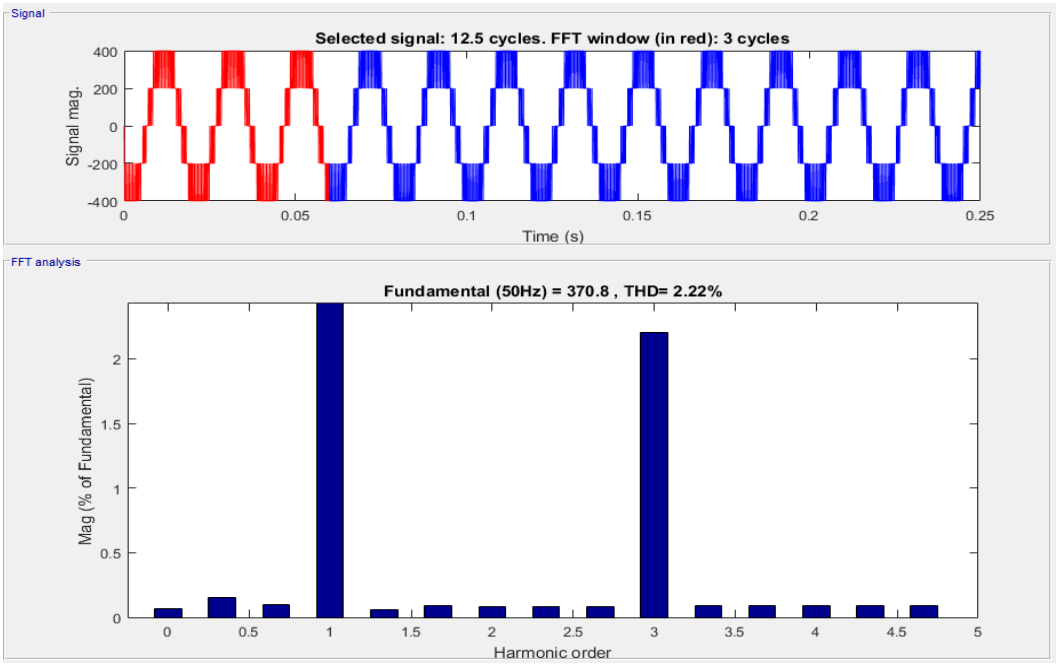

Figure 4.17 Output phase voltage and FFT analysis

(f_m=50Hz, f_{cr}=250Hz, m_a=1.0)

The output phase voltage waveform five level cascaded multilevel inverter and its FFT analysis is shown in Figure 4.18.

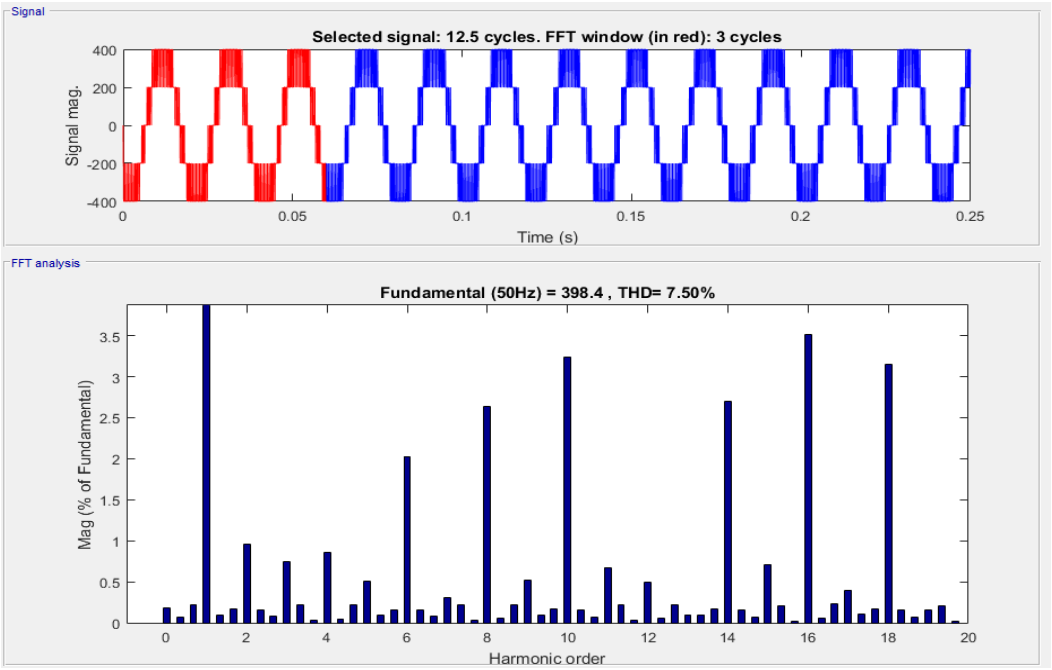

Figure 4.18 Output phase voltage and FFT analysis

(f_m=50Hz, f_{cr}=1000Hz, m_a=1.0)

When there is change in the values of the magnitude of the reference wave, the 'm' value is also changed. Table 4.1 shows analysis of the THD values of 5 level CMLI for different switching frequency and modulation index.

Table 4.1 THD values of 5 level CMLI

THD values of 5 level CMLI for different modulation frequency and modulation index			
Switching frequency (fs)	Modulation index (ma)		
	0.8	0.9	1
2000	9.47%	7.52%	7.60%
1000	8.66%	6.55%	7.50%
500	7.05%	6.15%	7.44%
250	2.40%	1.77%	2.22%

From Table 4.1 the researcher observed, the value of THD is improved when the value of switching frequency is decreased. But the performance of the system is less when the carrier

frequency is decreased. The graphical representation of variation of THD with the switching frequency is shown in Figure 4.19.

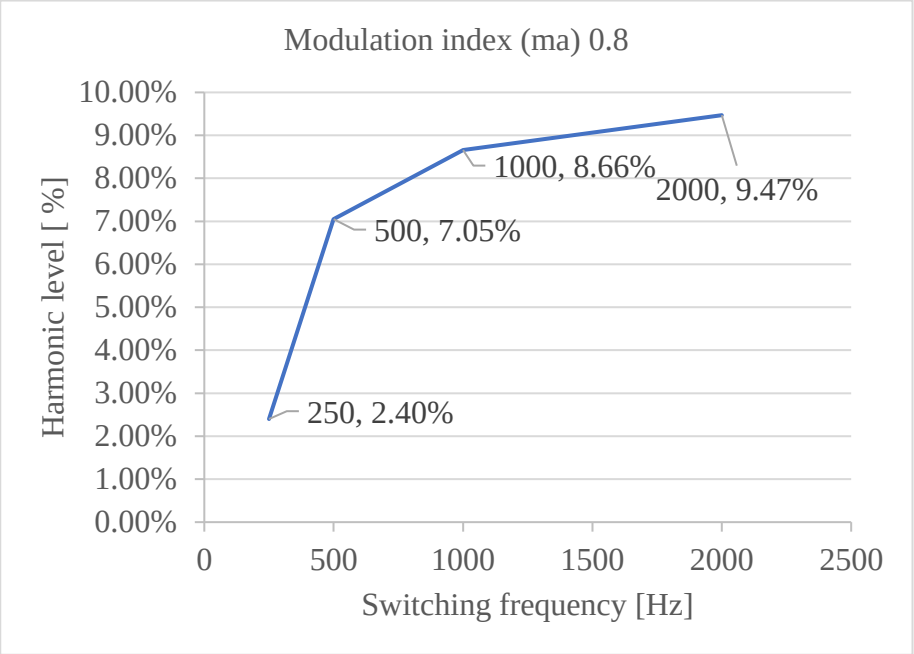

Figure 4.19 Variation of THD with switching frequency

Figure 4.19 clearly shows that, the variation of THD with the switching frequency at modulation index (ma=0.8). When the switching frequency decreases from 2kHz to 0.252kHz, the THD is improved from 9.47% to 2.40%. Table 4.2 shows the voltage values of 5 level CMLI for different switching frequency and modulation index.

Table 4.2 Voltage values of 5 level CMLI

Voltage values of 5 level CMLI for different Modulation frequency and modulation index			
Switching frequency (fs)	Modulation index (ma)		
	0.8	0.9	1
2000	314	354.2	395.5
1000	318.8	357.4	398.4
500	318.7	358.8	398.3
250	331.7	351	370.8

Table 4.2 shows that, the voltage profile is increased when the modulation index is increased. The performance of the system improved when the modulation index is increased.

The graphical representation of variation of voltage with modulation index is shown in Figure 4.20.

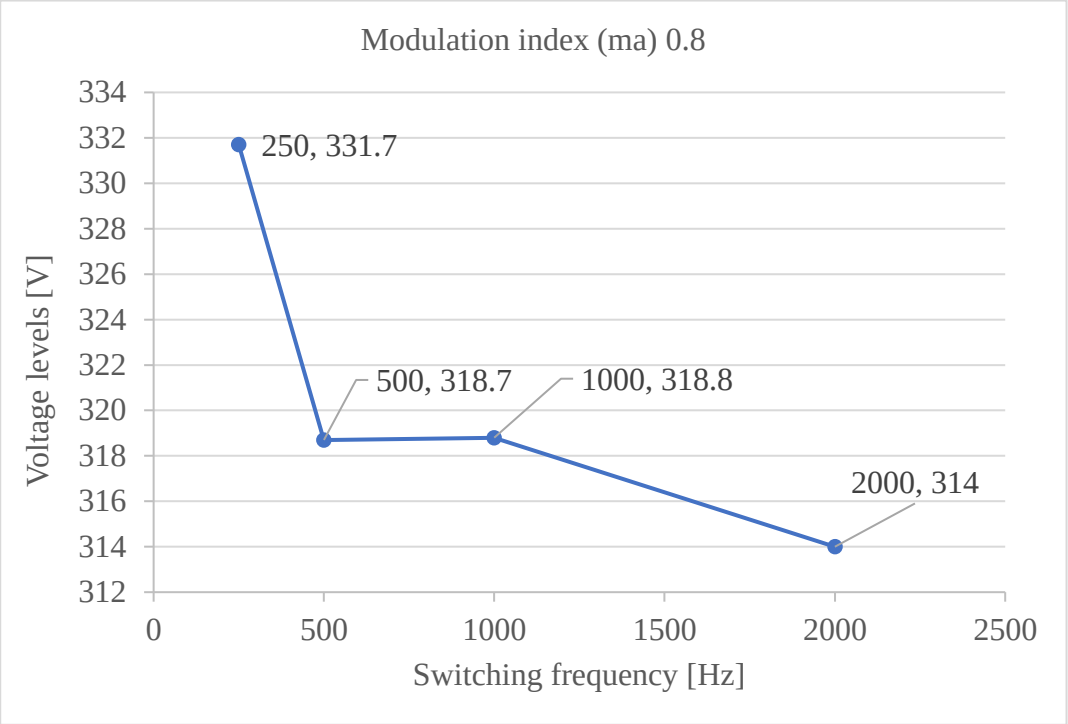

Figure 4.20 Variation of voltage with modulation index

4.4. Simulation Results of Homer Software

4.4.1. Cost Survey and Estimation

To model a system the cost of each and every component has its own effect. Globally the cost of wind and PV cells decreasing year to year and it hopes the bright future in terms of the energy demand [53]. Resource is one the most important thing and common input to the system. It applies to anything coming from outside the system that is used by the system to generate electric power. The type of source used for electric energy is like solar system input is particularly important to find out the feasibility of the system.

The monthly average solar radiation for selected area with latitude and longitude of 8.514 and 39.269 respectively fed into HOMER. The solar irradiance profile (input to PV system) of Koka in Adama which is located at South-Eastern part of Ethiopia, which was obtained from NASA, is illustrated in Figure 4.21, where it highlights the monthly average solar Global Horizontal Irradiance (GHI) data, which shows the irradiance peaking in February with 6.57 kWh/m^2/day.

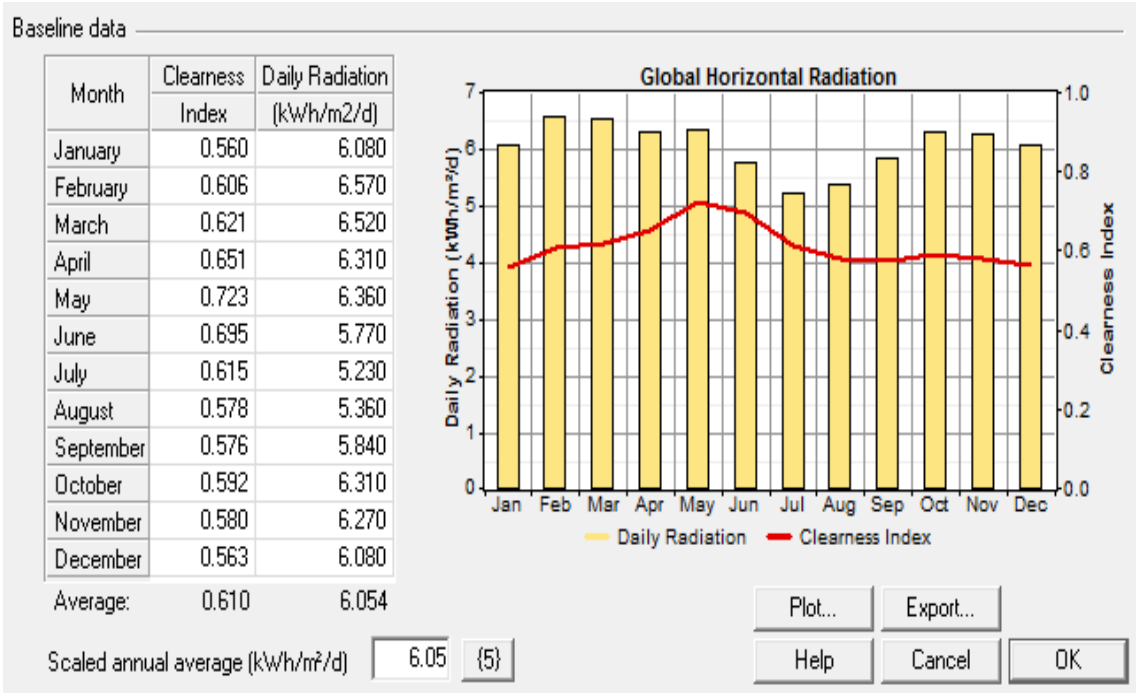

Figure 4.21 Synthesized input solar resource

The schematic representation of the standalone solar energy system is shown in Figure 4.22. The schematic diagram of the system contains solar panel and converter power generator.

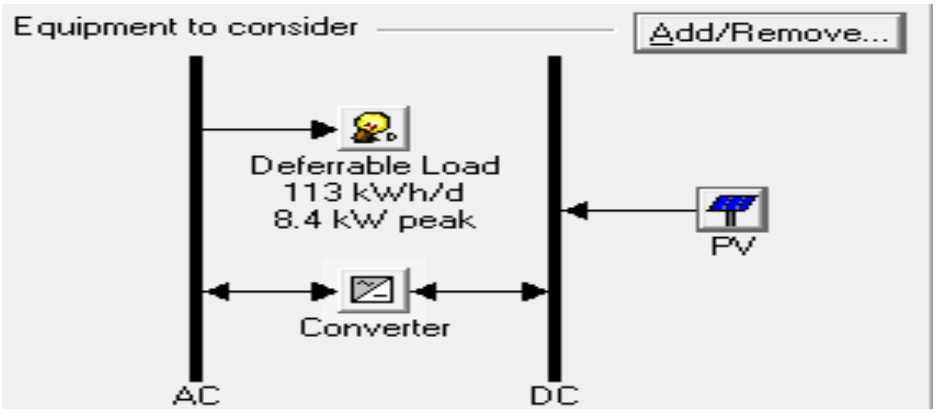

Figure 4.22 Schematic diagram of the standalone energy system

Deferrable load is the load that should be fulfilled after the primary load demand is supplied except in especial cases when water tank left empty below the required level, regardless of the time. The main aim is to provide water for farm irrigation system of the selected area. The total deferrable load of the system (total consumption of electricity by the pump) is 112.533kWh/day. In order to distribute the load throughout the year, some exceptions are considered. In the rainy season from 5% to 30% of deferrable load can be expected to

decrease because water consumption from the pump is expected to be shared by river and rain water ponds [54].

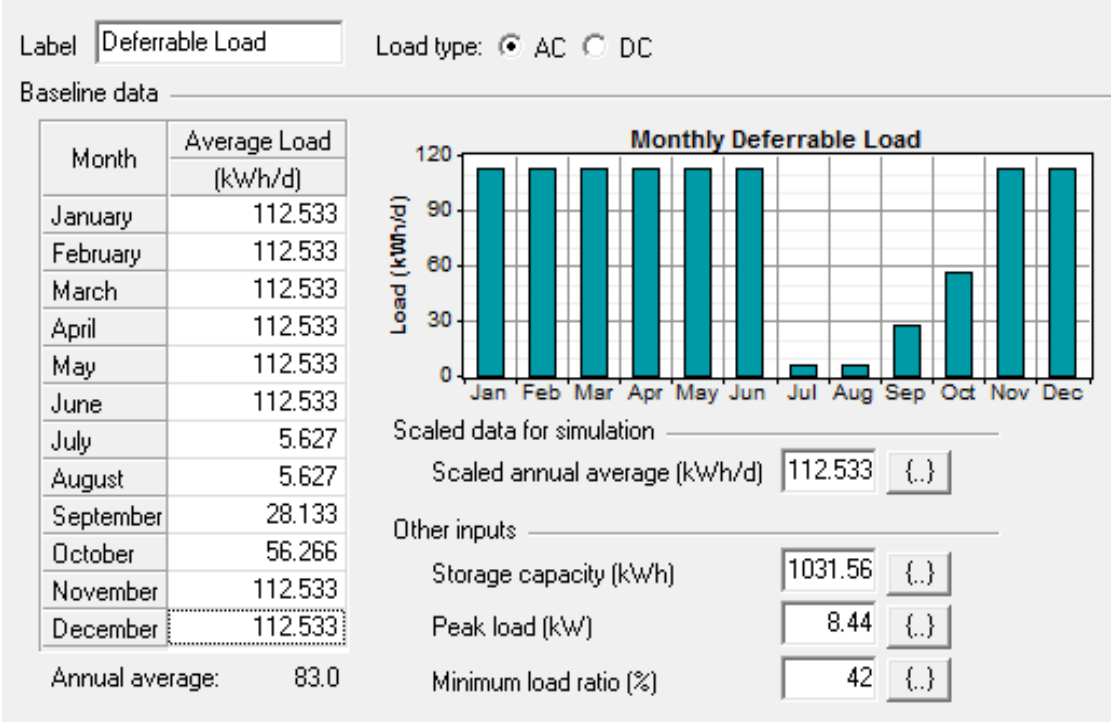

Figure 4.23 Energy used by deferrable loads

The 5% deferrable load has been decreased for July and August, 25% for September and 50% for October are assumed. The models are configuring standalone solar energy system that feeds Koka in Adama South-Eastern part of Ethiopia deferrable load. Figure 4.23 shows the energy used by deferrable loads. The total kilo-watt-hour energy required for the farm irrigation system is the watt-hour energy required for deferrable load which is 995.917kWh/day and for the future load demand 24.897kWh/day as reserve. Therefore, the total kilo-watt-hour energy demand including the reserve is 1020.814kWh/day.

After inserting the available data to the software, to determine the optimum solutions from different system configurations. HOMER software is simulated several times by varying decision variables that have effect on the output. The decision variables that affect the output are the size of PV panel and the size of converter according to this research work. The HOMER software shows the result for the inputs in either an overall form in which the top ranked system configurations are listed according to their net present cost (NPC) or in categorized form in which only the most cost-effective configuration is considered from each system type. The categorized optimization result of the standalone solar energy system

which selects the optimal combination of each component with the least capital cost is shown in Figure 4.24.

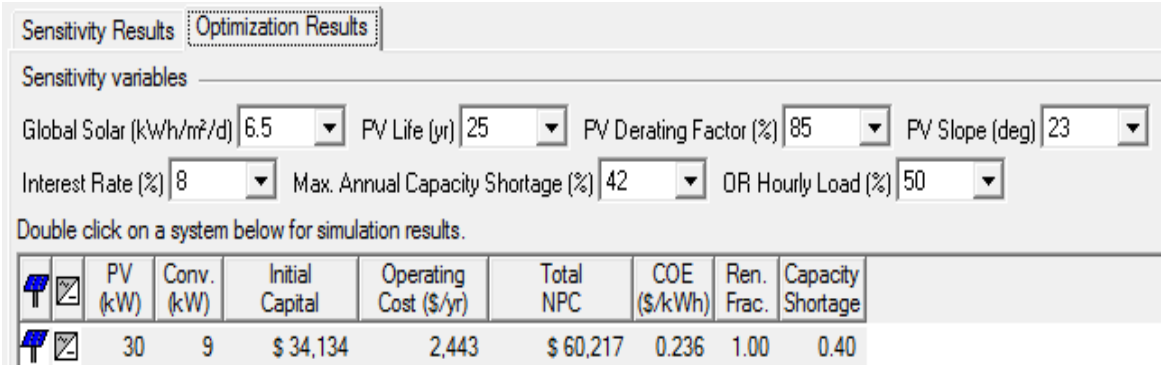

Figure 4.24 The categorized optimal result of the system

The optimization result obtained from simulation is with COE $0.236/kWh, NPC 60,217, Operating Cost per year $2,443. Figure 4.24 shows the total NPC is $60,217 is the best optimum standalone energy system configuration without including the cost of pump, storage and all it's accessories.

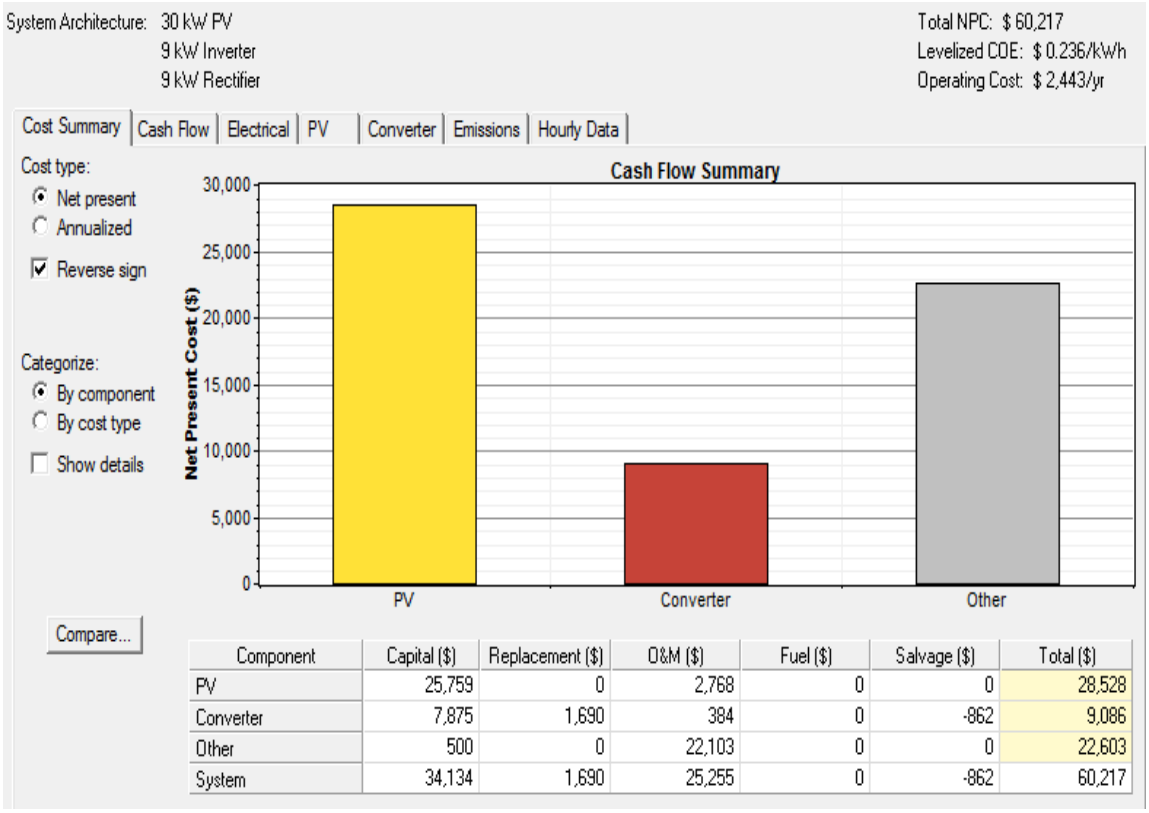

Figure 4.25 Cost of system components

The overall HOMER simulation result is shown in Appendix D. The cost of the system component is summarized in Figure 4.25.

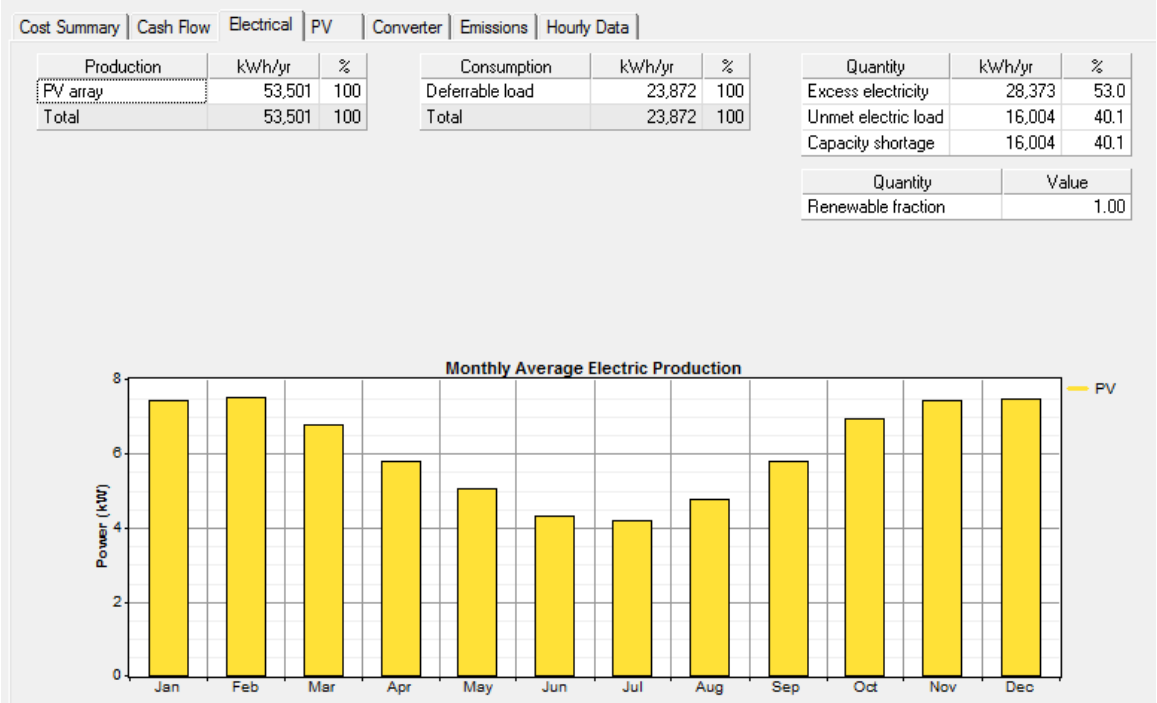

Figure 4.26 Electrical property of the system

The electrical property of the system is shown in Figure 4.26. Excess Electricity 53%, a capacity shortage 40.1%, unmet electrical load 40.1%, energy production /year is 53,501kWh and the model is 100% renewable.

The emission result of the system is shown in Figure 4.27 below. As the result shows, the system has zero emission of carbon dioxide (CO_2) and it is fully renewable.

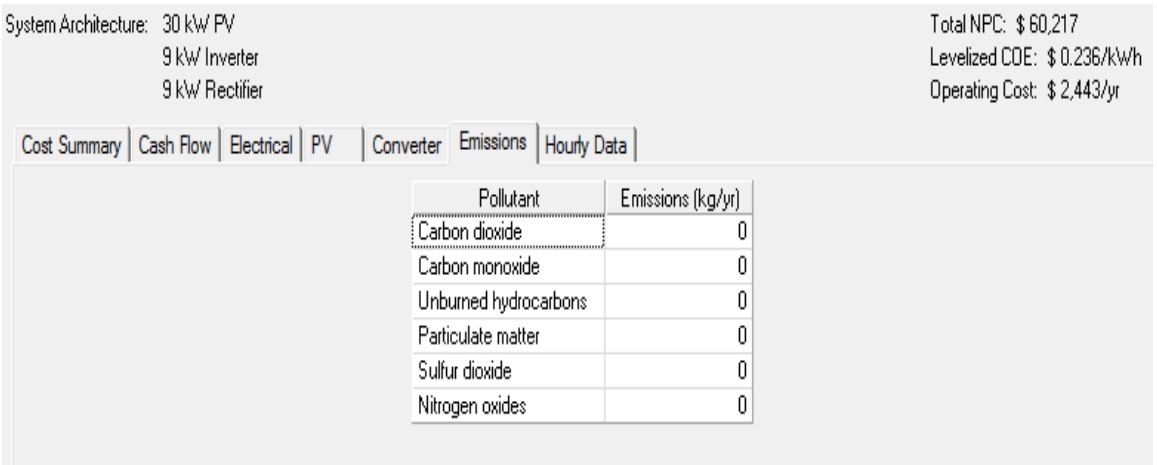

Figure 4.27 Emission result of system

CHAPTER 5

CONCLUSION AND RECOMMENDATIONS

5.1. Conclusions

In this chapter, the conclusions and recommendations from the findings are drawn. This research work presented suitable solution for solar based water pumping system which is affordable for the farmers in developing countries. Fossil fuels-based water pumping system is one of the major sources of CO_2 emission to the environment. On other hand, the cost of fossil fuels is tremendously increasing and its source is depleting. To overcome this problem, the renewable energy source has been focused. For this purpose, all the required data are collected from the specified site (daily load, solar radiation and etc). In this research work, HOMER software is used for the optimization analysis of the proposed system. According to the HOMER result, the initial investment cost is $34,134, total net present cost of $60,217 and cost of energy of selected area is found to be 0.236$/kWh.

A generalized PV module has been developed and verified with available module. The proposed model takes solar radiation intensity and cell temperature as input and outputs the I-V and P-V characteristics under various conditions. This model can be used for the analysis in the field of solar photovoltaic conversion system and MPPT technologies. The formula's developed for parameter extraction of photovoltaic module is useful as some of parameters may get change due to use in field because of dust, humidity, temperature and aging.

In the MATLAB Simulink model, the selected PV module is SCHOTT PERFORM poly240W. The energy demand of deferable load is 112.533kWh/day with peak load of 8.44kW has been used. Each module has a capacity of 240Wp. The total number of modules required is 65 modules. The PV array used in this thesis is a 15.6kW power that 13 are connected in series and 5 are connected in parallel.

The IPD-Cascaded H-bridge inverters for five-level with an induction motor are simulated using MATLAB/Simulink software. The firing pulses for the multilevel inverter are generated by using multi carrier triangular signals with a sinusoidal modulating signal and frequency respectively. This research work shows that, the value of the THD improved from 7.60% to 2.22% as the switching frequency is decreased from 2kHz to 0.25kHz (ma=1) and

the voltage profile of the system is increased from 314V to 395.5V (mf=2000) when the modulation index is increased from 0.8 to 1.

5.2. Recommendations

Assessment of solar power water pumping for farm irrigation system in Koka in Adama South- Eastern part of Ethiopia area indicates that the area has a huge potential of solar energy for water pumping and irrigation system. However, there are some challenges like: low purchasing power of the community and lower energy conversion of PV cell, towards the development and adaptation of solar powered water pumping system. It is an advisable technology since it has no environmentally hazardous outputs.

The researcher also recommends the government, NGO's and any party who are responsible for a water supply system of any given area; to use this most efficient method. It is thus recommended that the government, non-governmental organizations and the public make concerted efforts to overcome these challenges by using more flexible approaches to improve the current state of solar power water. If the artificial intelligence control system such as artificial neural network (ANN), fuzzy logic control (FLC) and genetic algorithm (GA) are used, the performance to generate power from the PV panel can be improved. Finally, the researcher recommends that the National Meteorological Agency of Ethiopia (NMAE) to make available the solar data in the form required for researchers of the country and to install direct solar energy measuring instruments at least in some areas of the country which are supposed to have higher potential of solar energy.

Acknowledgements: This research thesis was funded by Adama Science and Technology University under the grant number of **ASTU/SM-R/073/19**, Adama, Ethiopia.

References

[1] D. A. Mousse, A. Saudi, A. Beta and a. G. Asher, "Photovoltaic Pumping Systems Technologies Trends," *Lahr's Journal, ISSN,* pp. 127-150, June 2013.

[2] U. Report, "Eastern and Southern Africa Available from: https://www.unicef.org".

[3] M. Ababa, "Matching Induction Motors to PVG for Maximum Power Transfer," *Elsevier-Desalination,* pp. 31-38, 2014.

[4] I. Sefa and I. Altin, "Grid Interactive Photovoltaic Inverters-a Review," *JFac Eng Archit Gazi Univ,* pp. 24(3):409-24, 2017.

[5] I. Sefa, M. Demirtas and I. Colak, "Applications of One Axis Sun Tracking System," *Energy Convers Manage,* pp. 50:2709-18, 2015.

[6] J. S. Lai and F. Z. Peng, "Multilevel Converters- A New Breed of Power Converters," *IEEE Trans. Ind. Applicat.,* vol. 32, pp. 509-517, May/June 2013.

[7] L. Tolbert, F. Peng and T. Habetler, "Multivel converters for Large Electric Drives," *IEEE Trans. Ind. Applicat.,* vol. 35, pp. 36-44, Jan/Feb. 2015.

[8] Ethiopian Electrical Power in December 2016.

[9] V. Quaschning, Renewable Energy and Climate Change, John Wiley and Sons, 2010.

[10] Benghanem, M. and e. al., "Performance of Solar Water Pumping System Using Helical Pump for a Deep Well:," *Energy Conversion and Management,* p. 65, 2013.

[11] Breyer Ch., Gerlach A., Hlusiak M., Peters C., Adelmann P., Winiecki J., Schutzeichel H., Tsegaye S. and Gashie W., "Electrifying the Poor: Highly Economic Off-Grid PV Systems in Ethiopia a Basis for Sustatainable Development," 2009.

[12] Ethiopia, Mean Annuaul Surplus of Water in Available from: https:// energy pedia. info/wiki/File:Mean Annual Water Surplus in Ethiopia.jpg.

[13] F. Liu, S. Duan and Y. Kang, "A Variable Step Size INC MPPT Method for PV System," *IEEE Trans. Ind. Electron.,,* Vols. 55,No. 7, pp. 2622-2628, July 2008.

[14] H. Bodur and A. F. Bakan, "A New ZCT-ZVT-PWM DC-DC Converter," *IEEE Trans. Power Electron.,* Vols. 19, No. 3, pp. 676-684, May 2004.

[15] J. Lee, H. Bae and B. Cho, "Advanced Incremental Conductance MPPT Algorithm with A Variable Step Size,," *12th International Power Electronics and Motion Control Conference EPE-PEMC,,* Vols. 65, No. 6, pp. 603-607, Aug. 2006.

[16] Panels, the Planet's most Powerful Available from: http://us.sunpowercorp.com/ homes/sunpoweradvantage/more-electricity.

[17] Panels, the Photovoltaic Panels Work Available from: http:/www.Irc.rpi.edu/ programs/nlpip/lightingAnswers/photovoltaic/04-photovoltaic-panels-work.asp.

[18] A. R. Reisi, M. H. Mordi and H. Shokati, "Solar Energy, 88," pp. 154-162, 2013.

[19] L. Lui, Z. Wang, H. Zhang and Y. Xue, "Solar Energy Development in China-a Review," *Renewable and Sustainable Energy Reviews 2010,* 14(January) (1)):301-11.

[20] H. Mark, Stand-Alone Solar Electric Systems, 2010.

[21] M. Parimita, M. Tariq and K. Mohan, Solar Photovoltaic System Applications, 2016.

[22] Guide, The Kyocera Solar Inc. Solar Water Pump Applications Available from: http:/www.kyocerasolar.com.

[23] Energy, Information, Administration and (US)., *Annual Energy Review 2011.*, Government Printing Office 2012.

[24] E. Muliadi, "PV Water Pumping with A Peak Power Tracker Using Simple Six-Step Square Wave Inverter,," *IEEE Trans. Ind. Appl.,* Vols. 33, No. 3, pp. 714-721, May/Jun. 1997.

[25] N. Argaw, R. Forester and A. Ellis, "Renewable Energy for Water Pumping Applications in Rural, National Renewablle Energy Laboratory, Villages," pp. 19-26, July 2003.

[26] Tomoyuki Dansako and etal, "Slip Compensation of Induction Motor Using Sensorless Control," *International Symposium on Non Linear Theory and It's Applications, Japan,* Nov. 27th-30th,2016.

[27] Photovoltaic Powered Water Pumping Systems: Design and Optimization of an Irrigation System, Maria Ines Cardoso Bexiga 2014.

[28] A. Nasir, "Design, Simulation and Analysis of Photovoltaic Water Pumping System for Irrigation of Potato Farm at Gerenbo,," 2016.

[29] J. Malla, R. Mohana, K. S. Manoj and K. S. Pravat, "Study of PV Based Water Pumping System for Agricultural Sector," *Mater. Today Proc.,* Vols. 5, No.1, pp. 1008-1016, 2018.

[30] M. Benghanem, K. Daffallah, S. Alamri and A.A. Joraid, "Effect of Pumping Head on Solar Water Pumping System,," *Energy Convers. Manag.,* vol. 77, pp. 334-339, 2014.

[31] A. Mensur, H. S. A. S. Ghassan, U. S. Muhammad, T. A. Ali and M. E. Ibrahim, " A Review of Solar Powered Water Pumping Systems,," *Renew. Sustain. Energy Rev.,* vol. 87, pp. 61-76, Aug. 2018.

[32] G. Misrak, A. Abebayehu and M. Marta, "Feasibilty of Solar Photovoltaic Water Pumping System for Rural Areas in Ethiopia," *AIMS Journal 07/2015;2(3):697717.DOI:10.3934/Environsci.,* May 2015.

[33] M. M. Gilbert, "Renewable and Efficient Electric Power System," *Stanford University, Wiley and Sons, Inc., Hoboken, New Jersey,* April 2004.

[34] Dalelo and A., "Rural Electrification in Ethiopia,," *Opportunities and Bottlenecks, Addis Ababa University, College of Education,* 2003.

[35] A. Tadessie, "Feasibility Study of Small Hydro/PV/Wind Hybrid System for Off-Grid Rural Electrification in Ethiopia,," *AAU, Addis Ababa Institute of Technology Master's Thesis, Power Engineering Stream,* May 2011.

[36] A. September, "Renewable Energy Water Pumping System," July 2004.

[37] I. Kashif and S. Zainal, "An Improved Modeling Method to Determine the Model Parameters of Photovoltaic Models Using Differential Evolution,," *Science-Direct, Solar Energy, Elsevier Ltd.,* vol. 85, pp. 2349-23359, 2011.

[38] J. Abdul, A. Nazar. and A. R. Omega, "Simulation on Maximum Power Point Tracking of the Photovoltaic module Using LabView,," *International Journal of Advanced Research in Electrical, Electronics and Instrumentation Engineering,* vol. 1(3), pp. 190-199, 2012.

[39] T. Huan-Liang and S. Yi-Jie, "Development of Generalized Photovoltaic Model Using Matlab/Simulink,," *Proceedings of the World Congress on Engineering and Computer Science, San Fransico, USA,,* October 22-24 2008.

[40] N. Mohan and T. M. Undeland, Power Electronics, Converters, Applications and Design:, Wiley-India,2007.

[41] M. S. Rahman, "Buck Converter Design Issues," *Master Thesis, Linkoping Institute of Technology,* 2007.

[42] S. Naeim, "Design of DC-DC Buck Converter for Ultra-Low Power Applications in 65nm CMOS Process,," *Masster Thesis, Dept. Elec. Eng., Linkoping Institute of Technology,* 2012.

[43] B. Ashok and A. Rajendran, "Selective Harmonic Elimination of Multilevel Inverter Using SHEPWM Technique," *International Journal of Soft Computing and Engineering (IJSCE) ISSN:,* vol. 3, no. 2, pp. 2231-2307, May 2013.

[44] J. Rodriguez, J. S. Lai and F. Z. Peng, "Multilevel Inverters: Survey of Topologies, Controls, and Applications," *IEEE Transactions on Industry Applications,* Vols. 49, No. 4, pp. 724-745, Aug. 2009.

[45] P. Mosses, M. Stephen, N. Ponraj, K. Sathesh, K. Balamurugani and Karthikeyan, "Modified Cascaded H-Bridge Multilevel Inverter for House Hold Appliances,,"

International Research Journal of Engineering and Technology (IRJET), vol. 05, no. 03, 2018.

[46] A. Nabae, I. Takahashi and H. Akagi, "A New Neutral Point Clamped PWM Inverter," *IEEE Trans. Ind. Applicat.,* Vols. IA-17, pp. 518-523, Sept./Oct. 2005.

[47] T. A. Meynard and H. Foch, "Multilevel Choppers for High Voltage Applications for Power Electron Drives," Vols. 2, no. 1, p. 41, 2003.

[48] R. H. Baker and L. H. Bannister, "Electric Power Converter," *U.S. Patent 3 867 643,* Feb. 2006.

[49] L. M. Tolbert and T. G. Habetler, "Novel Multilevel Inverter Carrier Based PWM Method," *IEEE Transaction on Industry Application,* vol. 35 No. 5, pp. 1098-1107, Sept. 1999.

[50] H. Raffel, "Realization of a Quasi Direct Converter by a High Dynamic DC Link Voltage Regulator,," *PhD Thesis, University of Bremen,* 2003.

[51] G. E. Ahmad, "Photovoltaic Powered Rural Zone Family House in Egypt,," *Renewable Energy,* vol. 26, pp. 379-390, 2002.

[52] K. D. Dipak, "Voltage Control of DC-DC Buck Converter and It's Real Time Implementation Using Microcontroller,," *Master's Thesis, National Institute of Technology Rourkela,* 2012.

[53] The European Wind Energy Association (EWEA), "The Econonmics of Wind Energy" March 2009..

[54] D. Bekele and B. Palm, "Feasibility Study for a Standalone Solar-Wind Hybrid Energy System for Application in Ethiopia,," *Applied Energy,* vol. 87, no. 2, pp. 487-495, 2010.

Appendixes

Appendix A: The Dimension of Schedule 40 PVC Pipe

Schedule 40 Pipe Dimensions											
	Diameters			Transverse Areas			Length of Pipe per Sq. Foot of				
Size Inches	External Inches	Internal Inches	Nominal Thickness Inches	External Sq. Ins.	Internal Sq. Ins.	Metal Sq. Ins.	External Surface Feet	Internal Surface Feet	Cubic Feet per Foot of Pipe	Weight per Foot Pounds	Number Threads per Inch of Screw
1/8	.405	.269	.068	.129	.057	.072	9.431	14.199	.00039	.244	27
1/4	.540	.364	.088	.229	.104	.125	7.073	10.493	.00072	.424	18
3/8	.675	.493	.091	.358	.191	.167	5.658	7.747	.00133	.567	18
1/2	.840	.622	.109	.554	.304	.250	4.547	6.141	.00211	.850	14
3/4	1.050	.824	.113	.866	.533	.333	3.637	4.635	.00370	1.130	14
1	1.315	1.049	.133	1.358	.864	.494	2.904	3.641	.00600	1.678	11½
1¼	1.660	1.380	.140	2.164	1.495	.669	2.301	2.767	.01039	2.272	11½
1½	1.900	1.610	.145	2.835	2.036	.799	2.010	2.372	.01414	2.717	11½
2	2.375	2.067	.154	4.430	3.355	1.075	1.608	1.847	.02330	3.652	11½
2½	2.875	2.469	.203	6.492	4.788	1.704	1.328	1.547	.03325	5.793	8
3	3.500	3.068	.216	9.621	7.393	2.228	1.091	1.245	.05134	7.575	8
3½	4.000	3.548	.226	12.56	9.886	2.680	.954	1.076	.06866	9.109	8
4	4.500	4.026	.237	15.90	12.73	3.174	.848	.948	.08840	10.790	8
5	5.563	5.047	.258	24.30	20.00	4.300	.686	.756	.1389	14.61	8
6	6.625	6.065	.280	34.47	28.89	5.581	.576	.629	.2006	18.97	8
8	8.625	7.981	.322	58.42	50.02	8.399	.442	.478	.3552	28.55	8
10	10.750	10.020	.365	90.76	78.85	11.90	.355	.381	.5476	40.48	8
12	12.750	11.938	.406	127.64	111.9	15.74	.299	.318	.7763	53.6	
14	14.000	13.125	.437	153.94	135.3	18.64	.272	.280	.9354	63.0	
16	16.000	15.000	.500	201.05	176.7	24.35	.238	.254	1.223	78.0	
18	18.000	16.874	.563	254.85	224.0	30.85	.212	.226	1.555	105.0	
20	20.000	18.814	.593	314.15	278.0	36.15	.191	.203	1.926	123.0	
24	24.000	22.626	.687	452.40	402.1	50.30	.159	.169	2.793	171.0	

Appendix B: The MATLAB Implementation of Cascaded Multilevel Inverter

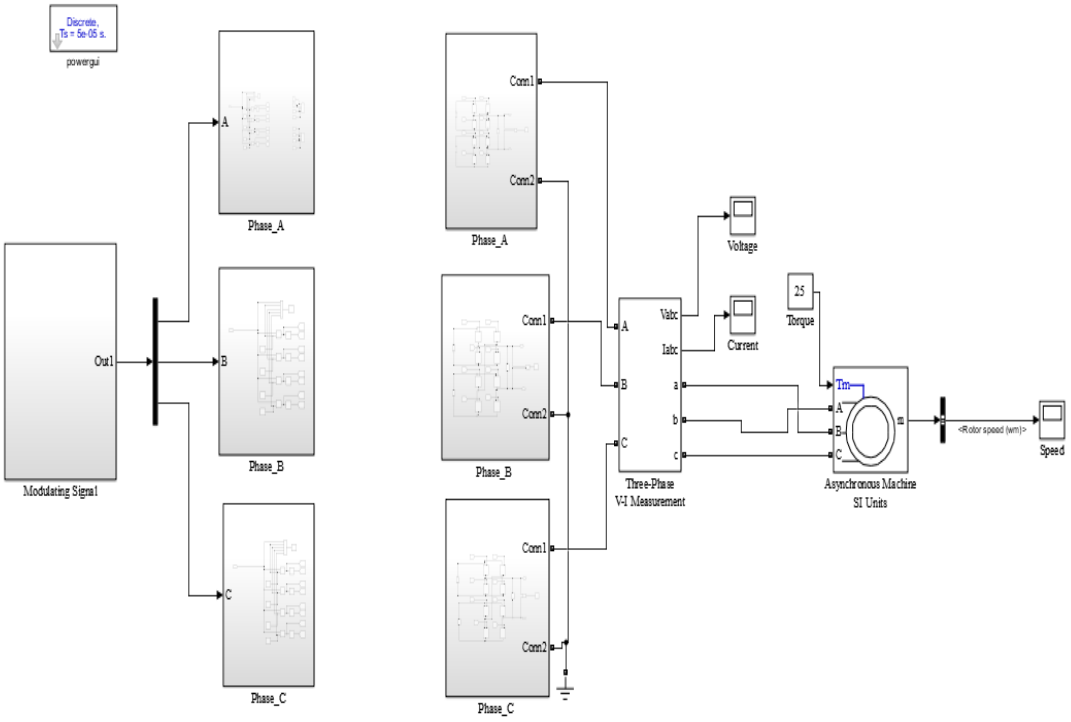

Appendix C: Multiplot Representation of PV System on MATLAB

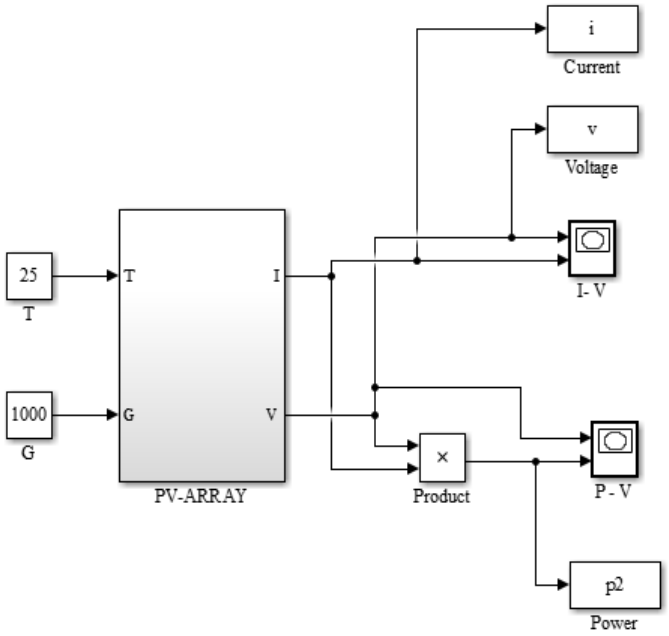

Appendix D: The overall HOMER Simulation Result

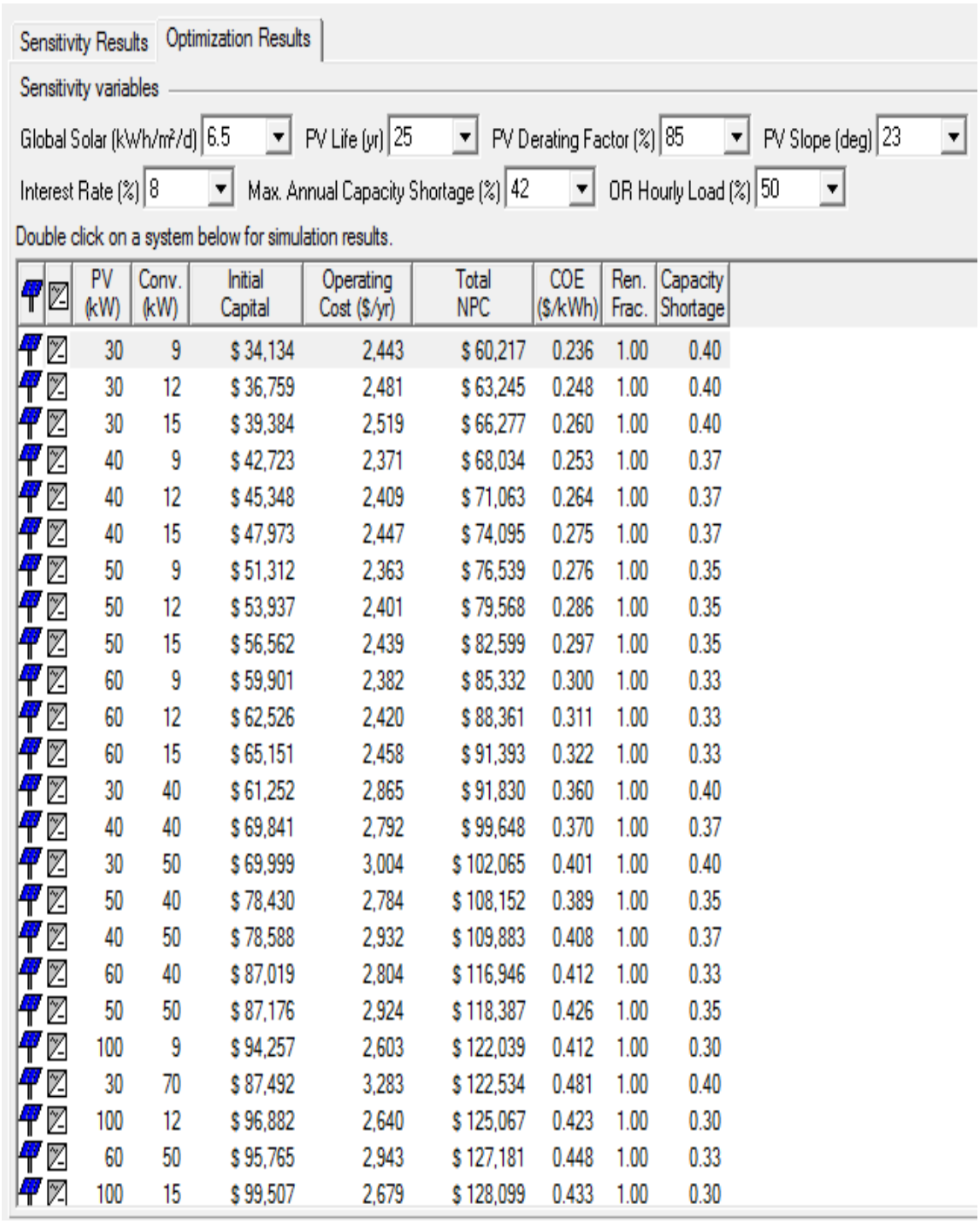

Sensitivity Results | Optimization Results

Sensitivity variables

Global Solar (kWh/m²/d) 6.5 | PV Life (yr) 25 | PV Derating Factor (%) 85 | PV Slope (deg) 23

Interest Rate (%) 8 | Max. Annual Capacity Shortage (%) 42 | OR Hourly Load (%) 50

Double click on a system below for simulation results.

PV (kW)	Conv. (kW)	Initial Capital	Operating Cost ($/yr)	Total NPC	COE ($/kWh)	Ren. Frac.	Capacity Shortage
30	9	$ 34,134	2,443	$ 60,217	0.236	1.00	0.40
30	12	$ 36,759	2,481	$ 63,245	0.248	1.00	0.40
30	15	$ 39,384	2,519	$ 66,277	0.260	1.00	0.40
40	9	$ 42,723	2,371	$ 68,034	0.253	1.00	0.37
40	12	$ 45,348	2,409	$ 71,063	0.264	1.00	0.37
40	15	$ 47,973	2,447	$ 74,095	0.275	1.00	0.37
50	9	$ 51,312	2,363	$ 76,539	0.276	1.00	0.35
50	12	$ 53,937	2,401	$ 79,568	0.286	1.00	0.35
50	15	$ 56,562	2,439	$ 82,599	0.297	1.00	0.35
60	9	$ 59,901	2,382	$ 85,332	0.300	1.00	0.33
60	12	$ 62,526	2,420	$ 88,361	0.311	1.00	0.33
60	15	$ 65,151	2,458	$ 91,393	0.322	1.00	0.33
30	40	$ 61,252	2,865	$ 91,830	0.360	1.00	0.40
40	40	$ 69,841	2,792	$ 99,648	0.370	1.00	0.37
30	50	$ 69,999	3,004	$ 102,065	0.401	1.00	0.40
50	40	$ 78,430	2,784	$ 108,152	0.389	1.00	0.35
40	50	$ 78,588	2,932	$ 109,883	0.408	1.00	0.37
60	40	$ 87,019	2,804	$ 116,946	0.412	1.00	0.33
50	50	$ 87,176	2,924	$ 118,387	0.426	1.00	0.35
100	9	$ 94,257	2,603	$ 122,039	0.412	1.00	0.30
30	70	$ 87,492	3,283	$ 122,534	0.481	1.00	0.40
100	12	$ 96,882	2,640	$ 125,067	0.423	1.00	0.30
60	50	$ 95,765	2,943	$ 127,181	0.448	1.00	0.33
100	15	$ 99,507	2,679	$ 128,099	0.433	1.00	0.30

Double click on a system below for simulation results.

PV (kW)	Conv. (kW)	Initial Capital	Operating Cost ($/yr)	Total NPC	COE ($/kWh)	Ren. Frac.	Capacity Shortage
40	70	$ 96,081	3,210	$ 130,352	0.484	1.00	0.37
30	80	$ 96,239	3,422	$ 132,769	0.521	1.00	0.40
50	70	$ 104,670	3,203	$ 138,856	0.500	1.00	0.35
40	80	$ 104,828	3,350	$ 140,587	0.522	1.00	0.37
60	70	$ 113,259	3,222	$ 147,650	0.520	1.00	0.33
50	80	$ 113,416	3,342	$ 149,091	0.537	1.00	0.35
30	100	$ 113,732	3,701	$ 153,238	0.601	1.00	0.40
100	40	$ 121,374	3,024	$ 153,652	0.519	1.00	0.30
60	80	$ 122,005	3,361	$ 157,885	0.556	1.00	0.33
40	100	$ 122,321	3,629	$ 161,056	0.598	1.00	0.37
30	110	$ 122,479	3,840	$ 163,473	0.641	1.00	0.40
100	50	$ 130,121	3,163	$ 163,887	0.554	1.00	0.30
150	9	$ 137,201	2,977	$ 168,983	0.559	1.00	0.29
50	100	$ 130,910	3,621	$ 169,560	0.610	1.00	0.35
40	110	$ 131,068	3,768	$ 171,291	0.636	1.00	0.37
150	12	$ 139,826	3,015	$ 172,011	0.569	1.00	0.29
150	15	$ 142,451	3,053	$ 175,043	0.579	1.00	0.29
60	100	$ 139,499	3,640	$ 178,354	0.628	1.00	0.33
50	110	$ 139,656	3,760	$ 179,795	0.647	1.00	0.35
100	70	$ 147,614	3,442	$ 184,356	0.623	1.00	0.30
60	110	$ 148,245	3,779	$ 188,589	0.664	1.00	0.33
100	80	$ 156,361	3,581	$ 194,591	0.657	1.00	0.30
150	40	$ 164,319	3,398	$ 200,596	0.664	1.00	0.29
30	150	$ 157,465	4,398	$ 204,412	0.802	1.00	0.40

Double click on a system below for simulation results.

PV (kW)	Conv. (kW)	Initial Capital	Operating Cost ($/yr)	Total NPC	COE ($/kWh)	Ren. Frac.	Capacity Shortage
150	50	$ 173,065	3,538	$ 210,831	0.698	1.00	0.29
40	150	$ 166,054	4,326	$ 212,230	0.788	1.00	0.37
100	100	$ 173,854	3,860	$ 215,060	0.727	1.00	0.30
200	9	$ 180,146	3,382	$ 216,253	0.707	1.00	0.28
200	12	$ 182,771	3,420	$ 219,281	0.717	1.00	0.28
50	150	$ 174,643	4,318	$ 220,734	0.795	1.00	0.35
200	15	$ 185,396	3,458	$ 222,313	0.727	1.00	0.28
30	170	$ 174,959	4,677	$ 224,881	0.882	1.00	0.40
100	110	$ 182,601	4,000	$ 225,295	0.761	1.00	0.30
60	150	$ 183,232	4,337	$ 229,527	0.808	1.00	0.33
150	70	$ 190,559	3,817	$ 231,300	0.765	1.00	0.29
40	170	$ 183,548	4,604	$ 232,699	0.865	1.00	0.37
50	170	$ 192,136	4,597	$ 241,203	0.868	1.00	0.35
150	80	$ 199,305	3,956	$ 241,535	0.799	1.00	0.29
200	40	$ 207,263	3,804	$ 247,866	0.811	1.00	0.28
60	170	$ 200,725	4,616	$ 249,997	0.880	1.00	0.33
30	200	$ 201,199	5,095	$ 255,585	1.003	1.00	0.40
200	50	$ 216,010	3,943	$ 258,101	0.844	1.00	0.28
150	100	$ 216,799	4,235	$ 262,004	0.867	1.00	0.29
40	200	$ 209,788	5,023	$ 263,403	0.979	1.00	0.37
250	9	$ 223,090	3,806	$ 263,716	0.857	1.00	0.28
100	150	$ 217,588	4,557	$ 266,234	0.899	1.00	0.30
250	12	$ 225,715	3,844	$ 266,745	0.867	1.00	0.28
250	15	$ 228,340	3,882	$ 269,777	0.877	1.00	0.28